

NASA TECHNICAL NOTE



NASA TN D-3332

@ 1

NASA TN D-3332

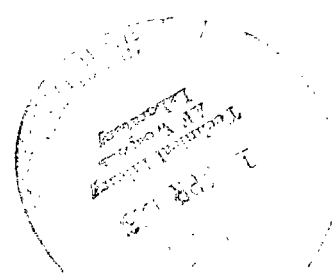
LOAN COPY: RETURN
AFWL (WLIL-2)
KIRTLAND AFB, NM



SURVEY OF ELECTROMAGNETIC ACCELERATORS FOR SPACE PROPULSION

*by Stanley Domitz, H. G. Kosmahl, Peter Ramins,
and N. John Stevens*

*Lewis Research Center
Cleveland, Ohio*





SURVEY OF ELECTROMAGNETIC ACCELERATORS
FOR SPACE PROPULSION

By Stanley Domitz, H. G. Kosmahl, Peter Ramins,
and N. John Stevens

Lewis Research Center
Cleveland, Ohio

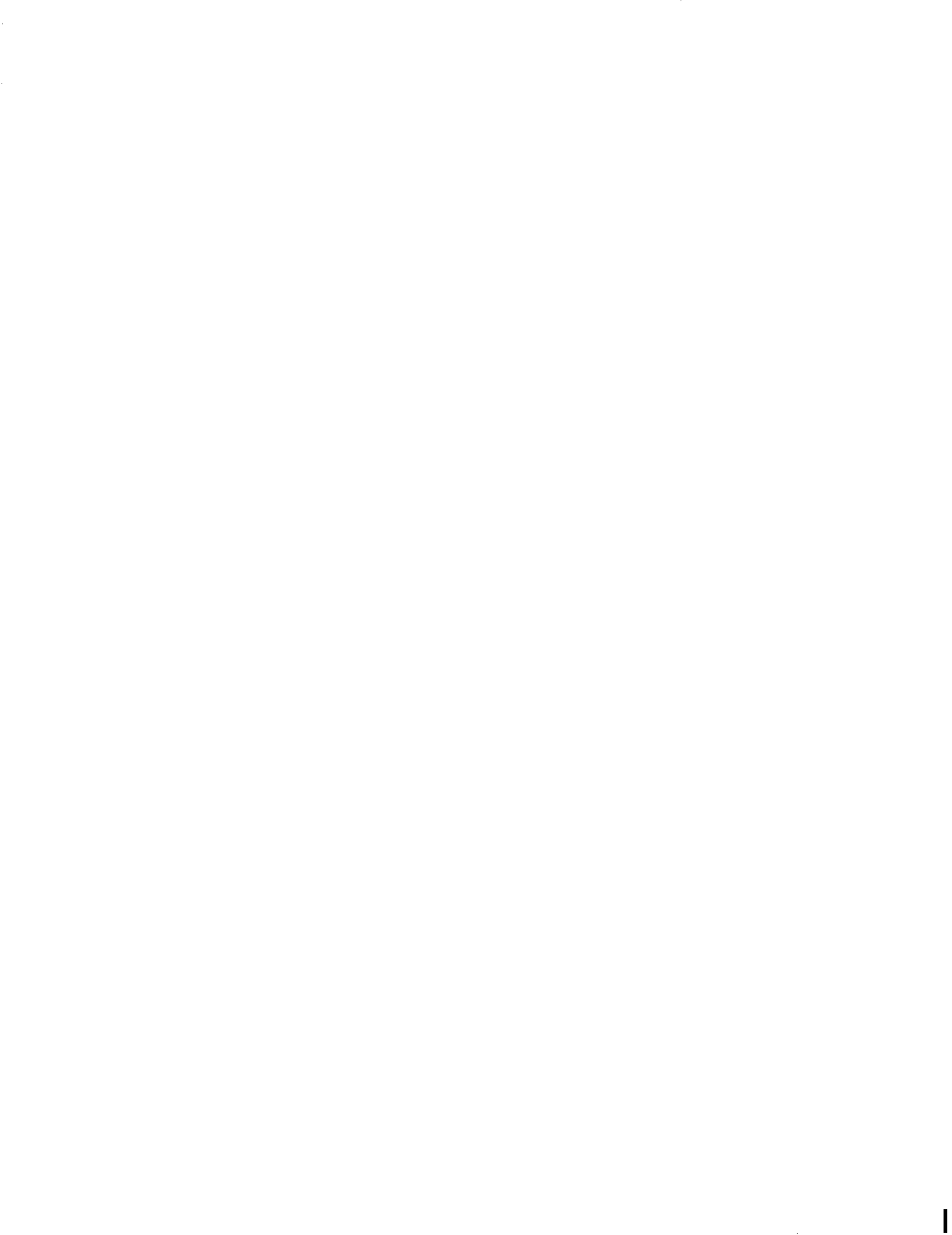
NATIONAL AERONAUTICS AND SPACE ADMINISTRATION

For sale by the Clearinghouse for Federal Scientific and Technical Information
Springfield, Virginia 22151 - Price \$1.60



CONTENTS

| Chapter | Page |
|---|------|
| I INTRODUCTION. | 1 |
| II PERFORMANCE EVALUATION AND COMPARISON. | 5 |
| III DIRECT-CURRENT ACCELERATORS | 11 |
| IV ALTERNATING-CURRENT PLASMA ACCELERATORS. | 61 |
| V PULSED PLASMA ACCELERATORS. | 87 |
| VI GENERAL CONCLUDING REMARKS. | 123 |



SUMMARY

A survey of the experimental status of electromagnetic or plasma accelerators is presented. This survey is limited to the major programs of recent years on plasma accelerators for spacecraft propulsion and does not cover the purely research activities in plasma physics.

At present plasma accelerators are at the stage of demonstrating feasibility collecting performance data and investigating the problems of operation. A broad approach covering a wide range of input power requirements and types of accelerators is being pursued. There is, however, a definite tendency towards devices using coaxial geometry, minimum electrode areas, and short interaction lengths.

CHAPTER I

INTRODUCTION

Accelerators for electric propulsion applications have traditionally been classified as electrothermal, electrostatic (ion), or electromagnetic (plasma) accelerators. Recent survey reports have been published for the first two categories (refs. I-1 and I-2). Surveys of plasma accelerators have been written by various authors (refs. I-3 to I-8), but the surveys that were comprehensive, do not have the latest results. The purpose of this report is to compile and interpret the latest representative experimental data in the propulsion-oriented, plasma accelerator program. In general this report represents the published state of the art as of July 1965. Recent theoretical and purely research-oriented efforts will be mentioned only when the results have a direct bearing on the accelerator program.

A plasma accelerator is a device in which a partially ionized plasma, a gas composed of free electrons, ions and neutral atoms, is accelerated primarily by means of the Lorentz (or $\vec{j} \times \vec{B}$) force. Most accelerators operate in a regime such that the force acts primarily on the electrons causing them to be accelerated in the thrust direction. The ions are accelerated by the electric field resulting from the separation of the electrons and ions. Finally, the neutral atoms, if they are to be accelerated, must be moved along by means of ion-neutral collisions. In this process the plasma remains electrically neutral on the average, that is, the electron density is approximately equal to the ion density.

Although the basic force law from which the thrust is derived is common to all plasma accelerators, there are numerous ways in which the current and magnetic field can be applied or induced. These can be used to distinguish the various types of accelerators. For example, in a linear cross-field accelerator a steady-state current and magnetic field are applied to accelerate the plasma; in Hall devices a steady applied magnetic field and induced currents are utilized; pulsed accelerators use a pulsed current and induced magnetic field; and traveling wave accelerators use an oscillating magnetic field and induced currents.

Another characteristic that distinguishes the different types of accelerators is the regime of operation. If the ratio of the ion mean free path to the accelerator dimensions is much lower than unity, then the accelerator is said to operate in the collision-dominated regime. In this regime the plasma is treated as a fluid and the usual magnetofluid-dynamic equations are used. If this ratio is much higher than unity,

however, then the accelerator is said to operate in the collisionless regime. Here the particle trajectory equations are used to represent the acceleration process. In the regime between these limits, there is no simplified theoretical approach.

As a result of this situation, it is doubtful if any single, simple theory will describe plasma phenomena well enough to predict operation over a broad operating range. Although present-day theories are useful for guiding the experimental research, most improvements in accelerator design and performance have come about almost entirely from an empirical approach and it is very likely that plasma accelerators will become operational before a theory sufficiently refined is available. A phenomenological approach will be used in this survey to explain the operation of the various accelerators. For those readers who desire a more complete theoretical background, references I-9 to I-14 are suggested.

The advantage of the plasma accelerator lies in its ability to produce high thrust densities, that is, the devices are not limited by fundamental space-charge laws. Their potential specific impulse ranges from 1000 to 20 000 seconds with no fundamental restriction on the upper limit. Thus with a high thrust density, relatively large thrusts (in the range of newtons) from small, simple, lightweight accelerators are quite feasible. The magnetic fields, where applied externally, can generally be obtained by relatively lightweight, permanent or low-loss magnets. The power-conditioning requirements do not appear to be severe. The dc devices require a low voltage and high current which can be obtained from present generators or conceivably from one of the direct energy-conversion schemes. The radiofrequency power for the induction accelerators can be generated using rotating machinery. The tubes for microwave-driven accelerators and the capacitor for pulsed accelerators will require a modest developmental effort.

The major experimental effort now is to study and evaluate the operation of the accelerators toward demonstrating feasibility for possible space propulsion applications. A number of different types of plasma accelerators requiring a wide range of input powers are being investigated. Development of flyable systems and the technology associated with these efforts has been logically postponed until acceptable performance of the accelerator has been established.

In this survey the division of the plasma accelerators will be by the power-input requirements. Prior to beginning this discussion, a chapter on performance evaluation and comparison is given to emphasize the fact that care is needed in interpreting and comparing data. A précis of current status containing the recent important results as well as problems precedes the discussion of each class of accelerator. A general-considerations section dealing with the particular acceleration process will be given before the discussion of the experimental results.

REFERENCES

- I-1. Mickelsen, William R. ; and Kaufman, Harold R. : Status of Electrostatic Thrusters for Space Propulsion. NASA TN D-2172, 1964.
- I-2. Wallner, Lewis E. ; and Czika, Joseph, Jr. : Arc Jet Thrustor for Space Propulsion. NASA TN D-2868, 1965.
- I-3. Brewer, G. R. ; Currie, M. R. ; and Knechtli, R. C. : Ionic and Plasma Propulsion for Space Vehicles. Proc. IRE, vol. 49, no. 12, Dec. 1961, pp. 1789-1821.
- I-4. Seikel, George R. : Generation of Thrust - Electromagnetic Thrustors. Proceedings of the NASA-University Conference on the Science and Technology of Space Exploration, vol. 2, NASA SP-11, 1962, pp. 171-176. (Also available as NASA SP-22.)
- I-5. Hess, Robert V. : Fundamentals of Plasma Interaction with Electric and Magnetic Fields. Proceedings of the NASA-University Conference on the Science and Technology of Space Exploration, vol. 2, NASA SP-11, 1962, pp. 313-336. (Also available as NASA SP-25.)
- I-6. Ellis, Macon C. , Jr. : Survey of Plasma Accelerator Research. Proceedings of the NASA-University Conference on the Science and Technology of Space Exploration, vol. 2, NASA SP-11, 1962, pp. 361-381. (Also available as NASA SP-25.)
- I-7. Demetriades, Sterge T. : Plasma Propulsion, pt. II. Astronautics, vol. 7, no. 4, Apr. 1962, pp. 40-42; 44.
- I-8. Dix, D. M. : A Survey of Some Plasma Acceleration Devices for Space Propulsion. Rept. No. TDR-169(3713-01)TR-1(SSS-TDR-63-120), Aerospace Corp. , May 17, 1963.
- I-9. Resler, E. L. , Jr. ; and Sears, W. R. : The Prospects for Magneto-Aerodynamics. J. Aeron. Sci. , vol. 25, no. 4, Apr. 1958, pp. 235-245; 258.
- I-10. Sears, W. R. : Magnetohydrodynamics in Aeronautics. Preprint No. 709-58, Am. Rocket Soc. , Inc. , 1958.
- I-11. Spitzer, L. , Jr. : Physics of Fully Ionized Gases. Intersci. Pub. Inc. , 1956.
- I-12. Chandrasekhar, S. : Plasma Physics. Univ. Chicago Press, 1960.
- I-13. Cowling, T. G. : Magnetohydrodynamics. Intersci. Pub. Inc. , 1957.
- I-14. Demetriades, S. T. ; Hamilton, G. L. ; Ziemer, R. W. ; and Lenn, P. D. : Three-Fluid Non-Equilibrium Plasma Accelerators. Progress in Astronautics and Aeronautics. Vol. 9 - Electric Propulsion Development. Academic Press, Inc. , 1963, pp. 461-511.



CHAPTER II

PERFORMANCE EVALUATION AND COMPARISON

INTRODUCTION

When the performance characteristics of a large number of plasma accelerators are available, a direct comparison of the various devices is inevitable. Although uniform standards for performance evaluation do indeed exist, they are not yet universally applied.

The status of plasma accelerators is such that, in many cases, the determination of the thrust efficiency alone is not a true indication of the potential of the accelerator for efficient operation. Rather, it is appropriate to examine the efficiencies of the various energy-transfer processes governed by plasma behavior. In many cases, the problem of achieving efficient energy transfer from the external source to the plasma region involves extensive development of circuit components and has largely been postponed. In other cases, the development of a propellant-injection scheme which does not a priori preclude a high mass utilization, and consequently the determination of a realistic thrust efficiency, has been postponed. Consequently, a large number of performance-evaluation techniques, each leading to different results and/or referring to different processes, has been employed. These sets of performance data are inseparable from the technique by which they were obtained and, in many cases, a direct comparison of the performance of various devices is meaningless. It is the purpose of this chapter to illustrate the various techniques and to show how they may differ.

Aside from weight and lifetime considerations, the thruster parameters of interest in mission analysis are thrust, specific impulse, and overall thrust efficiency. The quantities to be determined experimentally are the thrust T , total mass flow \dot{m}_t , and input power P . The efficiency η and specific impulse I_{sp} are calculated from

$$I_{sp} \equiv \frac{T}{\dot{m}_t g}$$

$$\eta \equiv \frac{T^2}{2\dot{m}_t P}$$

These five quantities, together with their interdependence, define the performance characteristics of any accelerator. However, each of the quantities may be evaluated by a number of distinct methods, each of which may have an uncertainty of unknown magnitude associated with it.

Thrust is generally measured by one of four techniques. Only the direct-reaction thrust measurement in a sufficiently low pressure environment is unambiguous. The accuracy of the other techniques is not known, although great care is exercised in their use to answer the elementary objections. The total mass flow through the accelerator is the sum of the admitted mass and of extraneous contributions such as eroded mass, mass desorbed from the electrodes and insulators, and recirculated gas. In many cases, these extraneous contributions so obscure the measured mass flow as to make it completely uncertain. The input power, although differently defined for the various classes of accelerators, can generally be accurately measured. The efficiency and \int_{sp} can be calculated from the particular measurements of thrust, mass flow, and power input, as made on a given device. This efficiency does not necessarily include all of the losses in components which have yet to be developed. Such losses must eventually be included to obtain the system efficiency. Alternately, η can be estimated from calorimetric measurements and \int_{sp} can be estimated from plasma velocity measurements. A more detailed discussion of all of the above measurements is presented in the following section.

THRUST

Thrust may be measured directly by (1) determining the reaction force on the accelerator or (2) on part of the accelerator (as on only the coils of the induction accelerator). It may be inferred from (3) the deflection of a target on which the exhaust beam is allowed to impinge, or (4) it may be calculated if the mass-velocity distribution of the exhaust is known. In the third case either a perfectly inelastic collision between the target and the plasma or a cancellation of axial components of momentum of any ablated mass must be assured. A distinction must be made between pulsed accelerators, where the instantaneous energy intensity can be extremely high, and the steady-state devices. For steady-state devices, outgassing is achieved and the energy intensity is generally too low to produce ablation of the target surface. Sputtering can be shown to be small. For pulsed accelerators, because of the high energy of the impinging particles, a large mass of material ablated from the target can be expected to introduce a significant error in the inferred plasma momentum. This difficulty can be largely overcome with the reentrant or closed configuration target. The ablated mass is contained and its possible momentum contribution to the observed target deflection is negated by trapping the material.

In measuring the reaction force on the coils of the induction accelerator, or the re-

action on the magnetic field coils of a dc accelerator the interactions of the plasma with the accelerator walls subsequent to its acceleration must be evaluated to obtain the true thrust. Only the direct thrust measurement is unambiguous. The calculated thrust efficiency is particularly sensitive to the accuracy of the thrust determination since it is proportional to the square of the thrust.

MASS FLOW

Because of the extraneous contributions to the total mass flow of eroded mass, mass desorbed from the electrodes and insulators, and recirculated gas, a necessary condition for proper determination of the mass flow rate is long term operation in a low pressure environment. Complete outgassing of the electrodes and insulators can then be achieved and, erosion can be evaluated. Beyond this, a distinction must be made between the pulsed and the steady-state devices.

A necessary but not sufficient condition for high mass utilization of the short pulse, low repetition rate pulsed accelerator is the requirement for discharge initiation after the admitted mass flow has ceased but before the gas flow has begun to leave the discharge region. Propellant-feed systems meeting this requirement have not been generally available. In these cases the a priori less than unity mass utilization has been needlessly charged to the accelerator as reduced η and f_{sp} .

In continuous-flow devices the effect of the environmental test-chamber pressure on accelerator performance has not been determined. Because of pumping-speed limitations, high mass-flow devices may operate with an ambient pressure high enough to permit some propellant to recirculate through the accelerating region resulting in underestimating the total mass flow. This can occur if the accelerating region is in contact with the gas in the test chamber. For the case where a pressure differential separates the accelerating chamber from the test facility, the high ambient pressure does not affect the mass-flow reading but may give a thrust reading that is too low.

INPUT POWER

The input power is defined differently for the various classes of accelerators. For dc devices the input power is determined from voltage and current measurements at the accelerator terminals. Because of possible ac fluctuations in both the current and the voltage, the input power must be checked; for instance, against the final energy balance in the accelerator. Magnet power, if any, is not counted. In ac-induction devices only the power to the plasma is considered. In the microwave-driven devices, by proper tun-

ing, the reflected power can be made negligible, and the total incident microwave power is used. In pulsed-plasma accelerators it has become apparent that the transfer efficiency of stored energy to the gun is related to the plasma processes and the input power is defined as the initially-stored capacitor energy times the pulsing rate.

SPECIFIC IMPULSE

Similarly to the η , the calculated J_{sp} depends on the accuracy of the measurements of thrust and mass flow. In many devices, where these parameters have not been measured or are only poorly known, the J_{sp} is still an unknown quantity. An alternate technique for determining the upper limit for the J_{sp} is integration over the mass velocity distribution in the exhaust if the distribution can be experimentally determined. Other measurements, such as luminous or magnetic-front velocities in the pulsed accelerators, have been used to estimate the plasma velocity. In general, however, the relations between these measurements and the actual J_{sp} of the accelerator are not known.

EFFICIENCY

The calculated thrust efficiency depends on the accuracy of the particular type of measurement of the thrust and of the mass flow. Any of the four ways of measuring the thrust, each with its own uncertainty, can be used. In many cases the uncertainty in the mass flow is so large as to make the calculation meaningless. An alternate technique for estimating the efficiency is by the measurement of the total beam energy by means of a calorimeter which captures the exhaust products.

The efficiency inferred from calorimetric measurements of total beam energy differs from the overall thrust efficiency by factors due to the presence of a velocity spread in the exhaust products, beam divergence, nonpropulsive energy components in the beam, and less than ideal mass utilization.

The thrust efficiency is a function of the mass-velocity distribution in the exhaust. For a given mass flow and total beam energy, the thrust efficiency decreases with both an increasing velocity spread in the exhaust and beam divergence and with a decreasing mass utilization. The calorimeter cannot discriminate between the various possible mass-velocity distributions, indicating identical efficiencies for all distributions.

Since cooling of the plasma and recombination take place within the calorimeter, calorimetric efficiencies are not valid approximations of the thrust efficiency in the cases where the sum of internal plasma energy, dissociation energy and ionization energy is large compared to the directed energy. For highly ionized light propellants and

low \mathcal{J}_{sp} , calorimetric measurements serve only to indicate the energy dissipation within the accelerator. For heavier propellants at high \mathcal{J}_{sp} ion energies are of the order of hundreds of electron volts per ion. For these cases the sum of the ionization and dissociation energies are known to be small compared to the directed energy of the ions. However, the internal energy must be shown to be small before calorimetric efficiency can be used as a meaningful approximation for the thrust efficiency.

The calorimetric efficiency represents the upper limit for the thrust efficiency and, as such, is frequently used as a standard for estimating accelerator performance for the cases where the frozen-flow losses are not a priori known to be large. However, even a direct comparison of calorimetric efficiencies of the pulsed accelerators is difficult since the collecting efficiency of calorimeters varies with the material and geometry of the calorimeter and with the exhaust-beam characteristics. In many cases the calorimetric efficiency is so low as to make the question of thrust efficiency and the other performance parameters an academic one.



CHAPTER III

DIRECT-CURRENT ACCELERATORS

SUMMARY OF CURRENT STATUS

The direct current accelerators to be discussed in this chapter have been separated into linear and coaxial devices. This geometric division is primarily a matter of convenience.

The linear crossed-field (or $\vec{j} \times \vec{B}$) accelerator is characterized by a steady-state magnetic field and current applied across the flowing gas stream. An arcjet is usually used as a preionization source. The accelerator operates in the pressure range of several torr, with high applied currents, and with moderate magnetic field strengths. The electrodes are mounted in a staggered or offset position to eliminate the Hall deflection.

The results indicate that the thrust is proportional to the current and the magnetic field as predicted by the simplified theory. Argon is the principal test gas but hydrogen, helium, and nitrogen have also been used. The specific impulse experimentally obtained is too low to be useful. With an argon mass flow rate of 1 gram per second and a power input of 250 kilowatts, the specific impulse of 1000 seconds was obtained. The highest reported value of specific impulse (2200 sec) was obtained using hydrogen as fuel. Calorimetric measurements have shown that about 60 to 70 percent of the total input power is in the exhaust, but the demonstrated thrust efficiency is less than 30 percent.

Diagnostic studies on the accelerator problems have not, as yet, clarified the solution to the problem of improving the thrust efficiency. A solution to the severe problem of the electrode and side wall erosion that does not increase the weight of the accelerator has not been found. Any further improvement in accelerator performance will require a basic study directed towards understanding the phenomena. At present the main effort in the crossed-field devices is concentrated in wind-tunnel applications.

In coaxial geometry many modes of acceleration are possible. Coaxial dc crossed-field accelerators of several different types have been operated at input powers from 10 watts to 250 kilowatts, specific impulse up to 12 000 seconds, and thrusts up to a few newtons. Thrust efficiency of 70 percent has been measured.

Magnetoplasmadynamic (MPD) arcs (high impulse arcs) have recently achieved efficiencies greater than 50 percent over a specific impulse range from 3000 to 10 000 seconds. The MPD arc is an annular arc operating in an external magnetic field. Several

acceleration mechanisms have been identified. The best accelerator performance to date has been obtained with lithium as the propellant.

Hall ion accelerators are plasma accelerators but can be looked upon as an ion engine without space-charge limitations. The concept is attractive but the accelerators must overcome the problem of the short circuiting electron diffusion to achieve high efficiency. A cesium accelerator shows some promise at a specific impulse of 1500 to 2500 seconds.

The oscillating electron ion engine or magnetic expansion thruster, which operates at low densities and low power, is similar in operation to a Phillips ionization gage (PIG)-type discharge. The engine has achieved an efficiency of above 30 percent at 3000 seconds for short-life operation.

INTRODUCTION

The accelerators to be discussed in this chapter are all dc, steady-state devices which operate over a wide range of thrust and specific impulse. The current is passed through electrodes that are in contact with the gas. The power input to the accelerator is simply the product of the current and the voltage across the electrodes. The relation between the currents and electric fields in the plasma, however, is quite complicated and is given by the generalized Ohm's law which takes into account the motion of ions, electrons and neutral particles.

A convenient form of this Ohm's law is:

$$\vec{j} = \sigma_0 \vec{E}' - \frac{\omega_e \tau_e}{B} \vec{j} \times \vec{B} + \frac{\omega_e \tau_e \omega_i \tau_i}{B^2} (\vec{j} \times \vec{B}) \times \vec{B}$$

where σ_0 is the scalar conductivity and $\vec{E}' = \vec{E} + \vec{u} \times \vec{B}$ is the electric field in the moving frame of reference (ref. III-1). An equivalent formulation of Ohm's law can be written by incorporating the right hand side of the preceding equation into the moving-frame electric field \vec{E}' and a tensor conductivity Φ or (ref. III-2):

$$\vec{j} = \Phi \cdot \vec{E}'$$

This latter form, while mathematically correct, suppresses the components of the resulting electric field and, hence, will not be used in the following discussion.

The $\vec{j} \times \vec{B}$ term represents the Hall effect which is caused by the drift motion of the electrons at right angles to the applied current and magnetic field. Since this term is perpendicular to the current density \vec{j} , it causes the electric field \vec{E} to have a com-

ponent perpendicular to \vec{j} , or a Hall field. The electric field is, then, at an angle relative to the current given by the Hall parameter $\omega_e \tau_e$.

The $(\vec{j} \times \vec{B}) \times \vec{B}$ term represents a phenomena known as ion slip. This effect is caused by the relative motion of the ions and neutrals. Under this condition a frictional force exists that retards the ions. This retardation can be considered as an ion resistivity, and hence, it is an additional loss mechanism representing an increase in heating of the gas. Ion slip can be neglected in accelerators that operate with a fully ionized plasma, that operate in the regime where the ion mean free path is larger than the channel dimensions, or that operate in a regime where there are sufficient collisions to insure that the neutrals and ions are locked together. Mathematically, this latter condition can be expressed as (ref. III-3):

$$\omega_e^2 \tau_e^2 < \frac{\omega_e \tau_e}{\omega_i \tau_i}$$

The accelerating force per unit volume is $\vec{j} \times \vec{B}$ where \vec{j} is the current density given by Ohm's law and \vec{B} is the magnetic field, which may be self-induced or applied externally. By choice of the accelerator geometry, and of the operating parameters, pressure, magnetic field, and power level, different modes of acceleration are possible. This chapter is divided into two sections, linear and coaxial accelerators. In general, linear accelerators utilize directly applied currents and magnetic fields whereas coaxial accelerators utilize both applied and induced (Hall) currents and applied and induced magnetic fields. The discussion of each half of this division will consist of a general considerations section in which the characteristics of the accelerator will be presented, an experimental data section, and finally, a concluding remarks section.

LINEAR CROSSED-FIELD ACCELERATORS

General Considerations

The linear crossed-field accelerator was originally proposed as an "afterburner" for the arcjet accelerator (ref. III-4): a means of extending the specific impulse of an arcjet. Since the arcjet exhaust was partially ionized, it appeared that it would be a simple matter to extend the nozzle section to confine the exhaust and add a magnet and electrodes to this section. The thrust would be increased due to the applied Lorentz force and the specific impulse would also increase since the mass flow remains constant. If the input power to the crossed-field section could be kept low, then the efficiency of the combination would also increase.

The idealized linear crossed-field accelerator is an application of the dc motor principle and can be represented schematically as shown in figure III-1. The exhaust from the arcjet is assumed to be flowing in the z-direction only and the magnetic field is in the negative x-direction. An applied current I is assumed to be flowing in the y-direction. The interaction of this current and the magnetic field will produce a volume force given by the Lorentz relation:

$$\vec{f}_v = \vec{j} \times \vec{B}$$

For the idealized model given here this relation can be easily integrated to obtain the accelerator thrust T_a :

$$T_a = BIh$$

Even with a diverging duct the thrust can be shown to be proportional to the same group of parameters (ref. III-4).

This Lorentz volume force acts only on the current-carrying elements of the plasma which is generally assumed to be only the electrons, and accelerates them in the z-direction. The resulting space-charge field, which may also be called a Hall field, set up by the separation of the electrons and ions, then accelerates the ions in the z-direction. Since the gas is only partially ionized, the more numerous neutral atoms are believed to be accelerated by ion-neutral collisions (ref. III-5). With varying degrees of approximation the magnetohydrodynamic equations expressing this process have been solved (see e. g., refs. III-6 to III-12).

The existence of a Hall electric field in the axial or z-direction implies that an axial Hall current can also exist. The Lorentz force due to this Hall current would produce an unwanted y-component of thrust or simply a deflected beam. This undesired effect can ideally be eliminated either by segmenting or staggering the electrode pairs which introduces an electric field that suppresses the Hall current. This principle is used in most of the experimental work. A practical configuration of this type of accelerator is shown schematically in figure III-2.

The pressure in the electrode region is generally in the range of several millimeters of mercury. In this range the electron mean free path is much less than the accelerator dimensions and the resulting collisions will produce appreciable Joule heating losses. The ion slip losses, however, can be neglected provided the magnetic field is limited to a few thousand gauss.

The electrode positions relative to the confining duct wall can also vary corresponding to two different modes of operation. If the electrodes are flush with the wall, then the accelerator is said to operate in the confined mode. If the electrodes penetrate into

the gas stream, then operation is in the unconfined mode. Even in the unconfined mode there are walls or baffles to raise the pressure in the electrode region so that an arc can be formed. Both configurations have been run as accelerators. The unconfined mode is used to reduce the viscous drag losses along the walls. In certain low-powered experimental devices, the drag losses were such that no net thrust could be produced (refs. III-13 and III-14). However, another investigator has shown that confined channel operation is possible at high-power input (ref. III-15).

The question of which mode of operation is best will not be satisfactorily resolved until an accelerator is tested in a vacuum tank with a very low back pressure. In experiments to date, the tank pressure has been fairly high (about 1 mm Hg), and it is possible to build up sufficient pressure to strike an arc in the electrode region. At the lower pressures comparable to a space environment, the arcjet exhaust may become too diffuse for unconfined operation. Furthermore, in the unconfined mode experiments there is a possibility of gas from the tank entering the electrode region and being accelerated. If this happens, the mass flow is incorrect and the performance data is optimistic.

The efficiency definition given in chapter II assumes that the gas is accelerated from rest. For the linear crossed-field accelerator this relation would give the thrust efficiency of the combined arcjet - plasma accelerator. Because of the variation in performance of the arcjets used by the different experimentors, a thrust efficiency for the crossed-field accelerator (η_a) has been defined by some investigators as:

$$\eta_a = \frac{\frac{1}{2} \dot{m}(u_f^2 - u_o^2)}{P_a} = \frac{T_a^2}{2\dot{m}P_a} + \frac{T_a u_o}{P_a}$$

where $T_a = \dot{m} \Delta u$ and is the thrust increment due to the crossed-field accelerator, $u_f = u_o + \Delta u$ where Δu is the velocity increment in the accelerator. Theoretical predictions of the maximum velocity increment obtainable from the linear crossed-field accelerator are limited by the assumptions that have been made to solve the equations. One such treatment predicts that the factor $\Delta u/u_o$ is, at most, 3.3 for a perfect monatomic gas in equilibrium (ref. III-16). In this survey only the combined arcjet - plasma accelerator efficiency will be given.

The discussion of the data will be divided into two main topics: accelerator performance results and accelerator problem-area investigations such as heat transfer to the electrodes, erosion, arc attachment and potential measurements. An additional discussion of the various loss mechanisms in crossed-field accelerators and their relative importance can be found in reference III-17.

Accelerator Performance

This discussion of accelerator performance is limited to the recent experimental results of Avco Corporation/Research and Advanced Development Division (Avco/RAD), Marquardt-MHD Research (MHD Research conducted the experimental investigation under subcontract to Marquardt Corporation), and Northrup Corporation. These three were chosen primarily because they were major, propulsion-oriented investigations. These results have not been obtained under sufficiently similar conditions to make comparative judgments, but they are indicative of the state of development of the accelerators and do show the operational trends. The earlier data of Demetriades (ref. III-18), Ragusa and Baker (ref. III-19), and Wood (ref. III-20), among others, can be found in the literature and will not be presented here. Before discussing the performance curves it is first mandatory that a background description of each experiment be given so that proper evaluation of the data can be made. A schematic representation of the accelerators can be seen in figure III-2.

Avco-RAD program. - This program (ref. III-14) was an experimental investigation of the use of a cross-field accelerator to extend the operating range of a 30-kilowatt arcjet accelerator. A single pair of radiation-cooled, staggered electrodes was mounted in the exhaust of the arcjet. The data was taken with the accelerator operating in the unconfined mode since the use of the confined mode yielded little thrust. The arcjet - accelerator combination was mounted on a thrust stand which was housed in a large vacuum tank. Hydrogen was used as the test gas simply because it was the best gas for arcjet operation.

The thrust of the arcjet originally was 125 grams. With the addition of the electrodes and the magnet (but still without applying the electric and magnetic fields), the thrust dropped to 110 grams indicating that there were still viscous drag losses even in this unconfined mode. Data were taken for accelerator power levels up to 30 kilowatts and magnetic fields up to 0.25 tesla at a mass flow rate of 0.12 gram per second of hydrogen. No information was reported on the erosion of the electrodes during these tests. The performance data is summarized in figures III-3 to III-5.

In addition to the above work a series of test runs were made to investigate the possibility of obtaining a high specific impulse with an arcjet crossed-field accelerator (ref. III-21). The emphasis was on the velocity and no thrust data were reported. These tests did achieve 2000-second impulse using a mass flow of 0.10 gram per second hydrogen and a magnetic field of 0.25 tesla. The available data are given in table III-1.

Marquardt-MHD Research program. - The accelerator in this joint program (ref. III-13) was a crossed-field device using three pairs of water-cooled electrodes powered by separate 25 kilowatt power supplies. The accelerator channel wall formed part of the vacuum system with the magnet pole faces, the electrodes, and the arcjet entering through seals. As a result of this arrangement, the ambient pressure was high, that is,

several torr. The test gas was argon and the accelerator operated in the unconfined mode. In these tests it was again found that the confined mode of operation produced little or no increase in thrust presumably due to the viscous drag along the walls.

The thrust was measured with a pendulum thrust target. In these experiments no attempt was made to correct for the Hall deflection of the exhaust so that the pendulum measured only the axial component of the thrust. The mass flow data reported was just the gas input to the arcjet. No quantitative measure of the mass addition due to eroded products was attempted even though this erosion was pictured as severe. The performance characteristics, summarized in figures III-3 to III-5, were obtained by cross plotting the information from several graphs in the report. Although these data have been plotted as a constant current curve, in reality the current varied up to 10 percent during the test run.

A program to test the thruster in a vacuum environment was also undertaken (ref. III-2). In this program the arcjet - accelerator combination was mounted on a thrust stand inside a vacuum tank. The accelerator itself was similar to the previous one with the exception that the water cooling circuits in the electrodes were to be improved to lessen erosion. Only one data point was taken before the program ended. However, some relative observations were obtained for operation with two pairs of staggered electrodes and these have been summarized in table III-II.

Northrup program. - The Northrup report (ref. III-22) covers the last year of effort on an Air Force contract. The performance data was obtained using an accelerator having a single pair of water-cooled electrodes staggered by a distance analytically and experimentally determined to give the minimum Hall deflection. The arcjet - plasma accelerator combination was mounted on a pendulum-type thrust stand in a vacuum tank capable of maintaining a tank pressure of 0.9 torr. Operation was in the confined mode. The test gas was argon at a flow ratio of 1.36 grams per second. The gas velocity entering the thruster was 1910 meters per second so that the arcjet thrust can be calculated to be 2.6 newtons. The performance characteristics are summarized in figures III-3 and III-4.

A large number of experimental parametric investigations to improve the performance can also be found in this report. Studied were the effect of heat transfer to the electrodes, the effect of ambient pressure and shaped magnetic fields, and the use of various electrode materials and insulator configurations to reduce losses and erosion.

Discussion of test results. - The data presented in figures III-3 to III-5 and in tables III-I and III-II illustrate several trends in the performance of the crossed-field accelerators. First, a definite thrust increase has been demonstrated. This increased thrust has been shown to be proportional to the applied current and magnetic field for the unconfined mode of operation. The results obtained by the Northrup investigators demonstrate the performance of a confined mode of operation. In the latter results the thrust

approaches the theoretical value only at high applied power levels. A possible explanation is that at lower power levels, the viscous drag at the walls greatly reduced the net thrust. The agreement between the thrust data reported by Northrup and Marquardt is surprisingly good in view of the differences in operation and measurement techniques.

The performance characteristic curves (fig. III-4) indicate that the specific impulses so far attained are too low to be of interest for propulsion applications. However, these curves do show that, for the range tested, the performance does improve by lowering the mass flow and by increasing the power input. If the argon results are extrapolated to the hydrogen case, then lower mass flows and higher power inputs should improve the performance of the accelerator. This turns out to be the manner of operation of the so-called high-impulse arcs to be discussed later in this chapter.

The question of which is the best propellant has not been answered. Argon has been used for convenience, but the performance is too poor. The hydrogen results are the best that have been obtained so far. Helium has been tried as a propellant (ref. III-23) but the efficiency is lower than that obtained with argon. An investigation into the use of an argon-helium gas mixture as a propellant (ref. III-2) has demonstrated only that the mixture has the breakdown characteristics of argon over a broad range of helium percentages.

The efficiency tends to increase with the magnetic field for the ranges investigated. In figure III-5 the increase in efficiency is shown to be approaching a limiting value. One possible explanation for this is the increasing effect of ion-slip losses.

The demonstrated thrust efficiencies of these accelerators are low. The calorimetric data of Russell, et al. for argon (ref. III-24) indicate that, for 20 to 40 kilowatts input power, approximately 60 to 75 percent is in the exhaust. From the other performance results it appears that less than half of the energy in the exhaust is directed or useful energy. John, et al. (ref. III-14) estimate that for hydrogen the Joule losses amounted to 25 percent of the input power. Because of the trend to higher currents to improve the performance, the minimizing of Joule heating of the gas is a problem that has to be solved. Seeded gases have been suggested as an answer but so far only Langley (ref. III-25) and A. R. O. Incorporated (ref. III-26) have plans to use seeded gases in wind-tunnel programs. Unfortunately, there will be no thruster performance data from these tests.

Problem Area Investigations

Heat transfer to electrodes. - The experiments conducted at Northrup (ref. III-22) accumulated a considerable amount of data on the heat losses to the electrodes by calo-

rimetric measurements. Data for argon were taken with the accelerator operating in the confined mode and using only one pair of water-cooled copper electrodes. The results (see fig. III-6) showed that, as the accelerator power input was increased above 10 kilowatts, the total heat transferred to the electrodes became significantly less when a magnetic field was applied as compared to the zero magnetic field case. For these tests this phenomenon was independent of the magnetic field strength between 0.086 and 0.146 tesla. The fraction of input power lost to the electrodes then becomes progressively less as higher accelerator power levels are applied. Hence, the efficiency could be improved by operating at high input-power levels.

In this series of tests, the anode and cathode heating were about the same. It was determined that the heat transfer to each was due to the flux of charged particles falling through the anode and cathode sheath voltage drops. The aerodynamic heating was negligible. This result has been verified by other independent experiments (ref. III-15).

At Aeronutronics, the total energy deposited in an argon gas stream and the heat losses to a heavily water-cooled copper anode and an uncooled thoriated tungsten-tipped cathode was measured (ref. III-24). For 32.5 kilowatts input the total energy in the plasma beam was 21.1 kilowatts and the total cathode and anode losses were 1.59 and 9.91 kilowatts, respectively. These data were for an applied current of 500 amperes and a magnetic field of 0.10 tesla. The total heat transfer to the electrodes as a function of power input and magnetic field is shown in figure III-6. These curves are the result of cross plotting the data given in the reference assuming that the difference between the total power input and the power to the plasma is the total electrode heat transfer. For these experiments the heat losses to the electrodes were approximately independent of the strength of the magnetic field up to 0.15 tesla.

Further collaboration of these trends can be found in the data of an Avco/RAD experiment using a nitrogen-fueled crossed-field gas heater (ref. III-15, also see fig. III-6). For these tests both the electrodes were water cooled: the anode was made of copper and the cathode was Avcomet - a mixture of copper and tungsten. These data also indicate that the heat transfer to the electrodes is approximately independent of the magnetic field strength. For the same device the heat transfer to the electrodes has also been determined for confined and unconfined modes of operation (see fig. III-7) and for various electrode materials (see fig. III-8). In this latter experiment the copper and Avcomet electrodes were water cooled whereas the tungsten electrodes were radiation cooled. The nitrogen mass flow rate for all phases of this work was approximately 2.2 grams per second.

If the trends predicted by the nitrogen work can be applied to the accelerator, then it appears that the lowest heat transfer to the electrodes is obtained when a tungsten radiation-cooled cathode and a water-cooled copper anode are used and when the cathode is flush with insulator wall while the anode penetrates into the gas stream. Another al-

ternative would be to increase the input power level since the fraction of heat lost becomes less as the power level is increased. However, this results in a higher total heat transfer to the electrodes and increased erosion.

Erosion. - There are only qualitative results on the degree of erosion that is to be expected during operation. The numbers that have appeared are the average losses during a particular test. These are determined by weight differences before and after a test and do not give any indication of the erosion rate. It can be postulated that either this rate is constant throughout the test or that it is initially very high and tapers off during the test.

A $3\frac{1}{2}$ -hour test run at 30 kilowatts power input with little if any erosion of the cooled electrodes and insulation has been reported by Aeronutronics (ref. III-24). The AVCO/RAD tests (ref. III-15) were for 5 minutes duration at power levels up to 250 kilowatts. However, at power levels up to 750 kilowatts severe erosion limited tests to 10 to 30 seconds. The Marquardt-MHD Research report (ref. III-2) flatly stated that the erosion was severe even with water-cooled electrodes and relatively low power inputs. In the Northrup report (ref. III-22) there is information on both electrode and side-wall erosion. For their configuration they found that the side erosion predominated and that there was little electrode erosion with water-cooled electrodes at power levels up to 40 kilowatts. At Langley Research Center (ref. III-25) a 2.5-square-centimeter accelerator with 24 pairs of radiation-cooled electrodes for wind-tunnel applications was built and tested. These results indicated that the erosion of the tungsten electrodes and boron nitride side-walls was still a problem even though the current through each electrode pair was only about 50 amperes.

This problem has not been solved as yet. At one time it had been suggested that the erosion could be minimized if the current through each electrode pair was kept low and the number of pairs increased to maintain the input power level. The work at Langley indicates that the solution is not that simple. Since this erosion has a direct influence on the lifetime of these accelerators, a satisfactory solution to this problem must be found to make these accelerators attractive for propulsion applications. This solution preferably should not substantially increase either the complexity or the weight of the thrusters.

Arc attachment. - The Marquardt-MHD Research report (ref. III-2) stressed the problem encountered in trying to force the anode attachment point to remain in the vicinity of the anode tip. The arc preferred to walk up the anode until it came to the copper-tungsten joint and then burned through the copper, terminating the test. This illustrates one facet of this phenomena. The other phase of this problem is the nonuniform current distributions caused by this distorted arc.

This report is not the only place that the attachment problem is mentioned. Other investigators (ref. III-27) have found that the arc attached to the metal cooling plates in the side walls and shorted out the insulation. To force the arc to stay in the desired area

mushroom-shaped electrodes (ref. III-15) have been used as well as a deviation from the standard linear geometry (ref. III-2). In this latter case the electrodes were mounted in the fringing magnetic field parallel to the gas flow. The preliminary results indicated a partial success.

The nonuniform current distributions arise from the tendency of the cathode to emit from the upstream side and the arc to attach on the downstream side of the anode. This problem has been studied analytically by several investigators (e. g. , refs. III-28 and III-22) and experimentally at Langley (ref. III-25) and at Electro-Optical Systems, Incorporated (EOS) (ref. III-29).

The EOS program was an analytical and experimental program to investigate current distributions. To determine these distributions both the 1-inch-square anode and cathode were divided into nine equal, electrically insulated, water-cooled segments. These segments were maintained at the same potential while the current through each could be measured. The observed results were as follows:

Cathode distribution: At $B = 0$ the cathode current was carried entirely by one segment but not always the same segment. At $B > 0.05$ tesla secondary discharges appeared on other segments for about 0.01 second but there still was the intermittent migration of the primary discharge. At $B = 0.30$ tesla the current was distributed over four or five segments but there were times when only one carried the full current. At higher B there appeared a tendency for the migration to be confined to the upstream segments.

Anode distribution: In general the distribution was more stable. At $B = 0$ the current was carried predominantly by the trailing edge segments. At $B = 0.07$ tesla the current was entirely carried by the three trailing edge segments. At higher B there was no evidence of spreading of the arc.

These tests were run with the accelerator operating at constant currents of 50, 100, and 150 amperes and with the magnetic field varying incrementally from 0 to 0.34 tesla.

Plasma potentials. - The study of the plasma potentials at EOS (ref. III-29) was accomplished using 19 tungsten pins mounted in the side wall. From these readings the sheath and boundary layer voltage drops could be measured as well as the axial voltages. The sheath and boundary layer voltage drops have been plotted in figure III-9. The combined electrode drop for no magnetic field agreed with the 21-volt drop reported by Northrop under similar conditions. The axial potential gradients were difficult to interpret. If the space-charge field that accelerates the ions existed, then the axial potential measurements should have measured this. Instead the potential gradients were erratic. This investigation is continuing.

Concluding Remarks

The operating characteristics of the linear crossed-field accelerators have been studied for the past 5 years. From these data the thrust has been shown to be proportional to the magnetic field and the applied current as predicted by the theory. The agreement between the theoretical value and the experimental thrust is reasonably good. The magnetic field cannot be increased without limit to increase thrust since it has been shown that the efficiency reaches a maximum as the magnetic field is increased. At low power inputs it has been shown that the accelerator must operate in the unconfined mode. At high power levels either confined or unconfined operation is possible.

The disadvantages of these thrusters are that the efficiency is low, the specific impulse is marginal, and the lifetime is dubious due to the erosion of electrodes and insulators. The inefficiency of operation is primarily due to Joule heating, of the gas heat losses to the walls and electrodes, and the nonuniformity of the current distributions.

The problem area investigations have so far lead to contradictory conclusions. To reduce the fraction of heat lost to the electrodes requires high power input. This increases the erosion. Therefore, the electrodes and the walls must have improved cooling which will increase the weight. In addition to this, the arc behavior in a magnetic field is not well understood. It has been shown that the arc will assume an S-shaped curve between the anode and cathode. This is detrimental to the thrust. The attempts to straighten this curved arc have not been entirely successful.

Therefore, many problems remain unresolved. Until these problems have been answered there is no justification for any further optimization studies. The primary emphasis now is to find the solutions for the wind-tunnel accelerators where size and weight restrictions are not as severe as for a spacecraft thruster.

COAXIAL DIRECT-CURRENT ACCELERATORS

General Considerations

The dc accelerators discussed in the previous section were all of rectangular geometry, sometimes referred to as linear accelerators, and the accelerating force $\mathbf{j} \times \mathbf{B}$ was obtained directly from externally applied electric and magnetic fields analogous to the dc motor.

In coaxial geometry this is not the case. If a linear accelerator is rolled up into coaxial geometry the $\mathbf{j} \times \mathbf{B}$ force becomes rotational. The rotational force can be utilized, as in a nozzle; however, to obtain a direct axial electromagnetic force requires either an azimuthal current J_θ or an azimuthal magnetic field B_θ . The circulating current J_θ

(Hall current) cannot be applied directly, and to produce B_θ from an external coil requires a toroidal winding which is not practical. Therefore, the acceleration mechanisms in coaxial geometry are indirect and often a mixture of several different types. The advantage of coaxial geometry is that in the symmetrical arrangement it is possible to utilize magnetic containment of the plasma which reduces wall erosion; and undesirable gas discharge effects such as arc filament formation can be eliminated.

The dc coaxial accelerators can be divided into three basic types: the magnetoplasmadynamic (MPD) arc, the Hall ion accelerator, and the magnetic expansion thruster (oscillating electron ion engine). This division is based on research programs in progress, but the classification is arbitrary in the sense that the same mechanisms can operate in all of the devices. They differ physically due to the two possible arrangements of the applied magnetic field and of the electrodes with azimuthal symmetry and due to the physical change required in passing from high power and density to low power and density. For example,

(1) The MPD arc with a virtual cathode extending downstream is similar to the Hall ion accelerator.

(2) If the power and density of the magnetic expansion thruster is increased, the mode of operation changes into an MPD arc-type accelerator.

The three types of devices will be discussed separately and the experimental results will be presented.

Magnetoplasmadynamic Arc

The MPD arc is sometimes referred to as the high-impulse arc, thermoionic accelerator, magnetic annular arc, and Hall arc accelerator. Essentially all of these accelerators are the same device with the difference being that the dominant acceleration mechanism depends on the magnitude of the applied magnetic field and the applied current. The devices are arc-like in character. They operate at low voltage and high current and require no preionization. Preliminary research work has been carried on for some time, but it was only in December of 1963 that high performance was reported by A. Ducati of Giannini Scientific Corporation (ref. III-30). The MPD arc is being investigated at Avco-Everett Research Laboratory, Avco Corporation/Research and Advanced Development Division, Electro-Optical Systems Incorporated, Giannini Scientific Corporation, NASA-Langley Research Center, and NASA-Lewis Research Center.

The basic scheme of the MPD arc is shown in figure III-10. The possible accelerating mechanisms are listed as follows with the coordinates and electrode-polarity as shown in the figure:

(1) Axial force $F_z = j_r B_\theta$ where B_θ is the self-induced magnetic field of the cur-

rent j_z . The quantity j_z is a function of j_r so that the force is proportional to j_r^2 . In general the force tends to expand any current-carrying circuit, so that downstream of the accelerator, the force acts to bow out the current loop.

(2) Axial force $F_z = j_\theta B_r$. For $\omega_e \tau_e > 1$ the interaction of the applied current j_r with the axial component of the magnetic field B_z produces the azimuthal Hall current j_θ . The Hall current can also be produced by the interaction of axial current j_z with the radial component of the magnetic field B_r . The axial current arises from bowing out of the electron current forming a virtual cathode downstream of the anode.

(3) Rotational force $= j_r B_z$. Under certain conditions the plasma can rotate as a solid body. The rotational energy can be recovered and converted into axial motion in a magnetic or physical nozzle.

(4) Radial forces $j_\theta B_z$ and $j_z B_\theta$. The radial forces can be utilized for containment or for axial acceleration resulting from a pinch pressure.

(5) Aerodynamic pressure forces. Current passing through the plasma heats the gas and results in an axial thrust due to the expansion. The MPD arc is not designed to utilize this energy in a physical nozzle due to heat-transfer limitations. Expansion in a magnetic nozzle, however, might be important.

The early experimental work leading to the MPD arc came from two sources. One was an attempt to increase the specific impulse of the conventional thermal arcjet which is limited in specific impulse by the maximum gas temperature that can be tolerated. The subject was first discussed in references III-31 and III-32. In retrospect it seems obvious that if the mass flow is decreased and the current is increased, the energy addition per particle becomes quite large. The trick in passing from the thermal arcjet concept to the MPD arc was to abandon the arc nozzle with the small throat diameter and to allow the action of electromagnetic volume forces. By increasing the power and decreasing mass flow the specific impulse is only limited by the heat transfer to the electrodes, and the minimum density at which operation is possible.

The second source of the present work was the early experiments performed on rotating arcs and high-pressure Hall current acceleration phenomena (refs. III-33 to III-37). In these and related plasma research studies various acceleration mechanisms were identified and their feasibility demonstrated.

Performance. - Two configurations of MPD arcs are shown in figures III-11 and III-12. Figure III-11 is a water-cooled version (Avco/RAD) that has been operated up to 200 kilowatts with various gaseous propellants and figure III-12 is a radiation-cooled accelerator (EOS) that was designed for use with lithium at lower powers. The configurations shown are typical, however there are many minor variations in the designs to date. For example, in order to operate at very low mass flow, requires a special design to keep the gas pressure near the cathode above a critical value. At high powers, above 30 to 40 kilowatts, it has been necessary to cool the anode.

Figure III-13 shows the performance attained to date with various propellants. The efficiency is calculated from

$$\eta = \frac{T^2}{2\dot{m}P} \quad \text{and specific impulse} \quad I_{sp} = \frac{T}{\dot{m}}$$

The thrust T is the reaction force of the engine usually measured on a thrust balance, the mass flow \dot{m} and the input power P (magnet power is usually excluded). The thrust has also been determined from a large target downstream of the engine (Langley) and from the integration of local force with a small thrust plate (Avco/Everett).

The primary experimental parameter is the choice of propellant. Thus far hydrogen, ammonia, argon, helium, nitrogen, deuterium, and lithium have been tested. The highest efficiency has been obtained with lithium in a radiation-cooled accelerator. Figure III-14(a) shows the results of the lithium tests at Electro-Optical Systems (EOS) for three different model accelerators. The scatter in the data is due primarily to changing the mode of attachment of the arc to the electrodes. The input power was from 5 to 25 kilowatts. The data point for the 10-hour life test was taken with a configuration (design model LAJ-AF-6) which utilized an extended cathode. The cathode geometry is important in controlling the arc attachment point which is a factor in determining the amount of electrode and insulator erosion. For the tests at EOS the lithium propellant was fed into the accelerator as a liquid and the mass flow measured by a volume displacement method. Highest efficiency was obtained when the propellant was fed into the accelerator through the anode. Details of the lithium accelerator tests can be found in reference III-38.

A great deal of data have been taken with hydrogen covering a wide range of input power, mass flow, magnetic field strength, and as a result of this hydrogen data has served as a standard for comparing new designs and for performing diagnostic measurements. Figure III-14(b) shows data for hydrogen taken with the same accelerator over a power range of 20 to 160 kilowatts (ref. III-39) showing that the input power is not a primary variable; the efficiency is a linear function of specific impulse.

After lithium the best results have been obtained with ammonia (ref. III-39). The data for ammonia is shown on figure III-14(c) with data for other propellants. The lithium curve is the upper envelope of the data points shown in figure III-14(a). Argon, helium, and nitrogen gave poor results. None of the efficiency data include magnetic coil power.

Ammonia is an ideal propellant in many respects, however, it was found to operate at a thermal efficiency, or calorimetric efficiency of about 50 percent which requires that half the input power be dissipated as heat in the accelerator. For hydrogen the thermal efficiency is about 70 percent.

Propellants. - Figure III-14 shows the frozen-flow efficiency of various propellants as a function of specific impulse. The frozen-flow efficiency is the maximum efficiency that can be obtained if the propellant is fully ionized. There are other factors to be considered, however, such as multiple ionization and radiation losses, except for hydrogen and deuterium. For example, in tests at Langley with argon (ref. III-40) it was found that doubly and triply ionized atoms were present. These losses may prevent the use of heavier atoms. While the frozen flow efficiency increases with increasing atomic weight, the energy density in the discharge required to accelerate the atoms must be very large, since it is impossible to lower the gas density beyond a certain point and still maintain a high-current arc. As shown by experiments at Giannini (ref. III-41), if the gas density is low enough the arc will begin consuming electrode material in order to continue operation. If the ambient pressure is very low, a true vacuum arc is established that operates only from cathode material.

Increasing the energy density results in higher electron temperatures and multiple ionization and radiation losses. Lithium appears to be an ideal propellant in this respect since its second ionization potential is the highest of all elements (75 eV) while its frozen-flow efficiency is adequate for low specific impulse operation.

Another factor not considered in the frozen-flow efficiency curves is that the propellant may be only partially ionized and neutral particles accelerated through momentum transfer or charge-exchange collisions. This requires higher densities and would not be practical for heavy propellants.

The fact that deuterium gave almost the same performance as hydrogen (ref. III-41) indicates that the mechanisms are not very well understood since the ionization and recombination losses are the same for both propellants, but the molecular weight differs by a factor of 2.

Heat loss to electrodes. - One of the major losses in the accelerator is the power loss to the electrodes. The cathode loss is usually small, on the order of a few kilowatts or less but the heat transfer to the anode can be very large, at times over 50 percent of the input power. The correlation of heat-transfer data with the experimental parameters shows that anode heat transfer is predominantly dependent on current. Figure III-15 shows a correlation performance of data taken from several sources (ref. III-39). The data taken with several different geometries are in good agreement which, in itself, shows that there is not a strong dependency on geometry. The curve is for hydrogen but data taken with ammonia, helium, nitrogen, and argon show the same trend.

It is possible to explain the data of figure III-15 by assigning approximately 25-volt loss at the anode. This implies a high electron temperature or an anode sheath or a combination of both. The other possible heat-transfer mechanisms such as radiation from the cathode and from the plasma, recombination at the anode, and aerodynamic heat transfer do not appear to be a large contribution. There is a weak correlation of heat

transfer with mass flow.

Reliability-electrode erosion. - At Giannini Scientific, 50-hour life tests have been conducted at specific impulse of 3000, 6000, and 10 000 seconds using hydrogen. Table III-3 shows the experimental parameters of the tests. The electrodes were weighed after the completion of the test to determine the eroded mass.

It was found that eroded material comes primarily from the anode. As mentioned earlier, cathode erosion is more severe at low pressures. The use of an external magnetic field reduced the amount of erosion. The magnetic field prevents the arc from settling at a fixed location, due to some local asymmetry.

After sufficient experience had been accumulated in early tests it became relatively easy to design an accelerator that had negligible erosion after 50 hours. However, several unexplained failures occurred after many hours of smooth operation, which indicate that life tests will be an influence on the ultimate design of a thruster.

Thrust mechanisms. - Several attempts have been made to determine the acceleration mechanisms in MPD arcs. The information is mainly deduced from gross parameters such as thrust, current, voltage, and wall pressure. Very little work has been done on determination of local plasma properties due to the fact that local probing of a high-power discharge is not a rewarding occupation.

Earlier work at Avco/Everett (ref. III-34) and Langley Research Center (ref. III-35) showed the existence of Hall currents in coaxial geometry. It was also shown (ref. III-34) that energy could be put into gas rotation and converted to axial motion through both viscous and magnetic containment.

Recent measurements of the Hall current in an MPD arc at Langley Research Center (ref. III-40) showed that Hall currents increased with arc current but decreased slightly with increasing magnetic field. The net result would be an increase in Hall thrust with the product IB .

At EOS, Hall current thrust was demonstrated by measuring the direct reaction thrust on the magnetic field coil (ref. III-37). Figure III-16 shows the fraction of the Hall current thrust. The $j_{\theta}B_r$ force reacts directly against the magnetic field lines. On the other hand thrust due to j_rB_{θ} would physically react against the arc electrodes.

In reference III-42 (Avco/RAD) the total thrust has been analyzed and is as shown in figure III-17. The components of thrust are broken down as follows:

(1) Aerodynamic thrust $T_r \mathcal{P}_c A_t$ where \mathcal{P}_c is the measured chamber pressure and A_t the exit area.

(2) Thrust due to the arc current interacting with its self-magnetic field. The thrust is proportional to the square of the arc current and is given by $T = I^2 \left(\frac{3}{4} + \ln \frac{r_1}{r_2} \right)$. This includes the pinch force at the cathode $j_z B_{\theta}$. The existence of the cathode force was

demonstrated in one experimental model by measuring the pressure at the cathode tip.

(3) The balance of the thrust is assigned to the Hall current force $j_{\theta} B_r$.

Most of the experiments indicate that the Hall thrust varies as the product IB , being linearly dependent on I and weakly dependent on B . One exception to this is the data taken at Avco/Everett where a definite optimum was found in the magnetic field strength. The thrust data was obtained by integration of the force of a small thrust plate over the area of the beam. The thrust profile showed that for large magnetic fields, the beam was strongly pinched with resulting losses in axial thrust. Apparently, there is an effect of the magnetic field shape, that is, the relative component of B_r and B_z , but the mechanism involved requires further investigation.

Voltage-current relation. - The input power to the MPD arc is controlled by limiting the arc current; the discharge establishes its own operating voltage, which is determined by the overall arc impedance. The impedance depends on such factors as electron emission, ionization and dissociation process, electrode sheath effects and electronic conduction across a magnetic field.

The magnitude of the voltage depends mainly on the propellant used. For a given propellant the voltage increases with increasing magnetic field and with anode diameter. In reference III-43 an analysis is presented for the slope of the voltage as a function of the magnetic field curve.

The radial arc voltage is given as

$$V = V_s + E\ell$$

where V_s is the sheath drops at the electrode, E is the radial electric field to be determined, and ℓ the characteristic radial dimension. Assuming the ion drift velocity to be E/B , the ion velocity can be related to the ionization energy which gives the result

$$V = V_s \sqrt{\frac{2\mathcal{E}}{m_i}} B\ell$$

where \mathcal{E} is the energy required for ionization and dissociation. Figure III-18 shows good agreement for the theory with experimental data of voltage as a function of coil current for various propellants.

Local Diagnostics

In high power discharges, probes for obtaining local measurements must be water cooled and consequently are bulky. Spectroscopic and microwave measurements are not

precise due to the fact that the discharge is nonuniform and is not in thermal equilibrium. The problems just mentioned are discussed in reference III-44 which gives the results of an experimental study of the beam diagnostics in a thermal arcjet at McDonnell Aircraft Corporation.

At Electro-Optical Systems, the axial current distribution in the plasma downstream of the accelerator has been mapped by measuring the azimuthal magnetic field with a Hall-effect probe (ref. III-45). The probe is swung through the beam and the axial current j is obtained from

$$B_{\theta}(r, z) = \frac{\mu_0}{\mathcal{A}} \int_0^{\mathcal{A}} j_z(r, z) r \, dr$$

Figure III-19 shows a typical current distribution for a 44-kilowatt hydrogen MPD arc. Although there may be errors due to misalignment of the probe, and asymmetry of the discharge, it can be seen that the measured values of the current substantiates the visual observation that the current from the cathode (cathode jet) extends downstream and loops back to the anode tending to follow the magnetic field lines. Measurement of plasma potentials with a bare wire probe tend also to substantiate the picture.

At Avco/Everett measurements of the mass flux in the beam have been made with a probe which swallows the mass flow that it intercepts. The mass flux is calculated from the measured pressure rise in an evacuated chamber. Preliminary measurements give qualitatively reasonable results (ref. III-43). The problem is to insure that the probe does collect the mass flow corresponding to its frontal area. In continuum flow this requires that the normal shock wave be inside the collecting tube. In free molecular flow, where the mean free path is larger than the probe dimensions the length to diameter ratio of the collecting orifice must be small enough to minimize backward diffusion.

An accurate measurement of the integrated mass flow will give an answer to the question of how much of the ambient gas is recirculated.

Mass entrainment. - Several investigators have demonstrated that the MPD arc can operate entirely on the ambient gas in the vacuum facility at pressures above 10 microns. That is, it acts as a pump recirculating the propellant which can be bled in through the tank wall. This raises the question of the validity of the performance data taken to date. The measured thrust and power are correct; however, the calculated efficiency and specific impulse would be in error since the true mass flow is unknown.

The situation cannot be resolved by a simple calculation of the mass efflux into the discharge region.

$$\dot{m}_0 = n_0 m_0 u_{th} A$$

where \dot{m}_0 is the entrained mass, n_0 is the neutral density, m_0 the atomic weight, u_{th}

the thermal velocity, and A the area of the discharge since not only is the area unknown but the mechanism for interaction with the plasma beam depends on whether or not the neutrals become ionized.

The problem of determining mass entrainment is best resolved by: (1) Operation at low background pressures with condensable propellants that cannot recirculate and (2) diagnostic measurements to determine an independent mass flow or velocity of the beam.

Problems and future efforts. - Almost all of the results that have been reported in this section were obtained in the period of a year. The data has not yet been fully digested and there is not a working theory for the design of new accelerators.

At the present time the MPD arc is under intensive investigation. Most of the present effort is involved in studying new propellants (alkali metals), investigation of optimum accelerator and magnetic field configurations and in the development of low-power radiation-cooled thrusters.

Assuming that an optimum propellant and an optimum geometry for a given power level is developed, there still remain several major problems to be solved before the MPD arc becomes a competitive thruster.

- (1) Magnet design for minimum weight and power consumption
- (2) Anode cooling at power levels above 30 kilowatts
- (3) Lifetime demonstration
- (4) Operation at very low ambient pressure

One fact that should be emphasized is that the MPD arc operates from low-voltage dc power and thus it offers an alternative in planning for primary electric power and power conditioning. Most of the schemes that have been considered thus far have been concerned with high-voltage dc power for use with electrostatic thrusters.

Hall Ion Accelerator

Figure III-20 shows another type of coaxial geometry that is used. The applied electric field is axial and B is radial. For large $\omega_e \tau_e$, j_θ is induced and the force $j_\theta \times B_r$ is in the axial direction. The applied electric field force on the ions is also in this direction. Thus it is possible to consider the device as an electrostatic ion accelerator without a space-charge limitation, since the electrons in the ideal limit perform stationary orbits distributed along the axis. This arrangement is sensible because in all other plasma accelerators an electric field is believed to be induced in order to accelerate ions in the thrust direction. It is a logical evolution to apply the electric field axially. There is one major difficulty to this arrangement: any amount of axial electron current is a loss. Essentially, it is short circuiting the device. An attempt is being made to construct a gas discharge device where the current is primarily being carried by the ions -

a very difficult thing to do.

The Hall ion accelerator is being investigated at Lewis and Langley Research Centers, AVCO/Everett, EOS, United Aircraft, and Curtis Wright. All of the devices are annular in geometry in order to produce a radial magnetic field throughout the acceleration region with the electric field applied along the axis. There are some differences in the methods used to preionize the flowing gas and in the power level of operation. The Hall ion accelerators can be grouped into two categories:

(1) Low power, low density without preionization; or preionization by a Phillips-ionization-gage-type (PIG) arrangement, contact method, or radiofrequency. The low-density device is conceptionally similar to an ion engine in which space charge is avoided, and in some cases it resembles an ion engine in physical appearance. The analysis usually follows a collisionless plasma approach in which neutral particles are not accelerated.

(2) Higher power, up to 200 kilowatts, and higher density with arcjet preionization. The arcjet is required to supply the ionization energy for the high mass flows. The problems here are similar to the $j \times B$ accelerator: hot gas containment and wall erosion. Continuum MHD equations are used in the analysis.

Figure III-21 is a schematic of a typical low-density accelerator (AVCO). The gas flows through the anode where ionization is produced by the PIG-type discharge near the anode. In the acceleration region, ions are electrostatically accelerated by the axially electric field imposed between the anode and the cathode (neutralizer). The accelerating potential is the applied dc voltage minus the sheath potentials. A radial magnetic field is produced by the coil and the iron magnetic circuit, part of which protrudes into the center body.

The neutralizer is a thermionic emitting cathode, usually a directly heated tungsten filament. The ideal operation discussed in the introduction is not attained. In practice, the following losses appear:

(1) The propellant is not fully ionized. For a low-density accelerator, neutrals are not accelerated.

(2) Ionization does not occur entirely at the anode. This produces a spread of ion velocities.

(3) A plasma sheath appears at the electrodes so that the accelerating potential is not the applied potential.

(4) The electron backflow from the neutralizer to the filament is "anomalously" high. This constitutes a power loss $j_e V$. The ratio of ion current to electron current is a measure of the efficiency of the device.

Item (4) is the most serious loss. The equation for motion of electrons across the magnetic field (neglecting ion slip) is

$$j_{ez} = \frac{\sigma E_z}{1 + (\omega_e \tau_e)^2} \approx \frac{n_e e^2 E_z}{m_e (\omega_e \tau_e)^2} = \frac{m_e n_e E_z}{B^2 \tau_e}$$

If n_e and τ_e are constant, the electron current varies inversely with B^2 and can, in principle, be controlled. However, electrons find other means of reaching the anode. As of today all investigators have concluded that anomalously high diffusion does exist and is caused primarily by plasma oscillations or turbulence. The maximum ion current is found to be about one half the total current which imposes an upper limit on efficiency of 50 percent. As a result most of the experimental effort now under way is an attempt to discover the mechanism involved in the electron diffusion. The results of these studies could be of importance to all plasma accelerators.

Table III-IV gives some experimental parameters of typical Hall ion accelerator experiments. Except for the United Aircraft study, which was an attempt to evaluate the performance of a cesium accelerator, the experiments are mainly diagnostic studies using argon as the working gas. The most important of the diagnostic measurements are listed as follows:

(1) Hall currents - The circulating electron currents j_θ furnish an independent measure of the thrust density $j_\theta B_r$. Hall currents have been measured with an inductive loop which acquires an induced emf due to the collapsing magnetic field when the discharge is shut off. It was found in reference III-46 that the Hall currents go through a maximum with increasing applied magnetic field. The variation has been interpreted in terms of joule heating and ion-slip losses.

(2) Axial electric field - One way of considering the device is as a hot cathode discharge in which the applied magnetic field redistributes the applied voltage over the entire length of the discharge. However, sheath effects still exist and the true accelerating potential must be determined by measurements. This is usually done by means of a Langmuir probe or an emissive probe. It is found that the sheath voltage can be as high as 40 volts which means that the higher applied voltage will in general give better efficiency. The electric field in the plasma varies with B and B^2 in some cases. Both of these dependencies can be explained, however the magnitude of E_z for a given current j_z is too low to be explained from classical arguments, and requires the introduction of plasma oscillations or instabilities.

(3) Ion current j_{iz} - As discussed previously, it is desirable to determine the ratio of ion current to total current. The measurement of ion current is made with negatively biased Langmuir probe as described in reference III-47 or inferred from thrust target measurements. The ion current varies throughout the accelerator due to wall collisions and ionization.

(4) Plasma density and electron temperature - The determination of the plasma

properties with a Langmuir probe enables a check of the conductivity equation. Typical results are listed in table III-IV.

(5) Plasma oscillations - A great deal of study has been given to plasma oscillations which have been experimentally determined with probes and pickup loop. The frequency, location, movement, and variation of oscillation with accelerator parameters have been studied. The interest in this problem is not confined to the Hall ion accelerator, and the literature in the field is vast. For this purpose it can be said that while the mechanism for enhanced diffusion is not understood, its effect is often catastrophic and the accelerator parameters must be controlled to minimize the electron backflow.

United Aircraft cesium accelerator. - One serious attempt to design a competitive Hall ion accelerator in which the losses previously cited were minimized is an experimental study by United Aircraft (ref. III-48). The configuration is shown in figure III-22. The accelerator was originally designed to operate with surface contact ionization; however, it was found that with cesium essentially complete ionization occurs near the anode by electron bombardment. The thrust was determined by a target and an independent check on the thrust was made according to

$$T = \dot{m}u_i = \dot{m} \sqrt{\frac{2eV}{m_i}}$$

where V is the effective accelerating potential determined by measuring the plasma potential outside the cathode sheath and \dot{m} is the cesium ion flow. Figure III-23 shows the efficiency against J_{sp} curve.

At an input power of 1.3 kilowatts, the efficiency at the highest impulse 1500 seconds was 40 percent, exclusive of neutralizer and ionizer power. The limit on specific impulse was due to voltage breakdown across the accelerator. The magnetic field strength in the experiment was between 400 to 1000 gauss. Below 400 gauss it is believed that streaming instability caused the large increase in electron backflow. Above this critical value the ion current was about half of the total discharge current.

The results of this study show that, even accepting the anomalous diffusion loss the Hall ion accelerator might be competitive in the specific impulse range of 1500 to 2500 seconds. However, all the data appear to limit the efficiency to less than 50 percent.

High-pressure Hall ion accelerator. - For this device, collisions are important and the analysis proceeds with the continuum magnetohydrodynamics (MHD) equations using a generalized Ohm's law under nonequilibrium conditions. Like the linear crossed-field accelerator, high-density Hall accelerators must operate at high power density in order to accelerate the flow. The currents required are appropriate to arc-type technology. In coaxial geometry preionization requires a complicated arrangement. Figure III-24 shows the configuration that has been studied at EOS (ref. III-37). Five arcjets are

equally spaced around the annulus to preionize the gas as it enters the accelerator region. A radial magnetic field is provided with an iron-core center body. The main discharge is from the tungsten tip cathode to the anode plate. Along the annulus, coaxial cylindrical segments are spaced to measure heat flux and axial potential gradient.

For this experiment, at input power up to 100 kilowatts, a velocity increment of about 3 or 4 was achieved. However, the specific impulse was low (300 sec) and while calorimetric efficiency was up to 30 percent, overall thrust efficiency was only a few percent. To reach good impulses and efficiencies, more power must be put into the gas to raise the temperature and percent ionization. Because losses to the wall of momentum and heat flux dominate the situation in a long accelerator, work on the high-pressure Hall accelerator has been discontinued in favor of the short MPD arc discussed previously. As the accelerator length is shortened, the two devices become physically similar.

Magnetic Expansion Thrustor or Oscillating Electron Ion Engine

The final dc accelerator to be discussed is the oscillating electron ion engine or dc magnetic expansion thrustor which consists of low-density hot cathode coaxial discharge in an axial magnetic field. Electrons emitted from the cathode receive almost the full anode voltage at the cathode sheath. The energetic electrons are utilized to ionize the gas and to accelerate the ions through means of an electric field set up in the plasma along the axis of the device. An electric field must be established in order to satisfy the condition that no net current can flow from the device. Microscopically the electrons can be viewed as oscillating in a potential well until they are collected at the anode.

The term "magnetic expansion" refers to an alternative macroscopic description of the acceleration process. If energy is added to the electrons in a nonequilibrium plasma immersed in a magnetic nozzle, the electron energy is converted into directed ion energy through expansion of the electron gas. From this point of view, the energy addition can be by means of radiofrequency, microwave, or, as in the present case, dc power. In this model it is assumed that the electrons attain a temperature that must satisfy a power balance between the input power and the various power-consumption processes. The accelerating potential is the difference between plasma potential and a floating potential necessary to achieve equal ion and electron exit rates. This potential difference might be expected to be on the order of five times the electron kinetic temperature.

These devices are geometrically similar to the MPD arc; therefore, it is possible that Hall current acceleration is also present to complicate matters further. Experimental work is being conducted at United Aircraft Corporation and Lewis Research Center.

United Aircraft Corporation has made experimental studies of the effect on overall engine performance of electrode geometry, shape and strength of the magnetic field and power level with nitrogen, argon, neon, and krypton. The details of this work are reported in reference III-54. The best results were obtained with argon at an anode potential of 150 volts. The maximum efficiency was 33 percent at a specific impulse of 2700. The efficiency η is

$$\eta = \frac{T^2}{2\dot{m}P}$$

where T is the measured thrust in the propellant flow, and P the power input exclusive of cathode heating power and magnetic coil power. Several cathode configurations were also studied (ref. III-54) in an attempt to increase cathode life. The longest cathode life quoted was 30 hours. At higher voltages, about 200 volts, the discharge undergoes transitions to the arc mode which gives poor results. In general, thrust increases with anode current, but a critical value of anode current cannot be exceeded. The optimum magnetic-field shape was one in which the magnetic field lines followed the contour of the anode surface. In general, a strong mirror geometry gave the best results. Typically, the magnetic field strength is about 500 gauss, but an optimum magnetic field strength usually exists depending on engine geometry and operating parameters.

Because there exists an optimum size thruster a seven-module array of thrusters was operated to produce higher thrust. There appeared to be no interaction effect or instability in the operation.

Analytical studies have not predicted accelerator performance but an iterative machine solution was computed for the plasma potential gradient taking into account beam current neutrality, local charge neutrality, production of charged particles, and diffusion of electrons to the anode. The solution agreed with the measured potential gradient for a particular case, but the method becomes too complex to take into account changes in some experimental parameters such as magnetic-field distribution. Also the effect of plasma oscillations, which are usually present, is not known.

A similar device (dc magnetic expansion thruster) is being investigated at Lewis Research Center with the main emphasis on the operation at lower anode voltages in order to prolong cathode life. At lower voltages, the efficiency is lower but there is some hope that if reliability can be increased, the device may have application as a satellite attitude-control thruster operating directly from solar cells. Where the solar-cell weight is not the dominant weight in the system, lower efficiency accelerators can still compete on the basis of lower system weight and higher system reliability.

A significant fact discovered in the tests at Lewis Research Center was the dependence of engine performance on the background pressure of the environmental test chamber. With a thruster configuration similar to that shown in figure III-25 the thrust measure was 60 percent of the thrust measured at an ambient pressure of 2.5×10^{-4} torr. This reduced the measured efficiency using argon propellant from 14.2 percent at 1375 seconds to 4.8 percent at 800 seconds (ref. III-55).

The exact mechanism of thrust loss is still to be determined, but it is obvious that plasma accelerators must be checked in a low-pressure environment. Since the engine design was optimized for higher ambient pressure operation it is probable that better results can be obtained at low pressures.

Ammonia was also used as a propellant and a performance map is shown in figure III-26. Figure III-27 shows the setup of the test apparatus. Although the efficiency with ammonia is lower, ammonia is competitive with argon because of lower tankage weight.

The outstanding problem to be solved for the successful operation of the thruster is the development of a reliable cathode for long duration operation.

CONCLUSIONS

The coaxial dc accelerators have shown progress in recent years operating over a wide range thrust and specific impulse. In coaxial geometry several different accelerating modes are feasible.

The MPD arcs have demonstrated high impulse for the first time in a dc device. The best performance has been with lithium and ammonia. Efficiencies greater than 50 percent have been achieved from 3500 to 10 000 seconds. Work is now in progress at Avco, EOS, Giannini Scientific Corporation, Langley Research Center, and Lewis Research Center.

The Hall ion accelerators are in a research state at the present time. To achieve efficient operation electron diffusion must be controlled. Efficiencies of 40 percent at 1500 seconds were achieved using cesium. Considerable effort is underway to understand the diffusion mechanism.

The magnetic expansion thruster shows promise for specific mission applications if long-life cathodes can be obtained for thrusters with adequate efficiency.

REFERENCES

- III-1. Cowling, T. G.: Magnetohydrodynamics. Intersci. Publ., Inc., 1957.
- III-2. Asam, A. R.; and Sunderland, R. J.: Magnetogasdynamic Rocket for Space Propulsion. Marquardt Corp. (NASA CR-54040), 1964.
- III-3. Hurwitz, H., Jr.; Sutton, G. W.; and Tamor, S.: Electron Heating in Magnetohydrodynamic Power Generators. ARS J., vol. 32, no. 8, Aug. 1962, pp. 1237-1243.
- III-4. Demetriades, Sterge T.; and Ziemer, Richard W.: Energy Transfer to Plasmas by Continuous Lorentz Forces. Magnetohydrodynamics, A. B. Cambel, T. P. Anderson, and M. M. Slawsky, eds., Northwestern Univ. Press, 1962, pp. 185-205.
- III-5. Wood, George P.; and Carter, Arlen F.: Considerations in the Design of Steady D.C. Plasma Accelerator. Preprint No. 903-59, ARS, 1959.
- III-6. Resler, E. L., Jr.; and Sears, W. R.: The Prospects for Magneto-Aerodynamics. J. Aero. Sci., vol. 25, no. 4, April 1958, pp. 235-245.
- III-7. Sears, W. R.: Magnetohydrodynamics in Aeronautics. Preprint No. 709-58, ARS, 1958.
- III-8. Oates, Gordon C.; Richmond, J. Kenneth; Aoki, Yoshio; and Grohs, Gerhard: Loss Mechanisms of a Low Temperature Plasma Accelerator. Magnetohydrodynamics, A. B. Cambel, T. P. Anderson, and M. M. Slawsky, eds., Northwestern Univ. Press, 1962, pp. 207-230.
- III-9. Ring, Leon E.: Optimization of MHD Crossed-Field Accelerators and Generators. Paper Presented at Fifth Symposium on the Eng. Aspects of Magnetohydrodynamics, M. I. T., Apr. 1-2, 1964.
- III-10. Sherman, A.; and Sutton, G. W.: The Combined Effect of Tensor Conductivity and Viscosity on an MHD Generator with Segmented Electrodes. Magnetohydrodynamics, A. B. Cambel, T. P. Anderson, and M. M. Slawsky, eds., Northwestern Univ. Press, 1962, pp. 173-183.
- III-11. Podolsky, Boris; and Sherman, A.: Influence of Tensor Conductivity on End Currents in Crossed Field MHD Channel with Skewed Electrodes. J. Appl. Phys., vol. 33, no. 4, Apr. 1962, pp. 1414-1418.
- III-12. Sutton, George W.: End Losses in Magnetohydrodynamics Channels with Tensor Electrical Conductivity and Segmented Electrodes. J. Appl. Phys., vol. 34, no. 2, Feb. 1963, pp. 396-403.

- III-13. Baker, J. M. : Feasibility Study of a Continuous Flow Magnetogasdynamic Rocket for Space Propulsion. NASA CR-56263, 1962. Blackman, V. H. ; and Sunderland, R. J. : The Experimental Performance of a Crossed-Field Plasma Accelerator. Preprint No. 2633-62, ARS, 1962.
- III-14. John, R. R. ; Bennett, S. ; Chen, M. ; and Connors, J. F. : Arc Jet Engine Performance Experiment and Theory, V. Paper Presented at Seventeenth Space Flight Exposition, ARS, Los Angeles (Calif), Nov. 13-18, 1962.
- III-15. Burkhard, K. ; Devine, R. ; Hogan W. ; and Kessler, R. : A Continuous Cross-Field Gas Heater for Re-Entry Simulation. Paper No. 63-203, AIAA, 1963.
- III-16. Cann, G. L. ; Marlotte, G. L. ; and Ziemer, R. W. : A Steady-State Hall Current Accelerator. Final Rep. No. EOS-3160, Electro-Optical Systems, Inc. (NASA CR-52499), 1963.
- III-17. Dix, D. M. : A Survey of Some Plasma Acceleration Devices for Space Propulsion Applications. Rept. No. TDR-169(3713-01)TR-1; SSD-TDR-63-120, Aerospace Corp. , May 17, 1963.
- III-18. Demetriades, S. T. : Experimental Magnetogasdynamic Engine for Argon, Nitrogen and Air. Eng. Aspects of Magnetohydrodynamics, C. Mannal and N. Mather, eds. , Columbia Univ. Press, 1962, pp. 19-44.
- III-19. Ragusa, Domenico; and Baker, Jerome: Experimental Results with a Direct Current Electromagnetic Plasma Accelerator. Eng. Aspects of Magnetohydrodynamics, C. Mannal and N. Mather, eds. , Columbia Univ. Press, 1962, pp. 56-63.
- III-20. Carter, Arlen F. ; Wood, George P. ; Savol, Alexander P. ; and Weinstein, Richard H. : Experiments in Steady-State High-Density Plasma Acceleration. Eng. Aspects of Magnetohydrodynamics, C. Mannal and N. Mather, eds. , Columbia Univ. Press, 1962, pp. 45-54.
- III-21. John, R. R. : Thirty-Kilowatt Plasma Jet Rocket-Engine Second Year Development Program. NASA CR-508 49, 1964.
- III-22. Lenn, P. D. ; Bodoia, J. R. ; Ward, D. L. ; Hamilton, G. L. ; and Demetriades, S. T. : Experimental and Analytical Investigation of Crossed-Field Plasma Accelerators. Tech Rept. No. ASD-TDR-63-307, pt. I, (NSL 62-113-10), Aeronautical Systems Div. , May 1963.
- III-23. Kontaratos, A. N. : Experimental Study of Magnetohydrodynamic Duct (JxB) Type Propellant Properties. Rept. No. NSL 62-149-8, Northrop Corp. , Mar. 1963.

- III-24. Russell, G. R. ; Byron, S. ; and Bortz, P. I. : Performance and Analysis of a Crossed-Field Accelerator. Paper No. 63-005, AIAA, 1963.
- III-25. Wood, G. P. ; Carter, A. F. ; Sabol, A. P. ; McFarland, D. R. ; and Weaver, W. R. : Research on Linear Crossed-Field Steady-Flow D. C. Plasma Accelerators at Langley Research Center, NASA. Arc Heaters and MHD Accelerators for Aerodynamic Purposes, pt. 1, AGARDograph-84, 1964, pp. 1-45.
- III-26. Windmueller, A. K. ; and Rittenhouse, L. E. : Status Report on the Design and Test Experience of a Pilot MHD Accelerator for Wind Tunnel Application. Proc. Fifth Symposium on Eng. Aspects of Magnetohydrodynamics, M. I. T. , Apr. 1-2, 1964, pp. 221-222.
- III-27. Brumfield, R. C. ; Demetriades, S. ; Lenn, P. D. ; Ward, D. L. ; and Bedjai, G. : Design and Performance Study on a 500 Kilowatt Linear Crossed-Field Air-Plasma Accelerator for a Re-entry Simulation Facility. Rep. No. MHD-648, MHD Research, Inc. (NASA CR-58543), 1964.
- III-28. Podolsky, Boris ; and Sherman, A. : Influence of Tensor Conductivity on End Currents in Crossed-Field MHD Channels with Skewed Electrodes. J. Appl. Phys. , vol. 33, no. 4, Apr. 1962, pp. 1414-1418.
- III-29. Denison, M. R. ; and Ziemer, R. W. : Investigation of the Phenomena in Crossed-Field Plasma Accelerators. Proc. Fifth Physico-Chemical Diagnostics of Plasmas ; AIAA and Northwestern Univ. , Gas Dynamics Lab. , Biennial Gas Dynamics Symposium, Northwestern Univ. Press, 1964, pp. 201-232.
- III-30. Staff of Special Projects Group: High Specific Impulse Thermo-Ionic Acceleration. Rept. No. PRE-114-a, Giannini Sci. Corp. , Dec. 1963.
- III-31. Hess, Robert V. : Experiment and Theory for Continuous Steady Acceleration of Low Density Plasmas. Vol. I of Proc. XI Int. Astronaut. Cong. , Carl W. P. Reuterswärd, ed. , Springer-Verlag (Vienna), 1961, pp. 404-411.
- III-32. Maecker, H. : Plasmastromungen in Lichtbögen infolge eigenmagnetischer Kompression. Z. Physik, bd. 141, 1955, pp. 198-216.
- III-33. Powers, William E. ; and Patrick, Richard M. : Magnetic Annular Arc. Phys. Fluids, vol. 5, no. 10, Oct. 1962, pp. 1196-1206.
- III-34. Patrick, R. M. ; and Powers, W. E. : Plasma Flow in a Magnetic Annular Arc Nozzle. Advanced Propulsion Concepts. Vol. 1. Gordon and Breach Sci. Pub. , Inc. , 1963, pp. 115-134 ; Discussion ; pp. 135-136.

- III-35. Hess, R. V. ; Burlock, J. ; Sevier, J. R. ; and Brockman, P. : Theory and Experiments for the Role of Space-Charge in Plasma Acceleration. Proc. Symposium on Electromagnetics and Fluid Dynamics of Gaseous Plasma, Polytech. Press of Polytech. Inst. of Brooklyn, 1962, pp. 269-305.
- III-36. Hess, Robert W. : Fundamentals of Plasma Interaction with Electric and Magnetic Fields. NASA-University Conference on the Science and Technology of Space Exploration, Vol. 2, NASA SP-11, 1962, pp. 313-336. (Also available as NASA SP-25.)
- III-37. Cann, G. L. : Annular Magnetic Hall Current Accelerator. Paper No. 64-670, 1964.
- III-38. Moore, R. A. ; Cann, G. L. ; and Gallagher, L. R. : High Specific Impulse Thermal Arcjet Thrustor Technology. Electro-Optical Systems, Inc., June 1965.
- III-39. John, R. R. ; Bennett, S. ; and Connors, J. F. : Arcjet Technology Research and Development. Second Quarterly Prog. Rept. No. RAD-SR-65-5, Avco Corp., Dec. 1964.
- III-40. Grossman, William ; Hess, Robert V. ; Hassan, H. A. ; and Oertel, G. : Experiments with a Co-Axial Hall Current Plasma Accelerator. Paper No. 64-700, AIAA, 1964.
- III-41. Ducati, A. C. : Recent Progress in High Specific Impulse Thermo-Ionic Acceleration. Paper No. 65-96, AIAA, 1965.
- III-42. John, Richard R. ; Bennett, Stewart ; and Connors, John F. : Experimental Performance of a High Specific Impulse Arc Jet Engine. Paper No. 64-669, AIAA, 1964.
- III-43. Patrick, R. M. ; and Schneiderman, A. M. : Performance Characteristics of a Magnetic Annular Arc. Paper Presented at Sixth Symposium on Eng. Aspects of Magnetohydrodynamics, Pittsburgh, Penn., Apr. 21-22, 1965.
- III-44. Checkley, R. J. ; Esker, D. W. ; McVey, F. D. ; Merrifield, S. E. ; Murch, C. K. ; Painter, J. H. ; Scognamiglio, V. S. ; and Van Camp, W. M. : Analysis of an Arc-Jet Exhaust. Rep. No. A984, McDonnell Aircraft Corp. (NASA CR-54102), 1964.
- III-45. Cann, G. L. ; Lenn, P. D. ; and Harder, R. L. : Hall Current Accelerator. Third Quarterly Prog. Rept., Electro-Optical Systems, Inc., Mar. 1965.
- III-46. Brockman, Philip ; Hess, Robert V. ; and Weinstein, Richard : Measurements and Theoretical Interpretation of Hall Currents for Steady Axial Discharges in Radial Magnetic Fields. Paper No. 63-382, AIAA, 1963.

- III-47. Janes, G. S. ; and Dotson, J. : Experimental Studies of Oscillations and Accompanying Anomalous Electron Diffusion Occurring in D. C. Low Density Hall Type Crossed-Field Plasma Accelerators. Proc. Fifth Symposium on Eng. Aspects of Magnetohydrodynamics, M. I. T. , Apr. 1-2, 1964, pp. 135-148.
- III-48. Brown, Clyde O. ; and Pinsley, Edward A. : Further Experimental Investigations of a Cesium Hall-Current Accelerator. Paper No. 46-697, AIAA, 1964.
- III-49. Chubb, D. L. : Hall Current Ion Accelerator. Paper Presented at Fourth Symposium on Eng. Aspects of Magnetohydrodynamics, Univ. Calif. , Apr. 10-11, 1963.
- III-50. Ellis, Macon C. , Jr. : Survey of Plasma Accelerator Research. NASA University Conference on the Science and Technology of Space Exploration, Vol. 2, NASA SP-11, 1962, pp. 361-381. (Also available as NASA SP-25.)
- III-51. Brandmaier, H. E. ; Durand, J. L. ; Gourdine, M. C. ; and Rubel, A. : An Investigation of Hall Propulsor Characteristics. AIAA J. , vol. 2, no. 4, Apr. 1964, pp. 674-681.
- III-52. Lary, E. C. : Ion Acceleration in a Space-Charge Neutral Plasma. Rept. No. UAR-A125, United Aircraft Corp. , June 21, 1962.
- III-53. Siekel, G. R. ; and Reshotko, E. : Hall Current Ion Accelerator. Bull. Am. Phys. Soc. , ser. II, vol. 7, no. 6, June 19, 1962, p. 414.
- III-54. Pinsley, Edward A. ; Walch, Allen P. ; Banas, Conrad M. ; Davis, Jack W. ; and Churchill, Thomas L. : Applied Research on the Oscillating-Electron Ion Engine. ASD-TDR-63-253, United Aircraft Corp. , Apr. 1963.
- III-55. Seikel, George R. ; Bowditch, David N. ; and Domitz, Stanley: Application of Magnetic-Expansion Plasma Thrusters to Satellite Station Keeping and Attitude Control Missions. Paper No. 64-677, AIAA, 1964.
- III-56. Meyerand, R. G. , Jr. : Momentum Transfer Through the Electric Fields. Advanced Propulsion Concepts. Vol. 1. Gordon and Breach Sci. , Pub. , Inc. , 1963, pp. 177-190; Discussion, pp. 191-197.
- III-57. Davis, J. W. ; Angelbeck, A. W. ; and Pinsley, E. A. : Plasma Behavior in an Oscillating-Electron Ion Engine. Paper No. 63003-63, AIAA, 1963.

TABLE III-I. - HIGH SPECIFIC IMPULSE

TESTS (AVCO/RAD)

[Hydrogen flow rate, 0.10 g/sec; arcjet power, 30 kW; magnetic field strength, 0.25 T.]

| Accelerator voltage, V | Accelerator current, A | Total specific impulse, I_{sp} sec |
|------------------------|------------------------|--------------------------------------|
| 0 | 0 | 950 |
| 175 | 200 | 1550 |
| 190 | 375 | 1950 |
| 0 | 0 | 892 |
| 155 | 200 | 1480 |
| 180 | 400 | 2120 |

TABLE III-II. - PERFORMANCE OF ACCELERATOR

USING TWO PAIRS OF STAGGERED ELECTRODES

(MARQUARDT-MHD RESEARCH)

[Argon flow rate, 0.25 g/sec; plasma jet voltage, 18 V; plasma jet current, 300 A; plasma jet power, 5.4 kW; upstream electrode current, 100 A; downstream electrode current, 90 A.]

| Magnetic intensity, B, T | Thrust ratio | Total electrode power, kW | Total power, kW |
|--------------------------|--------------|---------------------------|-----------------|
| 0 | 1.0 | 7.0 | 12.4 |
| .0275 | 1.5 | 9.2 | 14.6 |
| .0430 | 2.8 | 13.6 | 19.0 |
| .0875 | 4.5 | 18.0 | 23.4 |
| .1143 | 6.0 | 22.0 | 27.4 |

TABLE III-III. - AVERAGED VALUES OF MPD ARC
 THRUSTOR PERFORMANCE DATA FOR THREE
 50-HOUR ENDURANCE TESTS (GIANNINI
 SCIENTIFIC CORPORATION)

[Model A-1-2-H (water-cooled); propellant,
 hydrogen.]

| Performance | Specific impulse, I_{sp} , sec | | |
|--------------------------------|-------------------------------------|-------|--------|
| | 3000 | 6000 | 10 000 |
| Propellant flow rate, g/sec | 0.025 | 0.025 | 0.0135 |
| Electrical input power, kW | 82.3 | 126.8 | 162 |
| Arc voltage, V | 39.0 | 57.9 | 72 |
| Arc current, A | 2109 | 2115 | 2260 |
| Thrust (measured), g | 78.3 | 147.6 | 137 |
| Thrustor efficiencies, percent | | | |
| Overall (electric/kinetic) | 14.4 | 34.1 | 40 |
| Thermal (electric/gas) | 49.7 | 63.7 | 57 |
| Thrust (gas/kinetic) | 28.9 | 54.6 | 72 |
| Arc chamber pressure, mm Hg | 34.1 | 25.7 | 14 |
| Test chamber pressure, mm Hg | 0.05 | 0.6 | ----- |
| Total electrode erosion, g | 25.22 | 0.04 | 2.24 |

TABLE III-IV. - OUTLINE OF EXPERIMENTAL WORK WITH
HALL ION ACCELERATORS

| Parameter | Facility | | | | |
|--------------------------------|-----------------------|----------------------------|---------------------------|----------------------------------|-----------------|
| | Lewis Research Center | Langley Research Center | Avco/Everett | United Aircraft Corporation | Curtiss Wright |
| Propellant | Argon | Argon | Argon | Cesium | Argon |
| Preionization | Electron bombardment | None | Electron bombardment | Contact and electron bombardment | Radio-frequency |
| Pressure, μ | 4 | 16 to 40 | --- | --- | --- |
| Maximum current, A | 1 | 40 | 24 | 10 | --- |
| Maximum voltage, V | 300 | 500 | 400 | 160 | |
| Maximum magnetic field, G | 200 | 500 | 500 | 1000 | 10 000 |
| Maximum electric field, V/cm | 10 | 25 | --- | 50 | |
| Electron density, μ /cu cm | | | 10^{10} to 10^{11} | | |
| Electron temperature, V | | | 10 to 30 | | |
| Accelerator length, cm | 10 | 23 | 13 | 2.5 | 0.63 |
| Reference | 49 | 46 | 47 | 48 | 51 |
| Other measurements | | Hall current instabilities | Ion current instabilities | Thrust | |

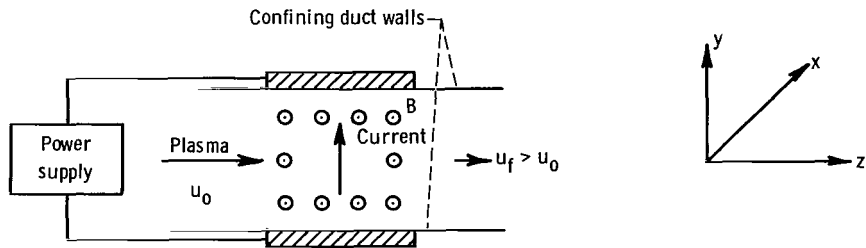
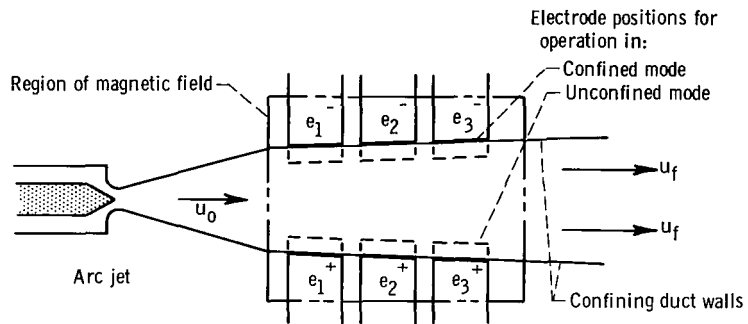


Figure III-1. - Schematic diagram of ideal accelerator.



CD-8181

Figure III-2. - Schematic of crossed-field accelerator combination.

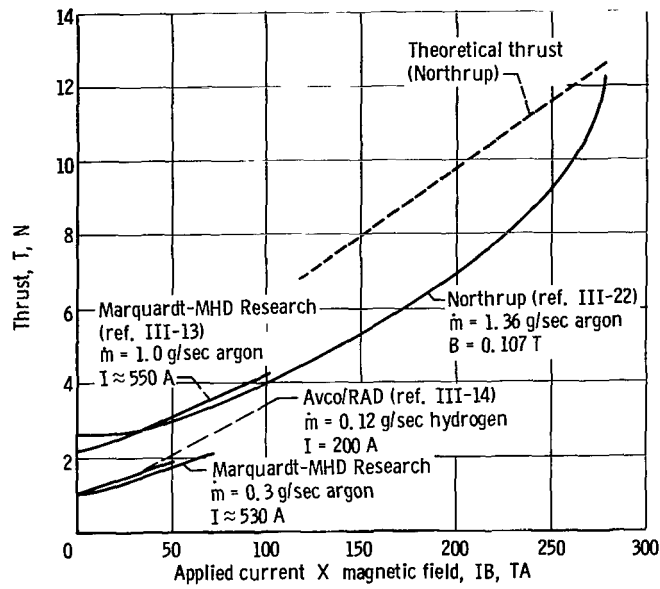


Figure III-3. - Thrust as function of product of applied current and magnetic field.

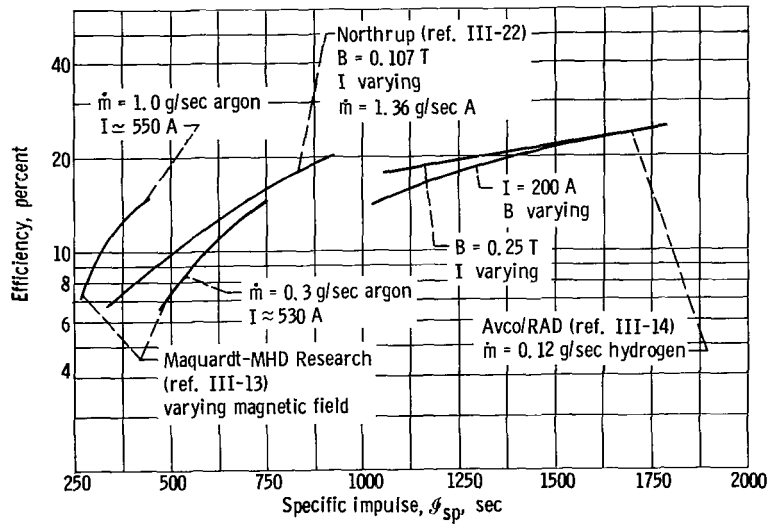


Figure III-4. - Efficiency as function of specific impulse.

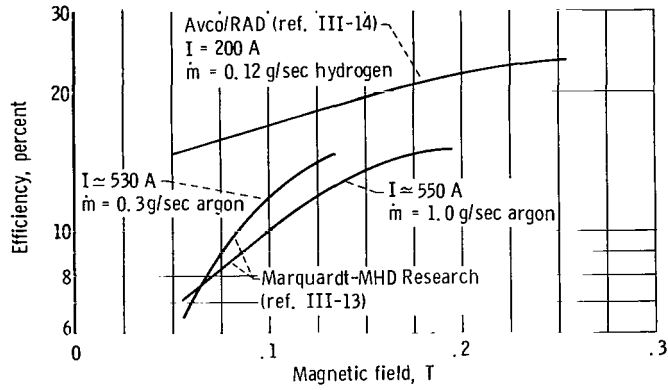


Figure III-5. - Efficiency as function of magnetic field at constant current.

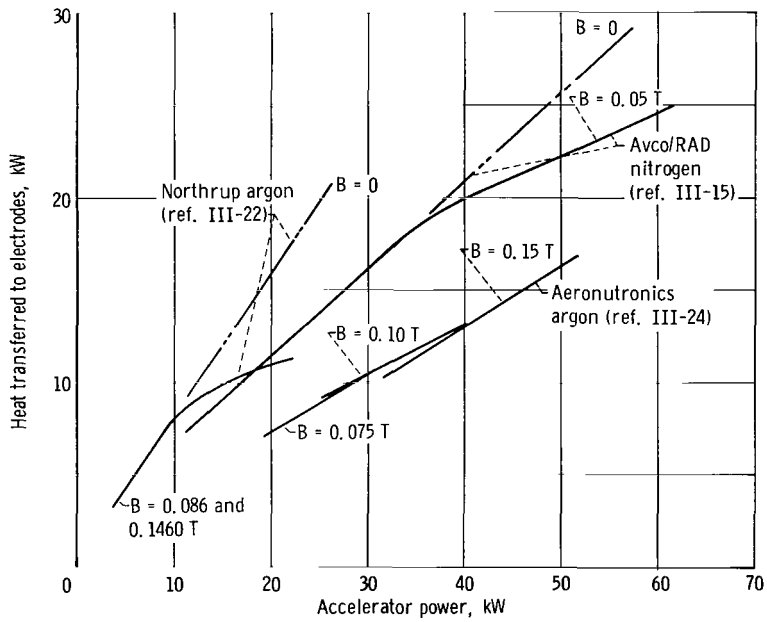


Figure III-6. - Heat transfer to electrodes as function of applied power with constant magnetic field.

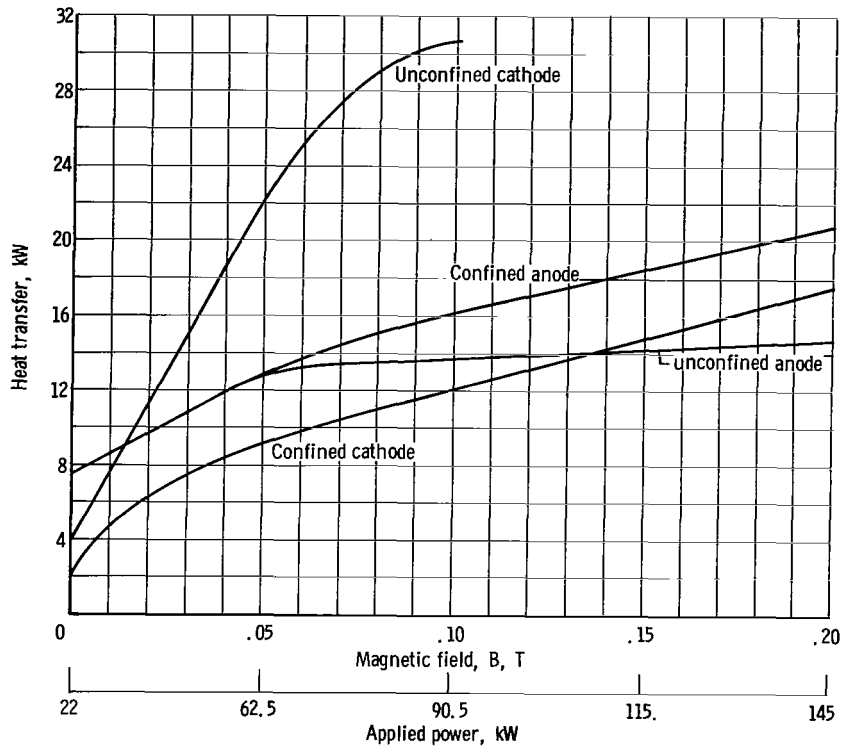


Figure III-7. - Electrode heat transfer for confined and unconfined operation. Propellant, nitrogen; current, 500 amperes (Avco/RAD, ref. III-15).

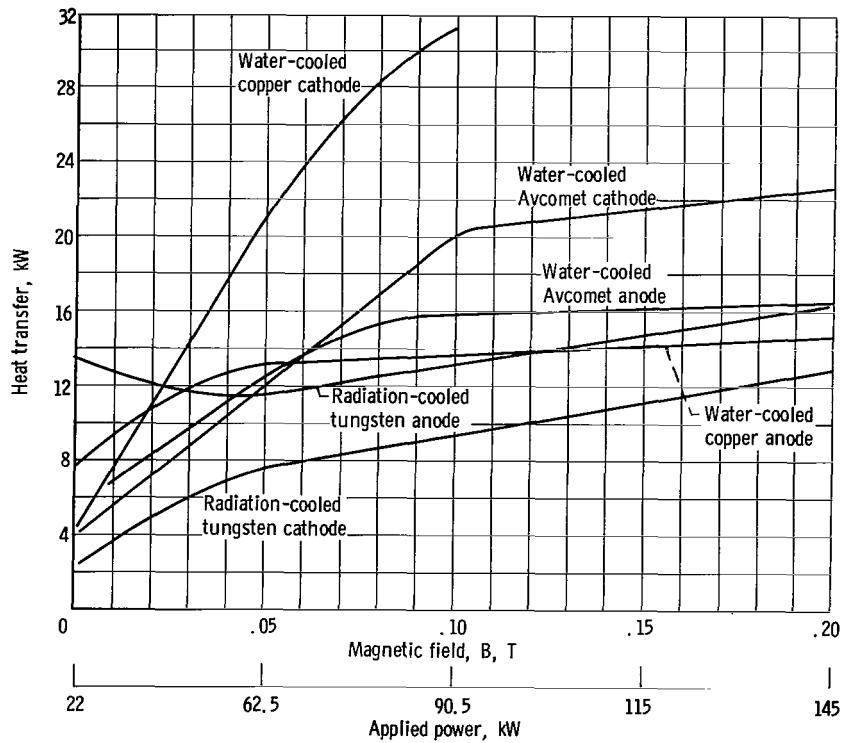


Figure III-8. - Effect of electrode material on heat losses. Propellant, nitrogen; current, 500 amperes (Avco/RAD, ref. III-15).

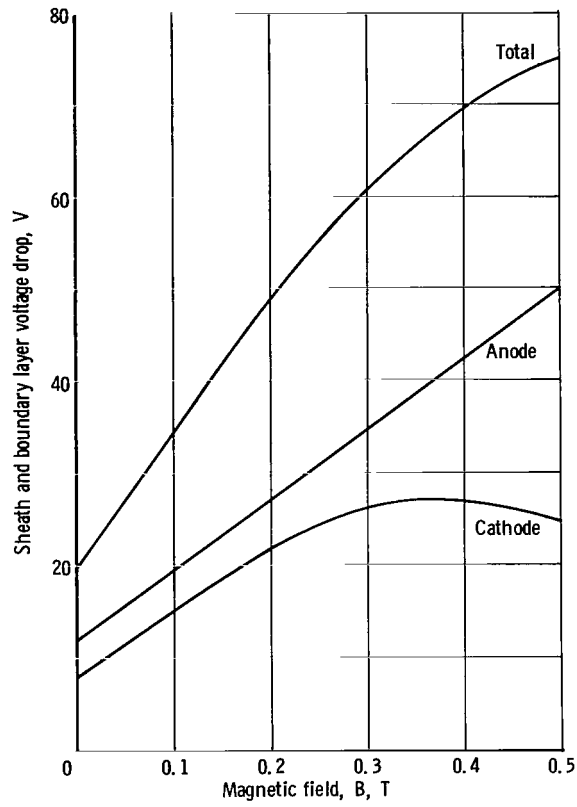


Figure III-9. - Sheath and boundary layer voltage drops as function of magnetic field. Propellant, argon; mass flow, 0.325 gram per second (EOS, ref. III-29).

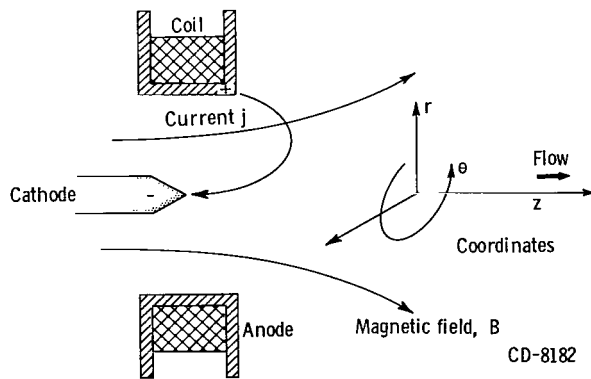
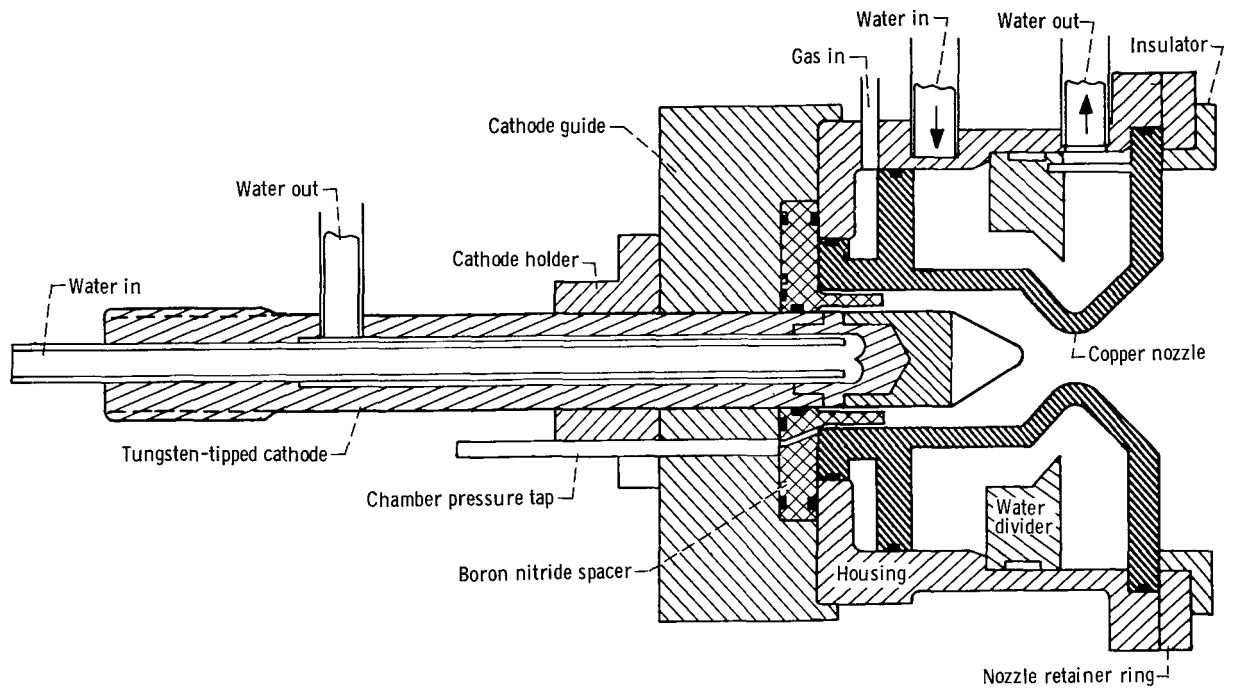
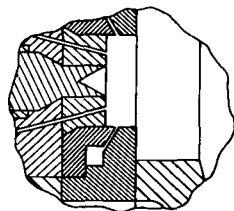
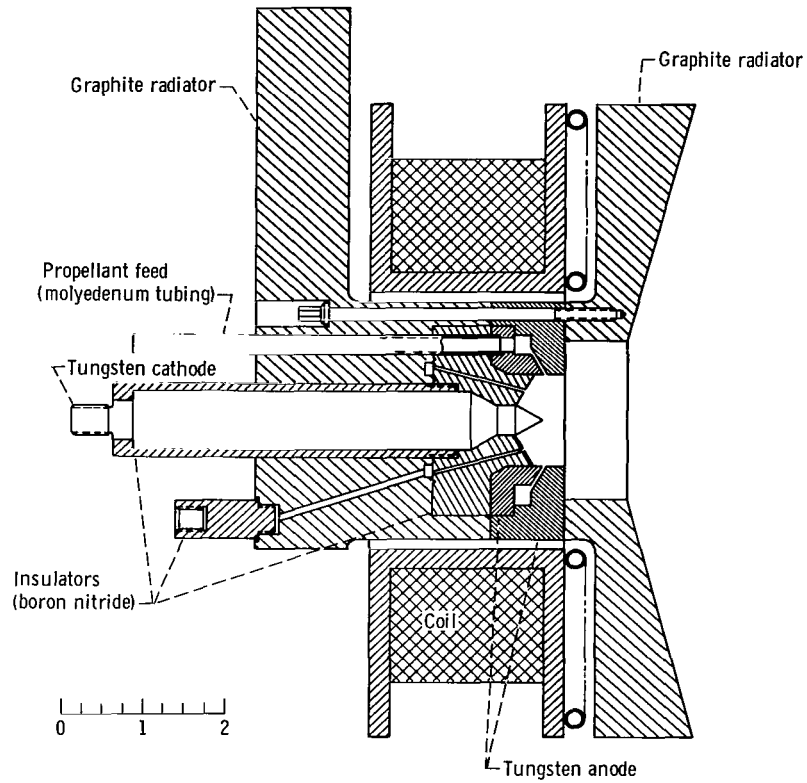


Figure III-10. - Magnetoplasmadynamic arc schematic.

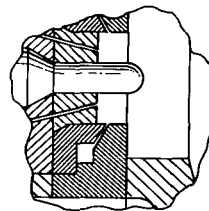


CD-64-9082

Figure III-11. - Magnetoplasmadynamic arc (AVCO/RAD).

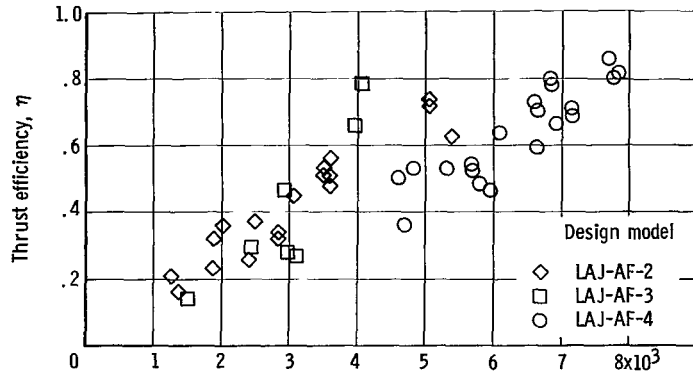


Model LAJ-AF-3
(Identical to model
LAJ-AF-2 except
as indicated.)

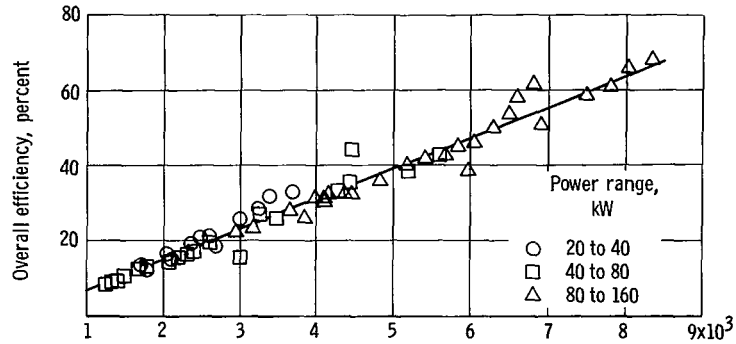


Model LAJ-AF-4
(Identical to model^s
LAJ-AF-3 except
as indicated.)

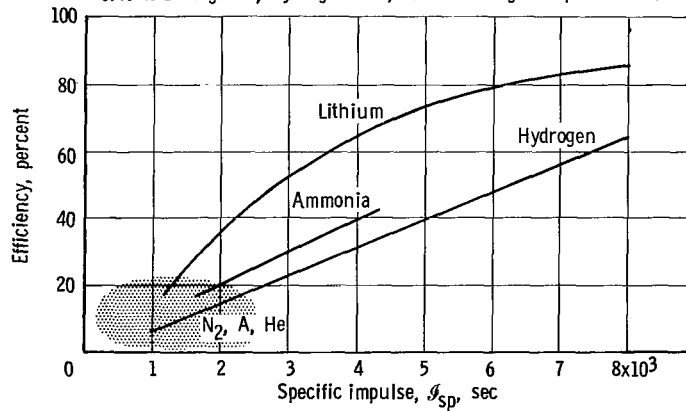
Figure III-12. - Magnetoplasmadynamic arc for alkali metals (EOS).



(a) Thrust efficiency as function of specific impulse (EOS). Lithium propellant; mass flow 0.005 to 0.02 grams per second; power 5 to 25 kilowatts.



(b) Efficiency as function of specific impulse for hydrogen (Avco/RAD). Arc current, 300 to 1600 amperes; arc voltage, 55 to 105 volts; applied field, 0.75 to 2 kilogauss; hydrogen flow, 0.02 to 0.05 grams per second.



(c) Magnetoplasmadynamic arc efficiency as a function of specific impulse for various propellants.

Figure III-13. - Performance data for several propellants.

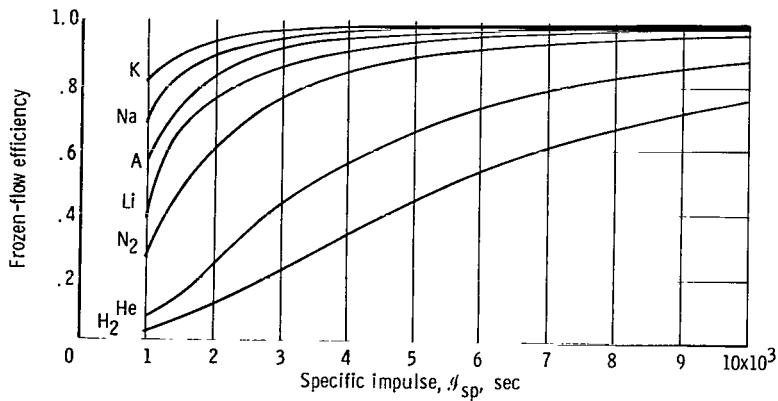


Figure III-14. - Frozen-flow efficiency as function of specific impulse for various propellants (singly ionized, fully dissociated).

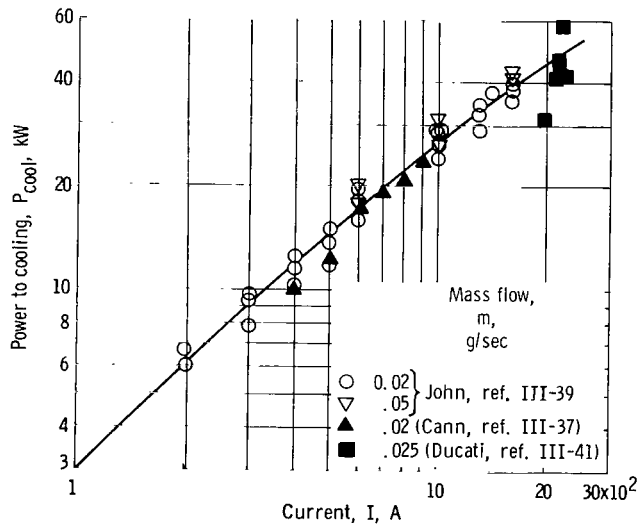


Figure III-15. - Power to cooling as function of current for hydrogen propellant. Mass flow, 0.02 and 0.05 gram per second; magnetic flux density, 500 to 2000 gauss.

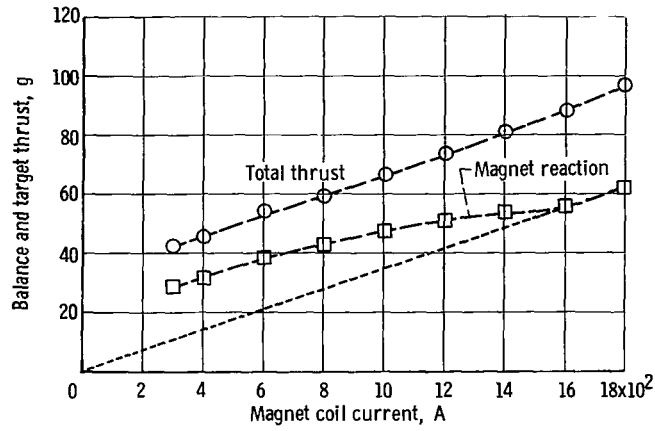


Figure III-16. - Balance and target thrust as function of magnet coil current. Propellant, hydrogen; current, 800 amperes; mass flow, 0.02 gram per second.

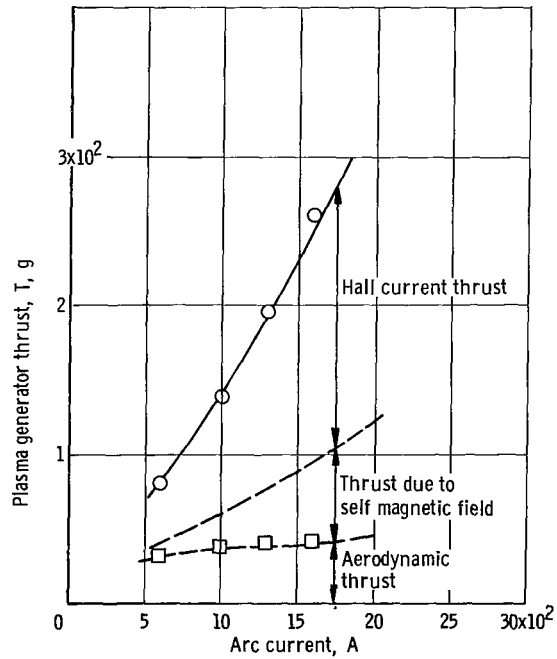


Figure III-17. - MPD arc thrust as function of arc current (hydrogen). Hydrogen flow rate, 0.03 gram per second; coil current, 1155 amperes (maximum axial magnetic-field density about 2000 gauss); arc voltage, 80 to 95 volts.

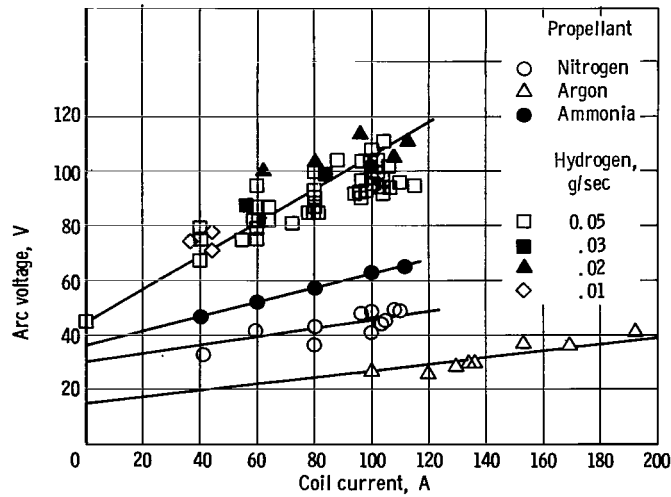


Figure III-18. - Characteristics of MPD arc operating with several propellants and various mass flows.

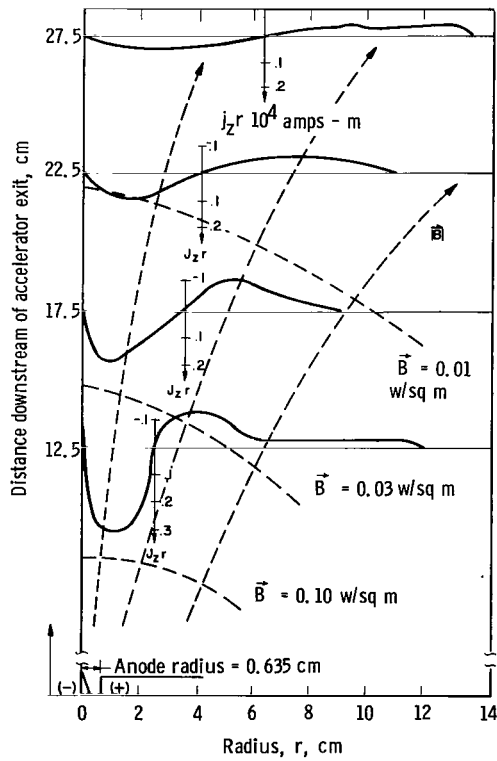
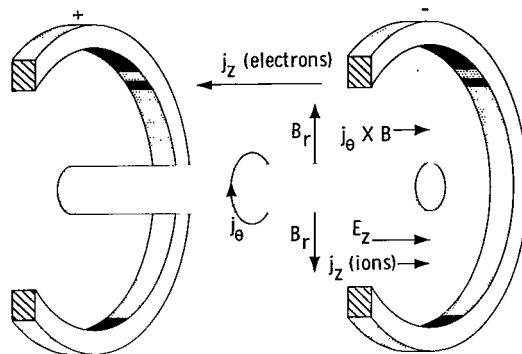
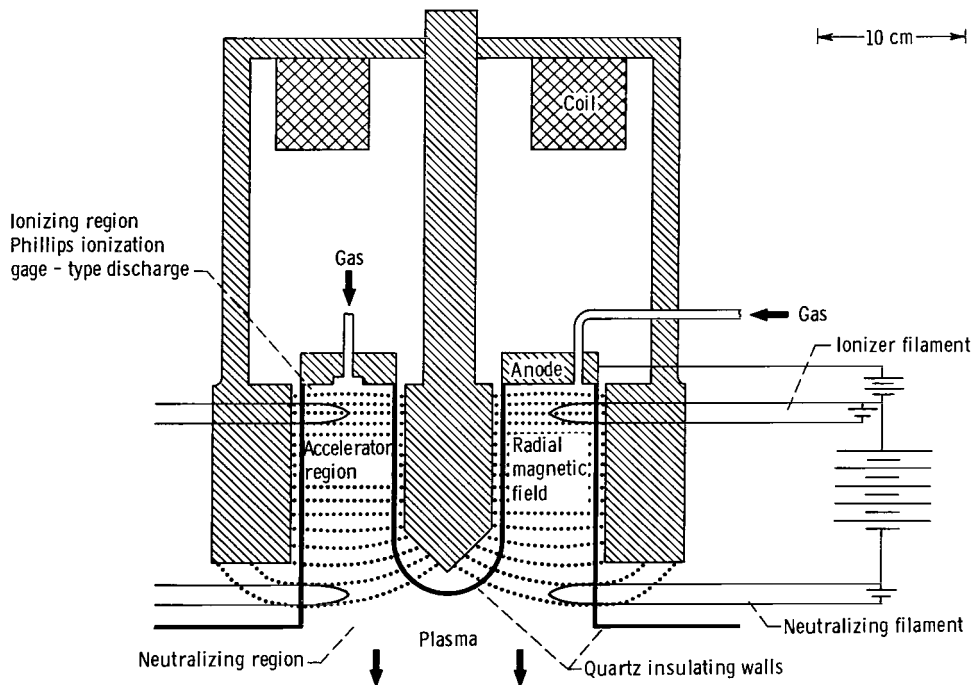


Figure III-19. - Axial and radial distributions of axial current density and applied magnetic field with contours of constant magnetic field strength.



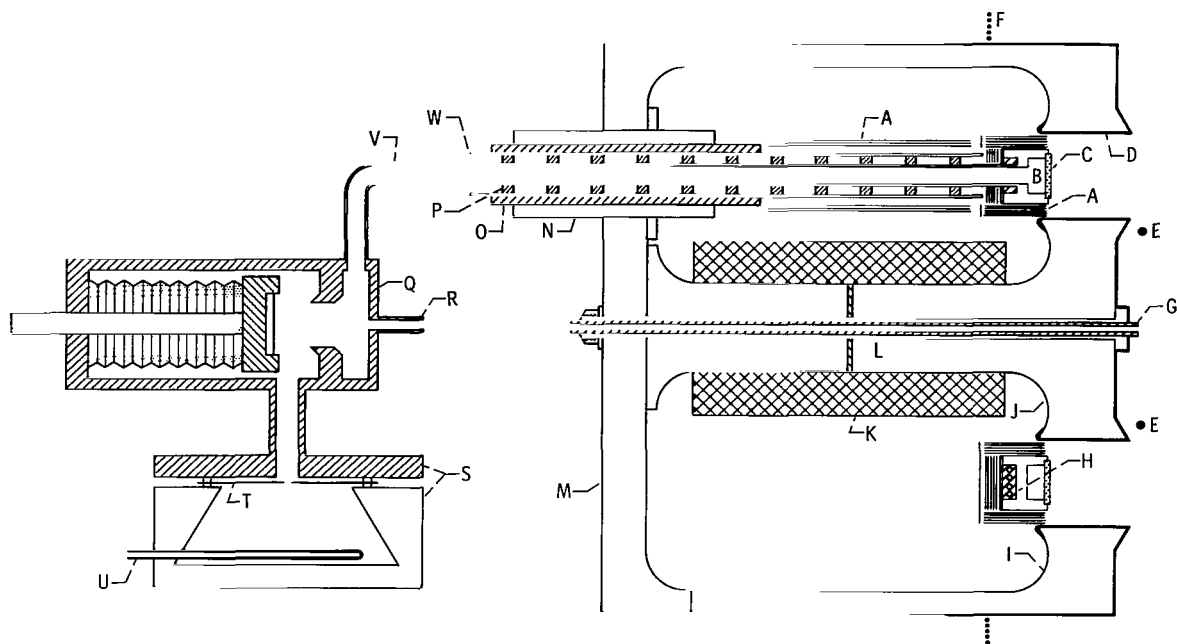
CD-8184

Figure III-20. - Hall ion accelerator.



CD-8185

Figure III-21. - Typical low-density Hall ion accelerator.



Legend

CD-8186

- | | | |
|--|-------------------------------------|----------------------------|
| A-Tantalum foil heat shields | H-Ionizer heater | P-Alumina separators |
| B-Cesium vapor duct | I-Outer pole piece (steel) | Q-Valve and manifold |
| C-Porous tungsten ionizer | J-Central pole piece (2V permendur) | R-Argon purging port |
| D-Pole face insulator (spray coated alumina or zirconia) | K-Solenoid | S-Cesium boiler and flange |
| E-Accelerator-neutralizer | L-Space gap for B measurements | T-Metering orifice |
| F-Shield | M-Steel backplate | U-Thermocouple tube |
| G-Electrical feed-thru for accelerator-neutralizer | N-Metal collet | V-Cesium vapor feed tube |
| | O-Alumina support tube | W-Tantalum support tube |

Figure III-22. - Schematic diagram of experimental Hall ion accelerator (United Aircraft).

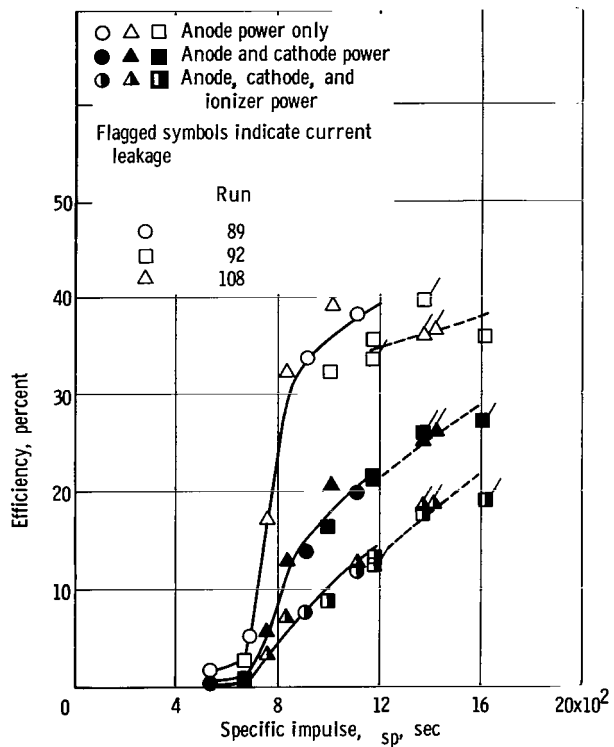


Figure III-23. - Efficiency as function of specific impulse for United Aircraft cesium accelerator.

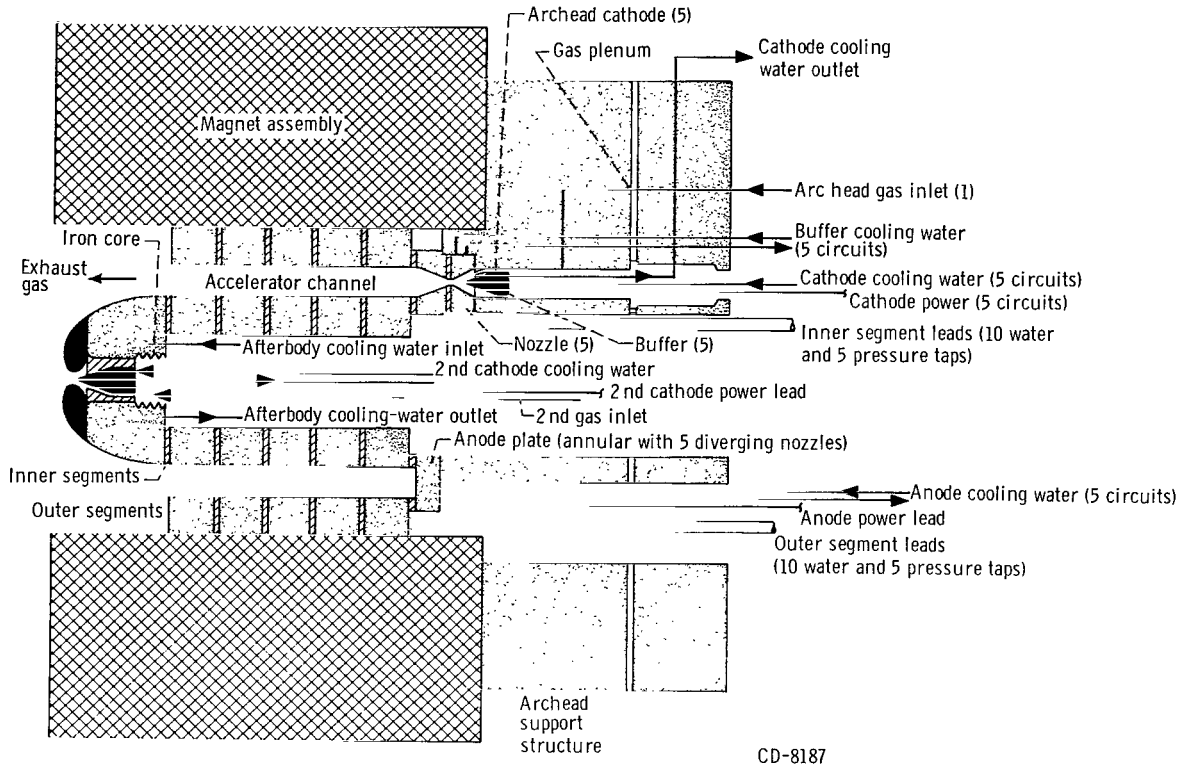
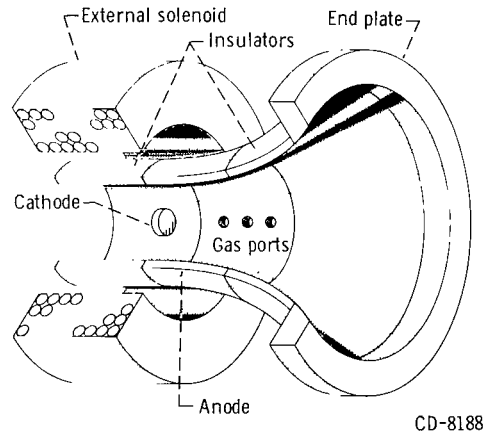


Figure III-24. - High-pressure Hall ion accelerator (EOS).



Maximum anode power efficiency, 33 percent;
 Thrust at maximum efficiency, 2.5 millipounds;
 Specific impulse, 2700 seconds
 Maximum thrust, 6.2 millipounds

Figure III-25. - Engine schematic and oscillating electron ion engine performance data for United Aircraft Corporation engine model D4a.

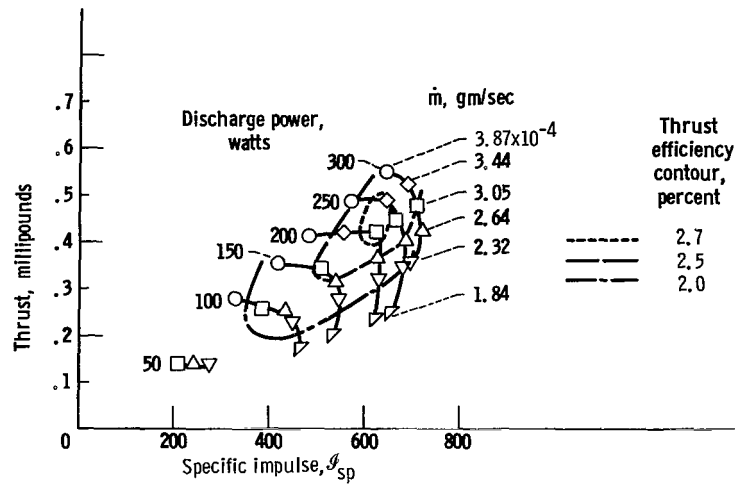


Figure III-26. - Thrustor performance. Ammonia propellant; 50-volt discharge; $\frac{1}{2}$ -inch-diameter anode.

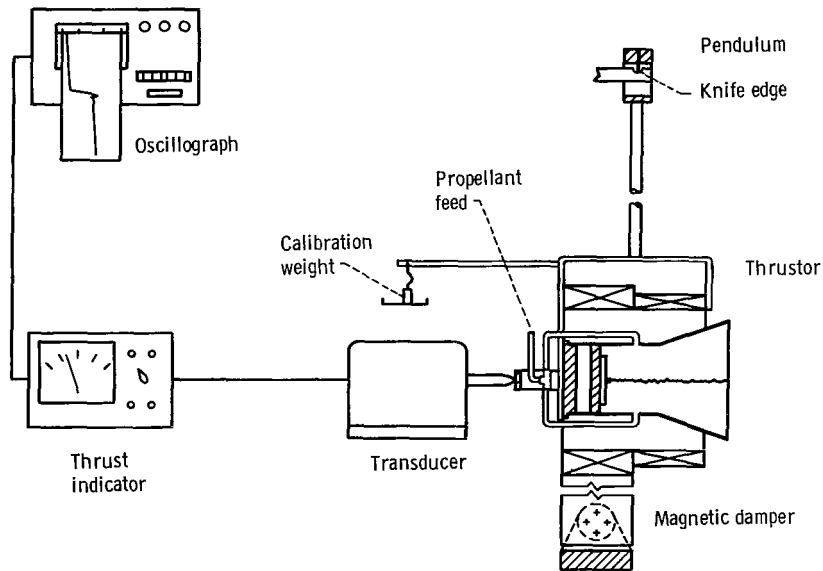


Figure III-27. - Magnetic expansion thruster.

CHAPTER IV

ALTERNATING-CURRENT PLASMA ACCELERATORS

INDUCTION-TYPE MAGNETIC ACCELERATORS

Summary of Current Status

Major experimental programs on induction-type accelerators are being conducted by several industrial and government groups. Since some of the experimental work is still in progress and none of the accelerators has reached the state of engine development, final conclusions regarding limitations of performance or ultimate feasibility are not appropriate at this time even though present indications for obtaining high overall efficiencies from most of the devices are not promising.

Three configurations of the electromagnetic circuit have proven useful: a polyphase resonant circuit producing a traveling magnetic wave, a distributed transmission-type circuit, and a radiofrequency (rf) fringe-field accelerator.

Performance measurements available from different sources indicate a plasma calorimetric efficiency, that is, an efficiency not including skin effect and other electric circuit losses, of up to about 50 percent and a corresponding thrust efficiency of 25 percent for traveling magnetic-wave thrusters and thrust efficiencies around and above 50 percent for the rf fringe-field device. The latter data require more confirmation, however.

The data cover a specific impulse range from about 2000 to 6000 seconds combined with thrust levels of up to several newtons in pulsed operation. The operational frequencies lie between 150 and 500 kilohertz.

General Consideration

The most important feature of induction-plasma engines is the fact that an externally supplied oscillating magnetic field induces a current which then interacts with the magnetic field thereby accelerating the plasma. As a consequence, no electrodes are needed. Electrode erosion, voltage drops, and heating are eliminated. On the other hand, operation at high ac frequencies is necessary and skin-effect losses and rf power-generation problems have to be solved satisfactorily.

Typically, for induction accelerators the plasma electrons are accelerated parallel to the axis of symmetry by a radial component of \vec{B} and azimuthal current j_θ , induced by B according to Maxwell's equation:

$$(\text{Curl } \vec{E})_r = - \frac{\partial B_r}{\partial t} \propto \omega B_r \propto \frac{\partial E_\theta}{\partial z} \quad (\text{IV-1})$$

where $\vec{B} = |B| \cos \omega t$. Thus, for ω in the range of kilohertz, sufficiently large currents j_θ which are proportional to E_θ can be induced with relatively weak magnetic fields, and gas breakdown can be achieved with no additional external ionization. This mode of coupling is known as "transformer coupling" with the coils being the primary and the plasma acting as the secondary winding of a transformer. In absence of any materials this coupling can be made essentially lossless. However, difficulties in phase performance may arise, as will be mentioned later, due to unsymmetrical loading of the coils by the plasma.

Essentially three configurations of the exciting B fields have been investigated.

(1) The coils are part of a polyphase resonant circuit (AVCO, Litton Industries, General Technology, NASA-Lewis), in which the formers are spaced along the system axis and fed with such a phase as to resemble a wave traveling with the desired phase velocity.

(2) The coils are part of a transmission delay line (Space Technology Laboratories, Aerospace Corporation) constructed for a desired phase velocity. This scheme is closely related to wave structures used for traveling-wave electronic amplifiers in which the axial phase velocity is delayed approximately by the ratio of pitch (distance between windings) to circumference of winding.

(3) The coils are part of a single-phase resonant circuit (Litton Industries).

All schemes may be used in a continuous or pulsed mode of operation. It is important, however, that the pulse length be substantially longer than the period of the exciting field so as to establish a continuous wavelike operation for the driving field. Otherwise transient effects will dominate the operation, making overall efficiency small.

Similar to processes involved in most plasma devices, the primary action is exerted on electrons, since the ion inertia is much larger, causing a slight separation of charges. This separation generates an axial space-charge field which in turn accelerates the ions, so that charge neutrality is maintained. The existence of this steady-state potential along the channel axis has been confirmed experimentally (ref. IV-1). For a tenuous plasma the existing theories (refs. IV-2 to IV-4), seem to agree in trends and within a factor of about 2 to 5 with experimental results. The wavelength, and hence the phase velocity, may be constant down the axis or it may increase to provide a better match between the gradually increasing plasma velocity and the driving field.

Collisionless equations of motion can be written by extending to ac cases Busch's theorem which relates the change in magnetic flux to the change in the angular momentum of electrons. Through inclusion of the self fields - which largely complicates the case - generally valid equations have been derived and are being investigated by Pennfold (refs. IV-2 and IV-3). These self-generated fields are important since they lead to the well-known pinching or self-confinement of plasma.

Induction engines operating in higher pressure regimes where collisions are important can be treated from a continuum point of view (ref. IV-5). One deals here with bulk currents and conductivities instead of with individual particles. Equation (IV-1) is more suitable for this case than for describing the collisionless-like motion of single charges.

The continuum regime of operation requires a finite resistivity of the plasma for finite efficiencies, as can be shown from equation (IV-1) and other Maxwell equations. Since Joule heating increases with resistance, there is an optimum conductivity for most efficient performance. Present theories fail, however, to derive accurately its value. The lower bound of σ will be given in equation (IV-3).

The efficiency of the engine depends critically upon many parameters, several of them either known only with a varying degree of accuracy or not yet understood or explainable. First, the plasma has to be coupled effectively to the magnetic field. It is evident that full magnetic pressure

$$\frac{B^2}{\mu_0} \propto j_\theta B_r \quad (\text{IV-2})$$

is exerted only on the plasma that is located in the magnetic cusps, where $B_z \approx 0$, and only if the magnetic field is prevented from penetrating rapidly into the plasma during the acceleration time (ref. IV-6). Otherwise excessive slippage of the plasma results in a detrimental effect on efficiency. The condition for the degree of acceptable slippage can be determined from the equation (IV-3) which describes the plasma conductivity

$$\sigma = \frac{1}{65.3} \frac{\mathcal{T}_e^{3/2}}{\ln \Lambda} \left(\frac{\text{mhos}}{\text{m}} \right) \quad (\text{IV-3})$$

which requires a certain minimum electron temperature \mathcal{T}_e (ref. IV-7).

In the preceding discussions the importance of high plasma conductivity for piston-like operation of the traveling-wave engine has been stressed. There exists, nevertheless, an alternative possibility for operating an accelerator if the plasma does not satisfy the requirement of equation (IV-3), that is, if the conductivity is not high enough to prevent substantial leaking. In this latter case there will be a relative motion of the plasma

and the magnetic field (in other words a point of constant phase will not be "frozen" into the very same volume of plasma). As a consequence of this relative motion, azimuthal currents will be induced in the plasmas and still exert a $j \times B$ force on the plasma. This case, however, requires stronger fields for the same thrust.

There are also relations to be fulfilled between the magnetic pressure and the static and stagnation pressures $B^2/2\mu_0$, $nk\mathcal{J}$, and ρu^2 , respectively. The condition that $nk\mathcal{J}/(B^2/2\mu_0) < 1$ everywhere is desirable for radial confinement of the gas. The condition that $\rho u^2 < (B^2/2\mu_0)$ is necessary at the inlet in order to permit close coupling to the moving field. For good efficiency the condition $\rho u_f^2/(B^2/2\mu_0) \gg 1$ at the exit is mandatory (ref. IV-1).

The large number of parameters and assumptions makes final predictions about actual performance questionable. It can be stated, however, that for high efficiency, certain design conditions and requirements must be satisfied. The phase velocity must be tapered or matched to the changing plasma velocity even if the exciting field is smooth enough to maintain efficient coupling to the plasma because, for constant wavelength (phase velocity), calculations indicate a maximum thrust efficiency to be about 50 percent (ref. IV-8). It is obvious that energy transfer from the wave to the plasma can take place only if the field velocity is larger than the plasma velocity.

It would seem desirable to construct an accelerator with a large ratio of the outlet to inlet magnetic-field velocities. However, a satisfactory theory for predicting the minimum number of wavelengths necessary for high exit velocity without excessive slippage of plasma through the field is not available. On the other hand, experience indicates that some few wavelengths in interaction length should not be exceeded and that is difficult to obtain a ratio of magnetic field velocities larger than about four or five (ref. IV-3), which would be very satisfactory.

For efficient coupling the plasma should be "locked" to magnetic field cusps only where a strong and desirable B_r component exists. In this case the plasma will not experience any serious difficulty in leaving the magnetic field at the exit (ref. IV-3). However, if there is some plasma at locations with strong axial magnetic-field components, radial acceleration will drive this plasma to the walls at the outlet. If no precautions are taken, the relative motion of the moving plasma and the stopping magnetic field will induce strong ring currents in the plasma, leading to its heating rather than acceleration. One promising method of eliminating this "end effect" (which is not limited to traveling-wave thrusters) is to taper the amplitude of B gradually with distance to zero or close to zero at the end of the accelerator. A moving plasma would not, then, have to cross a "standing," strong magnetic field and no energy would be transferred back from the plasma to the field. A successful elimination of end losses may very well prove decisive for the ultimate feasibility of the traveling magnetic-wave plasma engine.

Another problem is the power loss to the accelerator walls. In the case of devices

working with a more or less smooth distribution of gas throughout the tube, it is the axial component of B which prevents highly conducting gas from diffusing to the walls by pinching it radially inward. However, in regions of strong B_r and hence weak B_z , a radial electric field would be necessary and consistent for ion containment. In case of torroidal-plasma rings (ref. IV-2) it is the self-magnetic field which leads to a pinch effect and stability of the torroids over times sufficient to complete the acceleration cycle.

A problem of general importance to all wave type of magnetic-wave thrusters is the quality of the wave itself. To date, this problem has been treated only for the less important case of constant-phase velocities (refs. IV-9 and IV-10). From the equation describing the time and position dependence of the magnetic-flux density B along the symmetry axis (as derived in refs. IV-9 and IV-10) it follows that requirements for constant velocity and constant amplitude cannot be met entirely but can be kept to acceptable levels. The results may be expressed in terms of a parameter $\Psi = \frac{\delta}{r}$ where δ is the distance between adjacent coils and r is the coil radius. Operation at values of $\Psi < 1$, though desirable from a "ripple" standpoint, is inefficient in generating a field B from a given amount of coil current. Operation at large values $\Psi > 1$, on the other hand, is characterized by the presence of both forward- and backward-running waves, a fact resulting from the presence of an infinite number of space harmonics, all of them having the same frequency but different phase and group velocities. From these considerations, two quality factors are defined, representing the average B available on the axis and the amount of ripple. Computations show then that there is little difference in quality of performance between finite and infinite coil systems for $0.5 < \Psi < 5$ and 90° phase between subsequent coils (fig. IV-1). Thus, short systems seem to be feasible, a fact of high importance in plasma propulsion. A value of $\Psi = 1.0$ was selected for preliminary experimentation, a choice representing a slight sacrifice in B in order to produce a smooth wave. In a later investigation (ref. IV-11) the before-mentioned parameters have been expressed in terms of the magnetic wavelength as reference. An optimum in useful plasma energy is obtained for a coil radius to magnetic-wavelength rates of 0.35. At this optimum value, the useful energy in the wave is independent of the number of phases per wavelength when that number is greater than three.

Finally one remark should be made regarding the operation of pulsed networks. These must not be simply terminated in the characteristic impedance because such an arrangement would set an upper limit for achievable efficiency of 50 percent. Schemes have been proposed to recuperate the magnetic-field energy by feeding it back with proper phasing to the generator (refs. IV-12 and IV-13), but have not been checked out yet. A closed "ring" circuit has also been proposed as an effective remedy (refs. IV-12 and IV-13).

Discussion of Experimental Results

Polyphase-induction accelerators (AVCO, Litton Industries, General Technology, and NASA-Lewis). - Most comprehensive and complete diagnostic results so far were obtained by S. Janes and coworkers at AVCO/Everett Research Laboratories (ref. IV-1). Their accelerator was a 12-phase variable-field velocity induction engine approximately 5 wavelengths long (fig. IV-2). The frequency was 115 kilohertz, the chamber radius was tapered from 3 to 10 centimeters, the phase velocity was 1 to 4 centimeters per microsecond, and the ion density n was 10^{11} to 10^{12} per cubic centimeter. Two coil configurations, a 48-coil and a 54-coil arrangement were investigated. These devices were operated at low pressure such that the ion mean free path and cyclotron radius are one or more order of magnitudes higher than the tube radius. Under this condition a strong axial potential gradient should exist due to space-charge separation. Measurements yielded a total axial voltage of about 120 volts, which is slightly below the highest ion velocity observed in the exhaust but sufficiently close to support the theory of this type of acceleration.

Careful and significant data have been obtained on magnetic-field components, electric-field gradients, velocity and wall losses along the 120-centimeter-long chamber. The measurements show an increase in potential closely coupled with that in phase velocity up to an axial distance of 55 centimeters from the beginning of the tube, followed by a drop in potential gradient and finally followed by another increase of same in the exit region (fig. IV-3). Up to 55 centimeters length the radial component B_r is strong and smooth providing a strong coupling. Beyond 55 centimeters B_r is weakened and strongly perturbed resulting in a marked decoupling. In this region, moreover, there occurs a rapid heating of the ions. Axial velocity measurements coincide very well with the electric field data: a strong velocity increase for the first 55 centimeters, followed by a very weak one through the rest of the device and a modest increase again in the exhaust part. Wall heat-transfer data indicate clearly the detrimental effects on the containment of the plasma by abruptly terminating the magnetic field (fig. IV-4). The resulting radial force pushes the plasma outward toward the wall. This inability of the plasma to separate itself from the magnetic field is so serious that 60 percent of the total heat losses to the walls occur in the region of the last single coil and the remainder of 40 percent is distributed more or less evenly over the entire system of 47 or 53 preceding coils, respectively. If ohmic losses in coils and other circuit components are neglected, a thrust efficiency of 25 to 30 percent in argon has been measured. Calorimetric efficiencies have not been reported.

Two major difficulties can be seen clearly; the failure of the second half of the structure to produce any substantial directed energy and the severe losses at the end. A shorter device of only 40-centimeters length followed by an expansion nozzle has been

built using a 12-coil configuration. In contrast to the longer device, this shorter engine produces a steady increase of gas velocity. A considerable slippage has plagued the operation and no improvement in efficiency could be detected. The experimental program was terminated before a complete set of results could be obtained.

Another major experimental effort is in progress at Space Science Laboratories of Litton Industries, under A. Penfold (refs. IV-2 to IV-4). It involves a 50-kilowatt, steady-state engine operating with mercury vapor at a frequency of 240 kilohertz in the low-pressure regime. The choice of mercury as operating gas is motivated by the requirement that overall efficiency at \int_{sp} smaller than 5000 seconds be 90 percent or more.

With the help of an analog network fed into a computer, a number of geometries were studied to obtain an accelerator configuration having purely axial acceleration. It has been determined that this can occur to a degree only for plasma outside of the electric structure. A polyphase engine having this feature has been constructed. As yet, no accelerator performance has been obtained, even though many components have been tested.

An approach different from the two previously discussed has been pursued by members of NASA Lewis Research Center (ref. IV-9 and IV-10) with a very short polyphase system (fig. IV-5). The attractive feature of this device is a four-coil coaxial configuration producing a sufficiently smooth field in which the phase change from coil to coil is 90° . Thus, the total length of the system is considerably shorter than the device of AVCO/Everett. It operates at a frequency of 150 kilohertz and a maximum generator power of 25 kilowatts continuous wave.

To date, two untapered engines - the first, 1-magnetic wavelength long and the other $2\frac{1}{2}$ -wavelengths long, have been tested at Lewis Research Center with the following (refs. IV-9 and IV-10) results: The four-coil (1 wavelength) engine operated with argon produced an overall efficiency of 10 percent at $\int_{sp} = 3000$ seconds and 23 percent at $\int_{sp} = 4000$ seconds with xenon. Both results were thrust-based efficiencies as inferred from pendulum deflections. It has been determined that energy transfer to the walls was responsible for the major part of losses as was evident from calorimetric-efficiency measurements using xenon gas showing a thermal efficiency of 38 percent. Measurements with the 10-coil thruster resulted in 10-percent thrust efficiency at 3000 seconds for argon for a $2\frac{1}{2}$ wavelength thruster. (In quoting the efficiency data, coil and generator losses were disregarded.)

Since no probe measurements have been made, it was difficult to account for the difference in efficiency between argon and xenon. One could argue that for mass flow rates of 0.4×10^{-6} and 0.75×10^{-6} kilograms per second, xenon and argon, respectively, the pressure and density for the former must have been substantially smaller. Therefore, a more perfect ionization might be assured and smaller diffusion to the walls in xenon than in argon could be realized. Also, a larger cyclotron radius is certainly bene-

ficial for getting the ions out of a tube working in the low-density regime. Because no tapering of phase velocity was applied in either case, the 23-percent efficiency achieved with xenon may be considered a very satisfactory result. Tapered and otherwise improved configurations are being prepared and substantial gains in performance are indicated by theory.

The next program to be discussed is the traveling-wave accelerator work by General Technology Laboratories, under a NASA-Lewis Contract (ref. IV-14). Since all experience with this and many other types of plasma accelerators points in the direction of relatively high power operation for good performance, a pulsed-power oscillator capable of 8-megawatt peak power at 40-kilovolt plate voltage has been constructed and tested. Presently, however, only 100 kilowatts are being coupled into the plasma. It operates at a frequency of about 500 kilohertz with a pulse length of 1 millisecond. During 1 millisecond of constant power delivery, there will elapse 500 full oscillation periods and as far as the acceleration process of the plasma volume is concerned, a continuous mode prevails.

In contrast to the devices designed by AVCO and NASA Lewis, whose coils were coaxial about the axis of acceleration, the magnetic field in the General Technology device is produced by coils whose axis is perpendicular to the system axis. These coils have been wound on four pairs of ferrite cores, as shown in figure IV-6. In this scheme the magnetic field lines are more or less parallel and predominantly y-axis directed. There is no rotational symmetry about the system z-axis, and forces in the axial as well as in the transverse direction are present. These latter forces are likely to drive the gas into the walls. The advantage of this configuration, however, is that an excellent coupling of the field and the plasma exists over the entire cross-section. As to the smoothness in amplitude and phase velocity, the requirements for the General Technology design are identical to those described for other configurations. Another feature that distinguishes the General Technology thruster from other inductive plasma accelerators is the high plasma density.

The system has a mechanical gas valve and a simplified thrust stand which indicates the electromagnetic back reaction. A high-speed rotating mirror camera with a framing rate of 2×10^6 per second has been used to show the structure and motion of the plasma. The back impulse on the coils, \int_{tot} , was measured as function of the mass utilized m and energy input to the plasma ϵ_p . Derived performance parameters are defined as follows:

Thrust $T_{em} = \frac{\int_{tot}}{t}$, where t = time duration of run

Specific impulse $\int_{sp} = \frac{\int_{tot}}{g}$

Plasma directed kinetic energy $\frac{J_{\text{tot}}^2}{2m}$

Plasma input energy ϵ_p

Plasma efficiency $\frac{J_{\text{tot}}^2}{2m\epsilon_p}$

Figure IV-7 shows thrust and specific impulse as a function of mass for argon. It shows thrusts of some few newtons (in pulsed conditions) at J_{sp} around 3000 seconds.

To date, best efficiencies of up to 40 percent were obtained with helium. This number, however, does not represent a true propulsion efficiency due to strong gas-wall interaction which reduces the effective thrust to about one-half of the electromagnetic thrust T_{em} , as determined from independent target measurements. A possible cause for the strong gas-wall interaction might have been the lack of motion of the magnetic waves at the pole tips, where the field was essentially stationary for the geometry of figure IV-6. Another configuration was tested in which the coils have been rewound to produce a moving wave across the entire duct. Unfortunately, little, if any, reduction in wall interaction was obtained with the rewound system.

The power transferred to the plasma occurred at a level of about 100 to 200 kilowatts during the 1.25 millisecond pulse duration, which is substantially more than the continuous wave power levels applied in the AVCO and NASA-Lewis experiments.

Transmission-line networks. - The major effort on transmission-line traveling-wave accelerators has been carried out by a number of researchers at Space Technology Laboratories, Aerospace Corporation, and Massachusetts Institute of Technology (refs. IV-8, IV-12, IV-15, and IV-16).

The advantage of transmission-type networks as compared to polyphase systems is the fact that single-phase generator is used with all beneficial consequences resulting from such a simplification. However, every transmission line is equally affected by any unsymmetrical plasma loading as are polyphase systems. Because transmission lines need longer coils (e. g. , longer helical wire) than short polyphase systems, skin-effect losses are probably more severe in the former.

Devices of this type consisted of a doubly wound helix, wrapped around a glass tube confining the plasma and a number of capacitors distributed along the turns. The traveling magnetic field is produced by discharging the capacitor bank. The accelerator works in a manner similar to a shock tube. The radial component of B together with the induced ring current acts like a magnetic piston. If, due to high conductivity, the leakage of this piston through the plasma is small, a shock wave is driven into the gas.

The analysis (ref. IV-8) shows that for constant-phase velocity and negligible losses

at most 50 percent of the capacitor energy can be transferred to the plasma, the other 50 percent being left in the magnetic field. This magnetic energy can be used in case of steady-state operation, because the tube must be filled with it only once. For pulsed operation some of the recovery methods mentioned in the introduction may be applied. It can also be shown that the piston is always slowed down by the presence of plasma and that a small but finite (5 to 20 percent) part of the input energy will be dissipated in the annular current sheath between the plasma and the helix. Thus, a simplified and idealized theory predicts efficiencies above 80 percent also for transmission-line operation (ref. IV-8).

Subsequent experimental investigations confirmed qualitatively the piston-like action of the magnetic field behind the plasma and also the presence of a thin annular current sheath between the tube wall and a plasma cylinder. The following basic difficulties were identified and encountered: losses to walls, poor interaction around and at the center of the tube where $B_r \approx 0$ (so that the piston behaved like one having a hole at the center), and a higher than expected leakage rate. Performance measurements have not been reported.

Radiofrequency fringe-field accelerator. - The rf fringe-field accelerator is the most recent and probably the most promising induction-type accelerator. The rf magnetic field is derived from two concentric coils as shown in figure IV-8. These coils are composed of water-cooled copper tubing, are connected series-aiding, and have 20 turns. Two concentric pieces of high curie-point ferrite material are placed close to the coils on the left side. The operating frequency was chosen to be 250 kilohertz. The coils are part of a simple resonant circuit. The symmetric field has a radial and an axial component, the induced electric field only an azimuthal component. Figure IV-8 also shows the pattern of the magnetic flux which is identical to the lines of constant induced volts per turn. A saddle-point occurs in the magnetic field between the coils and the propellant is brought to this point by a series of various azimuthally placed nozzles. After ionization the E_θ field-driven azimuthal currents interact with the magnetic components to give rise to a predominantly axial acceleration.

The nature of the forces on the plasma can be best understood by considering two limiting cases: The plasma which comprises the secondary winding of the transformer has inertial, inductive and resistive properties and its behavior is determined depending on whether

$$R_p \gg \omega L_p$$

or

$$\omega L_p \gg R_p$$

where L_p symbolizes the inertia and inductance of the plasma and R_p its resistivity. In the first case the plasma currents are in phase with the primary voltage applied to the coils. Since B is in phase with the coil current the force $j \times B$ will have the form

$$j \times B \propto \sin \omega t \cos \omega t = \frac{1}{2} (\sin 2 \omega t)$$

The time average of this force is obviously zero and the device would function primarily as a heater. On the other hand, in the second case, the currents flowing in the plasma now dominated by inductive reactance will be obviously out-of-phase with the coil voltage similarly to magnetic fields and the force on the plasma will be

$$j \times B \propto \sin^2 \omega t = \frac{1}{2} (1 - \cos^2 \omega t)$$

which has a time average different from zero. Whether the device works in the resistive or inductive mode depends largely on the value of the parameter $\omega_e \tau_e$. For $\omega_e \tau_e \leq 1$ the plasma is collision dominated and appears in the circuit mainly as a resistance. If, on the other hand $\omega_e \tau_e \gg 1$, the plasma will act mainly as an inductance. Thus, for successful operation as an accelerator, tenuous plasmas are required. Like in all low-density cases the accelerating forces act almost entirely on the electrons which make up the azimuthal currents in the plasma. The ions are then accelerated by space-charge separation forces.

A thruster of the type shown in figure IV-8 has been developed and tested at Litton Industries and some results published by Penfold (ref. IV-17). Figure IV-9 shows thrust efficiency against specific impulse for two different values of mass flow rates with mercury as propellant. These efficiency numbers, if correct, compare very favorably with results obtained with other electric thrusters. However, due to inaccuracies involved in the determination of the rf input power and difficulties involving outgassing during operation and possible recirculation of mercury as well as other residual gases the quoted efficiencies may be in error and more unambiguous measurements are required. On the other hand it may be stated that, as far as efficiency is concerned, the performance of the rf fringe-field acceleration is better than that of the other inductive devices described in this chapter. A very likely reason for this improvement is the short axial extension of the thruster. Thus, wall losses which so much troubled the performance of other inductive devices are likely to be very small in this case.

Concluding Remarks

Substantial progress in the overall performance has been achieved with induction

thrusters over the last few years. It can be concluded that in all traveling-wave-type thrusters losses to walls, end effects and excessive leakage of the plasma through the field represent the more serious difficulties which must be resolved for efficient performance. On the other hand, specific impulse numbers between 1000 and 6000 seconds and thrust values of a few newtons (to date only in pulsed operation) are easily realizable. Work on reducing skin-effect losses and other circuit losses and on the rf power generators will have to begin soon to achieve an overall satisfactory performance. Also, it is difficult to raise the coupling efficiency from the generator into plasma above 80 percent in practical circuits: This difficulty arises from the necessity to use high Q circuits (in order to keep ohmic losses low) which are easily detuned by even small fluctuations in resistive and reactive plasma loading. Furthermore, there are limitations in designing a circuit with more than 90 percent of power going into the desired space harmonic in practical arrangements. Moreover, it is not likely that rotating machinery with more than 90 percent efficiency can be developed at frequencies above 100 kilohertz. These combined factors are liable to produce the before mentioned estimate of 80-percent coupling efficiency limit. Much more difficult to estimate is the actual efficiency limit from coupled rf power into directed exhaust-stream energy because all presently available measurements neglect skin effect and coupling losses and because of the lack of any accurate theory of plasma interaction with traveling magnetic fields.

In view of these difficulties and the progress achieved with other devices the work on traveling-wave-type accelerators has been almost entirely discontinued in the early part of 1965. The performance of the rf fringe-field accelerator - the latest development in the field of inductive engines - looks more promising than that of its traveling-wave type partners, not only because of higher efficiencies but also because of the simplicity of the fringe-field thruster.

CYCLOTRON RESONANCE THRUSTORS

Summary of Current Status

Compared with efforts expended on other types of plasma thrusters, relatively little work has been done on microwave-driven devices. Experimental results have been reported by General Electric (GE) and Radio Corporation of America (RCA) on geometrically similar devices which have been operated in the frequency range between 2 to 8 gigacycles and power levels from 200 watts up to several kilowatts. They are designed to excite the electron cyclotron frequency. They have been operated in the density regime of about 10^{12} or 10^{13} particles per cubic centimeter corresponding to $\omega_e \tau_e = 100$ to 1000. To date, calorimetric efficiency results up to 75 percent have been reported. Mass-

utilization efficiency and the specific impulse have not yet been accurately determined.

General Considerations

The basic operation of cyclotron resonance degree is best explained with the help of figure IV-10. A circularly polarized microwave enters a cylindrical tube filled with low-pressure gas. There exists in the vicinity of the gas injection plane the magnetic field of an intensity B such that

$$\omega_e = \frac{eB}{m_e} \approx \omega_{rf}$$

(equality of electron cyclotron and exciting microwave frequency). This field is fairly homogeneous in the central part of the magnet and diverges toward the ends. At power levels of a few hundred watts the low-density gas ($n \approx 5 \cdot 10^{18}$ per cu m, $\omega_e \tau_e \gg 1$) breaks down directly and remains ionized during the acceleration process. The electrons present in the system revolve around the magnetic field lines with cyclotron frequency. Simultaneously, they move with thermal gas velocity parallel to the tube axis along the field lines and their rotational energy is pumped up to higher and higher values. This happens because electrons draw power from the rf field near cyclotron frequency by increasing their cyclotron radii (only if the sense of polarization and cyclotron motion is the same) and gain between collisions an energy

$$\epsilon = \frac{(eE_0)^2}{4m\nu_{eff}^2}$$

(ref. IV-18). Where ν_{eff} is the effective collision frequency.

In the subsequent acceleration in the diverging region of the magnetic field the energized electrons drag out the ions due to space-charge coupling. The interaction of microwaves with plasmas has been studied by Daniel and Hurwitz (ref. IV-19). They showed that in order to avoid reflections of the incident power at the plasma front, the plasma density should, preferentially, increase exponentially. The effective collision frequency ν_{eff} in this tenuous plasma is determined by Doppler - broadening (damping) rather than by actual collisions with neutrals or ions. This broadening causes the conductivity of the plasma to become complex with the real part

$$\sigma = \frac{n_e e^2}{m_e \nu_{\text{eff}}}$$

and

$$\nu_{\text{eff}} = \frac{2\pi}{\lambda} \left(\frac{2kT_e}{\pi m} \right)^{1/2}$$

where λ is the wavelength of the driving wave in the plasma.

While high conductivity is desirable for low ohmic losses in the plasma, high and, if possible, total ionization is more important for an efficient operation since in the collisionless-like regime space-charge forces can accelerate ions only the neutrals remaining unaffected. For this tenuous plasma the acceleration process can be best described by considering the motion of individual charges.

An electron orbiting around a magnetic-field line represents a magnetic dipole moment given by

$$\vec{\mu} = I \cdot \vec{A} = e\nu_c \pi r_c^2 \vec{a}$$

where I is the current $e \cdot \nu_c$, $\vec{A} = \pi r_c^2 \vec{a}$, the encircled area and \vec{a} is the unity vector of the area. It has been shown (ref. IV-20) that $\vec{\mu}$ is almost a constant of motion in magnetic fields varying in time and in space if, taken over 1 cyclotron orbit, $\Delta B \ll B$. A magnetic moment will experience a force in the inhomogeneous part of B which is given by

$$\vec{F}_m = (\vec{\mu} \cdot \vec{\nabla}) \vec{B} = \left(\vec{\mu} \cdot \frac{\partial}{\partial \vec{s}} \right) \vec{B}$$

An electron finally thrown out of the magnetic field B_0 into a region at infinity where $B = 0$ will do a work against the field

$$\int \vec{F}_m \cdot d\vec{s} = \vec{\mu} \int \frac{\partial \vec{B}}{\partial \vec{s}} \cdot d\vec{s} = \mu \int_{B=B_0}^0 \partial \vec{B} = -\mu B_0$$

This work is being converted (due to space-charge coupling) into a uniform motion of both the electrons and ions. At infinity $u_i = u_e$ and thus the potential energy μB leads to a formation of a steady-state potential

$$m_e u_e^2 \ll m_i u_i^2$$

$$v = \frac{\mu B}{e}$$

Assuming constancy of $\bar{\mu}$ over regions of the exhaust, adjacent to the solenoid, a three dimensional, collisionless calculation of the acceleration process is feasible. It is of special interest to show that there will be little divergence of the exhaust in spite of diverging magnetic field. Three-dimensional equations coupling the space charge to magnetic fields have been formulated by one of the authors (ref. IV-21), and have been computed at NASA-Lewis with the help of the 7094 computer. They show clearly that the plasma does not strictly follow the magnetic-field lines but emerges at an angle of about 0° to 30° with respect to the axis depending on radial position. About 80 percent of the ultimate acceleration occurs within 1 radius of the solenoid out in the z-direction. Within 3 radii out along the z-axis, full steady-state conditions have been attained. This situation is very fortunate from theoretical point of view since the adiabatic conservation of $\bar{\mu}$ is very well satisfied in the region $z \lesssim r_c$. The space charge potential changes substantially only in the z-direction and it is quite flat over the radius for constant z. A more realistic treatment should include a distribution function for the magnetic dipole moments instead of assuming single average value as well as the rate of ion production in the rf boundary region.

The second microwave-driven accelerator to be described here has been reported by RCA, Princeton (refs. IV-22 and IV-23). There is a great amount of resemblance between this device and the cyclotron resonance propulsion system ("Cyclops") even though the interpretations of the proposed mechanisms as given by the respective workers are different. In the RCA model the acceleration process is being viewed as being due only to the distribution of electron energies. Due to the large mass ratio of the ions to the electrons there is no energy transfer to ions in the interaction region. Hot electrons, however, diffuse toward the exhaust. To maintain charge equilibrium both effluxes, that of ions and electrons, must be equal and a potential difference arises across the ion accelerating region. The latter can be calculated from equating both flux densities:

$$j_i = \frac{1}{2} \frac{nk \mathcal{F}_e}{m_i^2}$$

$$j_e = \frac{1}{2} n \left(\frac{2k \mathcal{F}_e}{\pi m_e} \right)^{1/2} e \text{ eV/k} \mathcal{F}_e$$

where V is the potential difference across the boundary.

Discussion of Experimental Results

Experimental investigations on "Cyclops" have been carried out by D. Miller (ref. IV-24) under a NASA-Lewis contract with General Electric for the last 4 years. They were begun at S-band frequencies and power levels of several hundred watts. Present efforts include a 5-kilowatt continuous-wave power klystron at 8.3 gigahertz and show a considerable improvement in performance as compared to low-power experiments. The plasma breaks down easily and no preionization is required. A coupling efficiency of up to 97 percent from rf into plasma has been accomplished. The plasma exhaust is confined to a narrow angle of about 10° to 15° . To date, up to 78 percent of the incident energy is measured as energy of the exhaust stream. The absorbed microwave power shows a maximum at $\omega \approx \omega_c$.

Two major difficulties have been identified: poor mass utilization efficiency and wall losses. From preliminary ion flux measurements taken across the exhaust stream with retarding potential probes, a mass utilization efficiency of about 75 percent has been estimated. Wall losses have been obtained by measuring wall power density with four small calorimeters along the wall. At 1 to 2 kilowatts of incident power about 30 percent is being lost to the side walls.

Other measurements include E fields found to be of the order of 15 to 20 volts per centimeter at the end of the magnet, a direct proof of the existence of a space-charge-caused potential, and velocities in the exhaust corresponding to 5000 seconds specific impulse. Various gases - argon, helium, and xenon, were tested at low power levels with the hope that xenon would yield lower specific impulses. The results obtained so far are inconclusive, however, and further parametric studies combined with changes in geometry and magnetic fields are being carried out.

As of October 1965, the following performance measurements were recorded on a thrust stand with the microwave driven accelerator ("Cyclops"): propellant xenon, at a flow rate of 0.8 milligram per second; microwave power input, $P = 1$ kilowatt; recorded thrust, 26×10^{-3} newton; resulting propulsive efficiency, 0.46; derived specific impulse, $T/\dot{m}g = 3200$ seconds; calorimetric efficiency, 0.78. If verified by further independent measurements the above quoted performance is very satisfactory.

The most recent experiments at RCA have been carried out at 2.45 gigahertz and $B = 0.087$ tesla. Langmuir probe measurements revealed the existence of an axial potential of about 90 volts which agrees fairly well with the number to be expected from the thermal energy of the electrons which had a temperature of 13.5 electron volts. Support for the assumed Maxwellian velocity distribution can be concluded from measured elec-

tron and ion current densities since it is the high-energy tail of electrons of temperature \mathcal{T}_e overcoming the retarding potential and joining the ions in the neutral beam. The energy spread of the ions was 6.5 percent (half width) with the peak being 78 electron volts. About 30 percent of the microwave power could be found as plasma energy in the exhaust stream by measuring the power in the beam from ion density and energy measurements over the area of the stream.

These experiments have demonstrated clearly a pronounced importance of the shape of the magnetic field on efficiency: by increasing the magnetic field at the exhaust of the wave guide by an auxiliary magnet and forming a magnetic "bottle" of approximately 2.5 mirror ratio, the efficiency went up to 30 percent as compared with only about 10 percent obtained within a purely solenoidal field. Radiofrequency probe measurements had been made to determine the penetration depth and also to gain an indication of the electron density. The latter has been found to be in fair agreement with the degree of ionization and total particle density concluded from Langmuir probe data.

Concluding Remarks

Despite great operational similarities between "Cyclops" and the "space-charge accelerator" of RCA, quite different interpretations of the physical scheme of operation are being given by the respective researchers. Whether this discrepancy is a real one or only due to the lack of accurate data is not known as yet. If density measurements were accurate to one, or perhaps a half order of magnitude, no substantial difference in $\omega_e \tau_e$ or in the mean free path could exist. Consequently, if heating of electrons dominates one experiment, it would be applicable to the other one as well. On the other hand, a diverging magnetic field must follow on every homogeneous region and acceleration of magnetic moments is taking place in the RCA device as well because there are hundreds of orbits between consecutive collisions. It appears possible that the combination of both effects (e. g. , electron heating and magnetic-moment acceleration) could be effective. However, order-of-magnitude agreements as derived from presently available data are insufficient for any quantitative conclusions.

At present, the experiments at GE have yielded a conversion efficiency of microwave-to-total beam energy up to 78 percent, and both the RCA and GE results confirm the axial electric fields to be the mechanism of ion acceleration. Actual energy-coupling efficiencies from microwave tube output into the plasma of more than 97 percent have been demonstrated. More experimental work is required to determine the mass utilization efficiency and its limitations.

As to the microwave power sources, presently available amplitrons and extended interaction klystrons are 75-percent efficient at 3 gigahertz and over 90-percent efficient

at 0.5 gigahertz. However, due to steady progress and heavy support, efficiencies in the vicinity of 90 percent at 10 gigahertz are likely to be achieved within the next 5 years (ref. IV-25). By replacing the experimental solenoid with a permanent magnet the cyclotron resonance devices will become extremely simple in construction and geometry. In general, cyclotron resonance devices can be applied as space thrusters wherever increased power is available in amounts of 50 watts or more aboard space vehicles, such as synchronous and nonsynchronous communication satellites.

A very specific application could be recommended aboard deep-space probes instrumented with mapping radars, TV cameras, and a communications system for data transfer to earth. Since such a system will require 10 to 50 kilowatts of microwave power for communications alone (ref. IV-26) a part of this power, about 5 kilowatts, could be branched off for the thruster or all power used during the communication "off" periods.

REFERENCES

- IV-1. Smotrich, H. ; Janes, G. S. ; and Bratenahl, A. : Experimental Studies of a Magnetohydrodynamic C.W. Traveling Wave Accelerator. Proc. Fourth Symposium on Eng. Aspects of Magnetohydrodynamics, Univ. Calif. , Apr. 10-11, 1963, pp. 73-93.
- IV-2. Penfold, A. S. : A Model for the Motion of a Rarefied Plasma in an Axially Symmetric Magnetic Field. Tech. Memo. No. 61-27, Litton Systems, Inc. , 1961.
- IV-3. Penfold, A. S. : Particle Motion in an Axially Symmetric Magnetic Field. Tech. Memo. No. 61-25, Litton Systems, Inc. , 1961.
- IV-4. Fonda-Bonardi, G. : The Design of an Electromagnetic Plasma Accelerator for Propulsion Applications. Tech. Memo. No. 60-9, Litton Systems, Inc. , 1961.
- IV-5. Neuringer, Joseph L. : Induced Forces in Annular Magneto-Fluid Dynamic Traveling Wave Devices. AIAA J. , vol. 2, no. 2, Mar. 1964, pp. 267-274.
- IV-6. Brewer, G. R. ; Currie, M. R. ; and Knechtli, R. C. : Ionic and Plasma Propulsion for Space Vehicles. IRE Proc. , vol. 49, no. 12, Dec. 1961, pp. 1789-1821.
- IV-7. Cowling, T. G. : Magnetohydrodynamics. Intersci. Pub. , Inc. , 1957, p. 4.
- IV-8. Schaffer, Allan: Plasma Propulsion with a Pulsed Transmission Line. ARS J. , vol. 31, no. 12, Dec. 1961, pp. 1718-1722.
- IV-9. Jones, R. E. ; and Palmer, R. W. : Traveling Wave Plasma Engine Program at NASA Lewis Research Center. Proc. Third Symposium on Magnetohydrodynamics, Rochester (N. Y.), Gordon and Breach Pub. , Inc. , 1964, pp. 383-399.
- V-10. Jones, R. E. ; and Palmer, R. W. : The Traveling Magnetic Wave Plasma Engine. Paper Presented at NASA Intercenter Conf. on Plasma Phys. , Wash. , D. C. , Dec. 3-5, 1963.
- V-11. Palmer, Raymond W. ; Jones, Robert E. ; and Seikel, George R. : Analytical Investigations of Coil-System Design Parameters for a Constant-Velocity Traveling Magnetic Plasma Engine. NASA TN D-2278, 1964.
- IV-12. Mayfield, Earle B. ; Meyer, Rudolph N. ; Head, Richard M. ; and Huddleston, Richard H. : Plasma Propulsion by Means of a Helical Transmission Line. Vol. 9 of Prog. in Astronautics and Aeronautics, Academic Press, Inc. , 1963, pp. 543-555.
- IV-13. Matthews, Clarence W. : A Theoretical Study of the Motion of an Idealized Plasma Ring Through Various Traveling-Magnetic-Wave Plasma Accelerators. NASA TN D-1636, 1963.

- IV-14. Heflinger, Lee; and Schaffer, Allan: Magnetic Induction Plasma Engine. General Technology Corp. (NASA CR-54063), 1964.
- IV-15. Mayfield, E. B.; and Head, R. M.: Plasma Propulsion. Nat. Aeron. Electronics Conf., IRE and IAS, Dayton (Ohio), May 2-4, 1960.
- IV-16. Covert, Eugene E.; Boedeker, Lawrence R.; and Haldeman, Charles W.: Recent Results of Studies of the Traveling Wave Pump. AIAA J., vol. 2, no. 6, June 1964, pp. 1040-1046.
- IV-17. Penfold, A. S.: Recent Advances in the Development of Electromagnetic Thrusters for Space Propulsion. Proc. Fourth Symposium on Advanced Propulsion Concepts. Palo Alto, Cal., April 26-28, 1965.
- IV-18. Lax, Benjamin; Allis, W. P.; and Brown, Sanborn C.: The Effect of Magnetic Field on the Breakdown of Gases at Microwave Frequencies. J. Appl. Phys., vol. 21, no. 12, Dec. 1950, pp. 1297-1304.
- IV-19. Ben Daniel, D. J.; and Hurwitz, Henry, J.: Matching Conditions at Gradual Plasma Boundaries. Final Rept., General Electric Co., Feb. 1962.
- IV-20. Hellwig, G.: Uber die Bewegung geladener Teilchen in Schwach Veranderlichen Magnetfeldern. (On the Motion of Charged Particles in Weakly Changing Magnetic Fields.) Z. Naturforsch., vol. 10A, 1955, pp. 508-516.
- IV-21. Kosmahl, H. G.; and Miller, D. B.: A Microwave Driven Magnetic Plasma Accelerator at Cyclotron Resonance. Paper Presented at Conf. on Electron Devices Res., Ithaca (N. Y.), June 24-26, 1964.
- IV-22. Ahmed, S. A.; and Hendel, H. W.: Space Charge Acceleration of Ions at Electron Cyclotron Resonance. Preprint No. 64-24, AIAA, 1964.
- IV-23. Hendel, H. W.; and Rebould, T. Todd: Continuous Plasma Acceleration at Electron Cyclotron Resonance. Preprint No. 63001-63, AIAA, 1963.
- IV-24. Miller, David B.; and Gibbons, Edward F.: Cyclotron Resonance Propulsion System. "Cyclops." Rep. No. SSL-63-4, General Electric Company (NASA CR-52336), 1963.
- IV-25. Okress, E. C.; Brown, W. C.; Moreno, T.; Goubau, G.; Heenan, N. I.; and George, R. G.: Microwave Power Engineering. IEEE-Spectrum, vol. 1, no. 10, Oct. 1964, pp. 76-86.
- IV-26. Anon.: Research on Spacecraft and Powerplant Integration Problems. General Electric Company (NASA CR-53398), 1963.

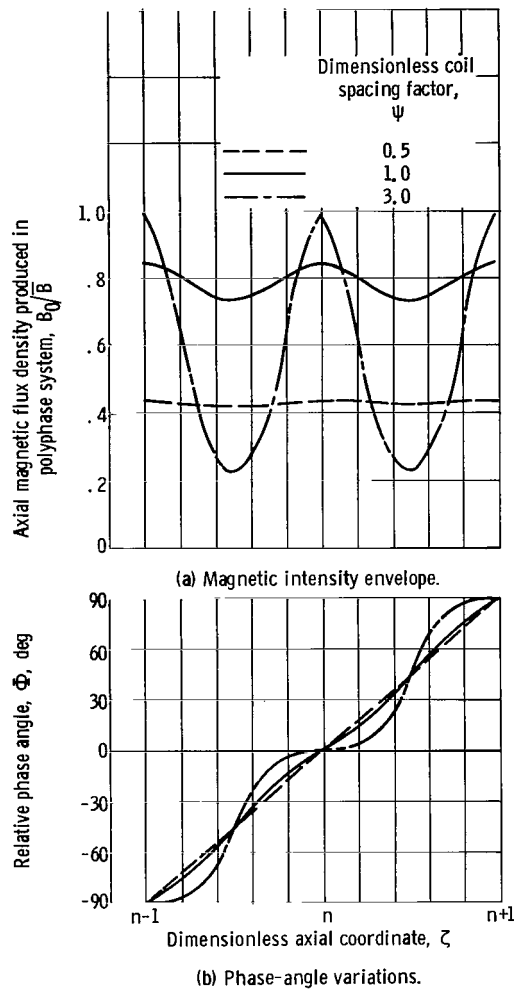


Figure IV-1. - Magnetic-intensity envelopes and phase-angle variations for an infinite field-coil configuration at 90° current phasing.

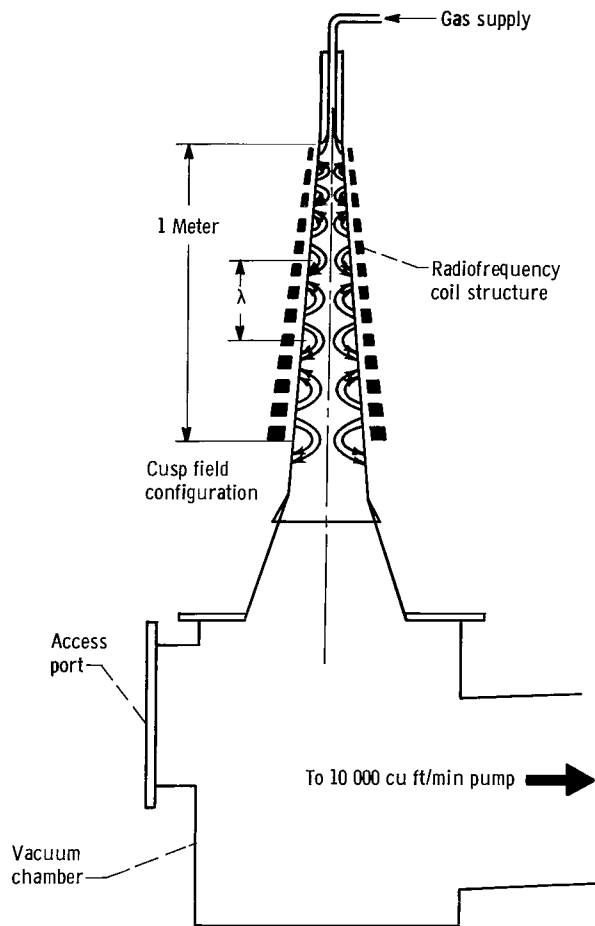


Figure IV-2. - Schematic of basic experimental arrangement of inductive traveling-wave accelerators. Length of accelerator chamber corresponding to full wave length of traveling cusped magnetic field.

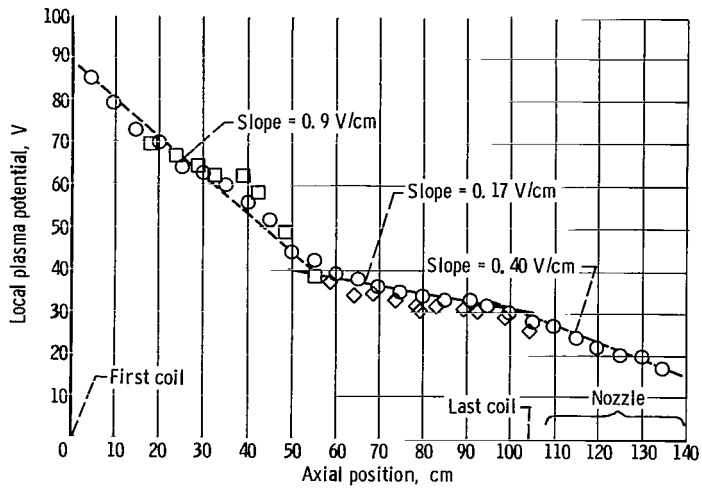


Figure IV-3. - Plot of local plasma potential measured on axis of accelerator as a function of axial position.

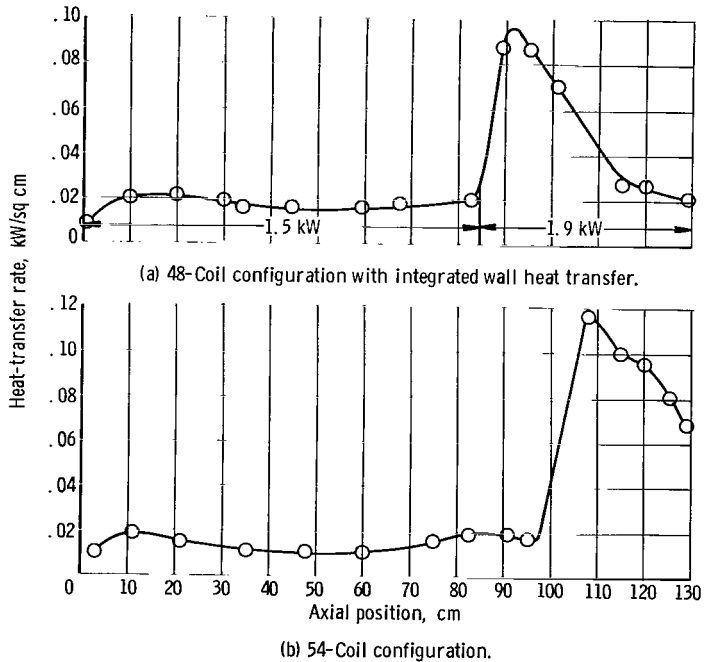


Figure IV-4. - Typical wall heat-transfer profiles for 48- and 54-coil configurations. Extension of coil configuration resulted in displacement of peak heating region.

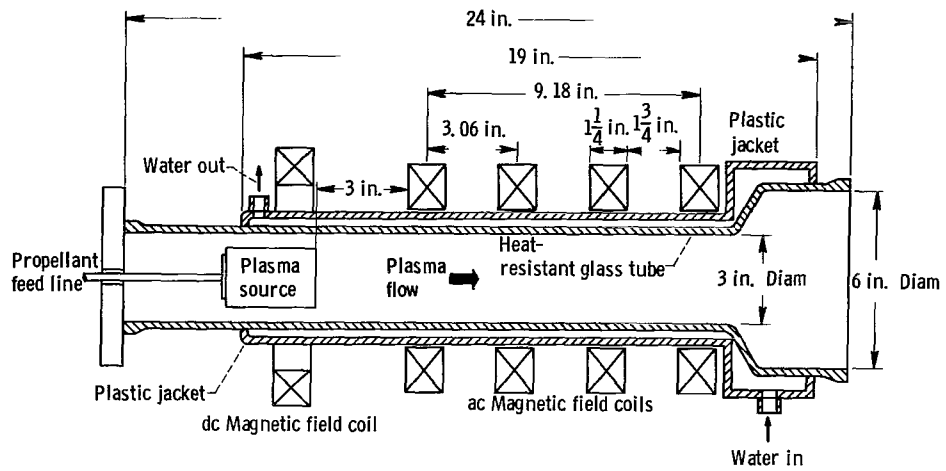


Figure IV-5. Sketch of four-coil four-phase traveling magnetic-wave plasma engine.

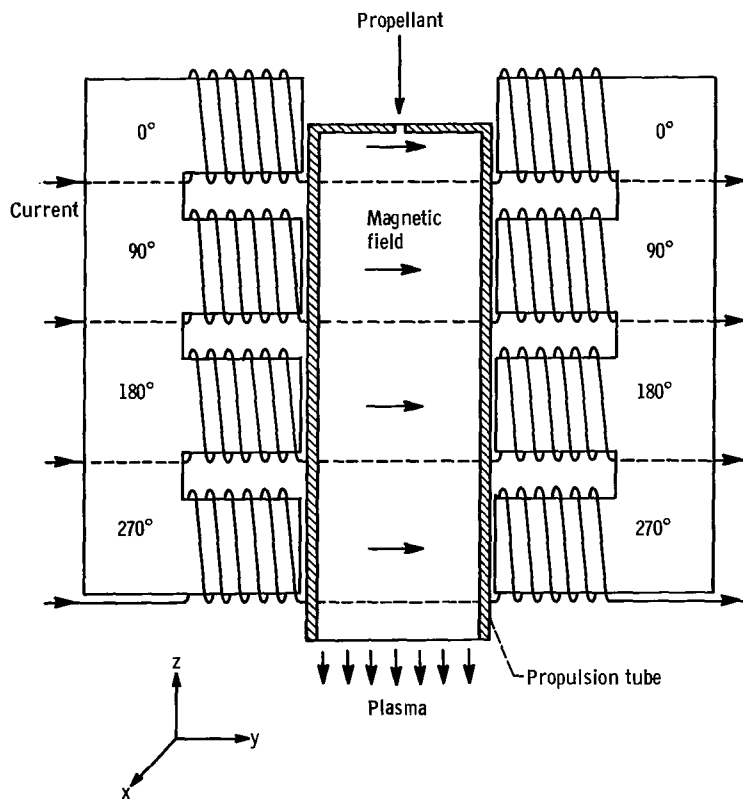


Figure IV-6. - Schematic of accelerator.

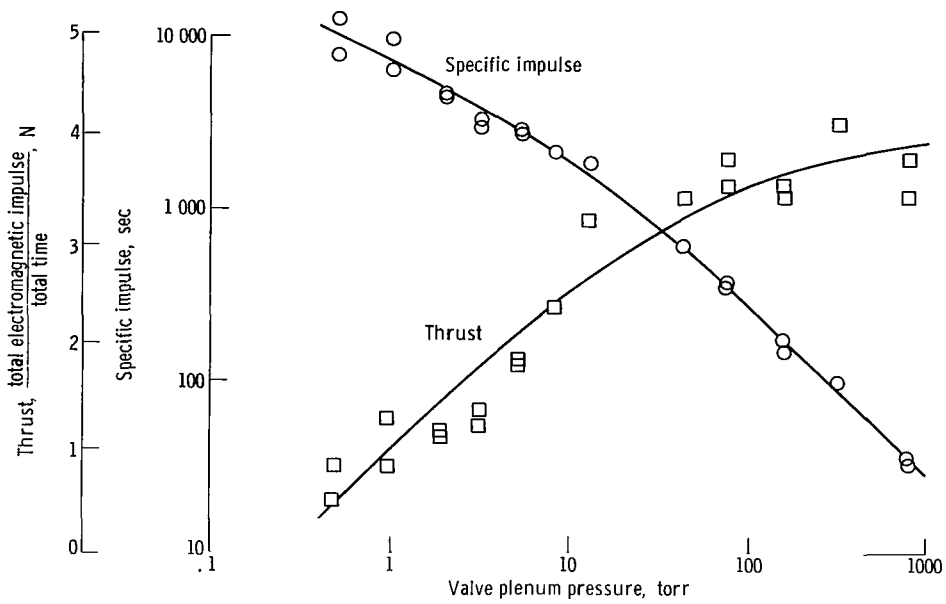


Figure IV-7. - Argon performance; charging voltage, 20 kilovolts; frequency, 465 kilocycles.

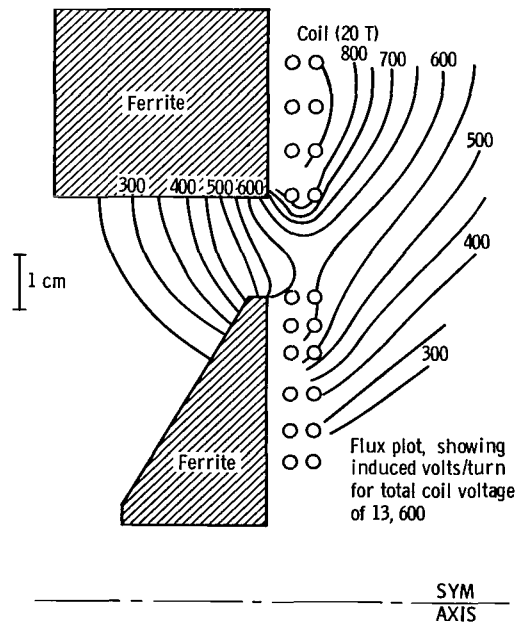


Figure IV-8. - Schematic of RF fringe-field accelerator.

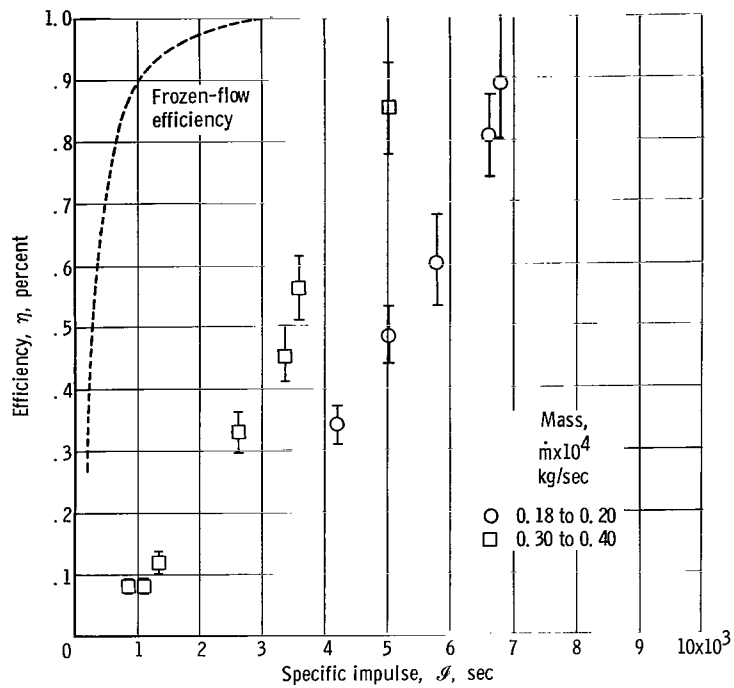
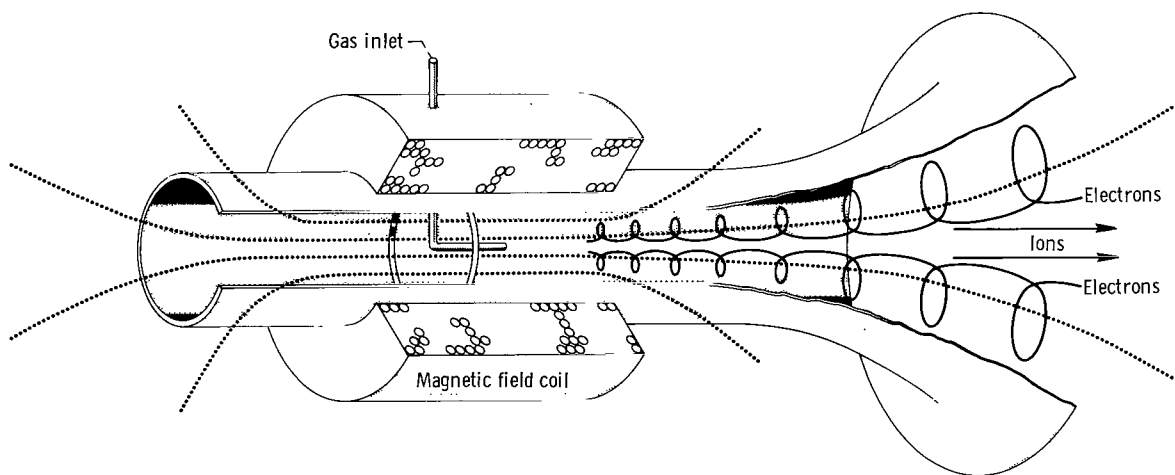


Figure IV-9. - Experimental results showing efficiency as function of specific impulse. Propellant: mercury.



CD-8189

Figure IV-10. - Cyclotron resonance plasma propulsion system.

CHAPTER V

PULSED PLASMA ACCELERATORS

SUMMARY OF CURRENT STATUS

In pulsed plasma accelerators, current is passed directly through the plasma and interacts with its self-magnetic field to produce the $\vec{j} \times \vec{B}$ accelerating force on the plasma. A wide variation of electrode geometries is possible. The most extensively investigated are the straight coaxial, the curved coaxial, and the parallel rail geometries. All of the accelerators require high currents and, at present, are driven by capacitor discharges.

Propulsion oriented experimental programs are at present being conducted at General Dynamics/Convair, The General Electric Company, and Lewis Research Center on the straight coaxial geometry accelerators, at Republic Aviation on the curved coaxial geometry, and at the Allison Division of the General Motors Corporation on the rail geometry.

In general, the status of pulsed plasma accelerators is such that the present experimental efforts are best described as feasibility studies. The accelerating mechanism has been found to be much more complicated than the existing theories predict. An understanding of the plasma behavior has not been achieved and the major loss mechanisms have not been identified. A realistic model of the detailed plasma processes to aid in the design of an efficient accelerator does not exist.

Nevertheless, the pulsed plasma accelerators show fair promise of becoming propulsion devices. Significant advances have been made, and it is only recently that the experimental programs have not been very seriously hampered by the deficiencies in certain critical system components. Efficiencies in excess of 50 percent have been reported. Erosion does not seem to pose a major problem at reasonable power levels. The only factor precluding the achievement of very high repetition rates is the heat handling capability of the accelerator system.

GENERAL CONSIDERATIONS

In pulsed plasma accelerators the current from the energy source is passed directly

through the plasma and interacts with its own magnetic field. The thrusters within this class differ with respect to electrode and insulator configuration, energy source and external circuit characteristics, propellant type, and propellant feed system. The coaxial plasma gun typifies the operation of these thrusters. Its simplest embodiment (see fig. V-1) is a charged capacitor in series with a pair of coaxial electrodes. When gas is admitted to the interelectrode region, electrical breakdown occurs at the breech. In a fraction of a microsecond the gas becomes a sufficiently good conductor to form a conducting sheet which separates the breech region containing the magnetic field from the field-free region beyond. The radial current interacts with the azimuthal magnetic field created by the electrode current to provide the electromagnetic acceleration force $\mathbf{j} \times \mathbf{B}$. Alternately, the highly conducting gas can be thought as being expelled by the force of the magnetic pressure, $B^2/2\mu_0$, acting on the current sheet over the area between the coaxial electrodes. The work done on the plasma is given by

$$\int \Delta \left(\frac{B^2}{2\mu_0} \right) dz$$

integrated over the area of the current sheet. $\Delta(B^2/2\mu_0)$ is the magnetic pressure drop across the sheet, and dz is an increment of current sheet travel (ref. V-1).

A short acceleration time is desirable (refs. V-1 and V-2). Thus the strong acceleration needed to produce high plasma velocities requires very large currents. These accelerators are pulsed in nature and final versions could have pulsing rates up to several thousand per second with pulse durations on the order of microseconds. A distinct advantage of this type of thruster is the capability of operation at the high instantaneous power levels while maintaining a tolerable average power level. The high instantaneous power operation may lead to higher efficiencies.

Electric Circuit Considerations

Some light can be shed on the circuit requirements for efficient operation by examining the over-simplified equivalent circuit for the plasma accelerator, depicted in figure V-2 (refs V-2 and V-3). The plasma is treated as the unconstrained series element of an inductive circuit. When current flows in the circuit the magnetic forces are always such as to increase the inductance of the circuit, producing motion of the unconstrained element formed by the plasma current loop toward the muzzle of the gun. The voltage at the gun terminals is

$$V(t) = \dot{\varphi}(t) + I(t)R(t) = L(t)\dot{I}(t) + I(t)[\dot{L} + R(t)]$$

The power delivered to the electrodes is

$$P = L\dot{I} + I^2(\dot{L} + R) = \frac{d}{dt}\left(\frac{1}{2} LI^2\right) + \frac{1}{2} I^2\dot{L} + I^2R$$

The term $\frac{1}{2} I^2\dot{L}$ represents the rate of work being done on the current sheet, independent of relative motion of the current sheet and plasma mass (ref. V-1).

The resulting energy delivered to the electrodes is

$$\int_0^t P \cdot dt = \frac{1}{2} LI^2 + \frac{1}{2} \int_0^t I^2\dot{L} dt + \int_0^t I^2R dt$$

The terms on the right-hand side represent field energy, work done on the current sheet, and ohmic losses, respectively. Not all of the mechanical work done on the current sheet will show up as useful kinetic energy of the plasma because of inherent loss mechanisms. However, for efficient operation, it is the second term which must be maximized.

Acceleration over several cycles of current is not practical because of the continued I^2R losses, the growth of instabilities, and the tendency of these devices to crowbar, that is, to set up secondary discharges near the breech following voltage reversal. Clearly, a ΔL large compared to L_0 must be realized before the current in the circuit begins to decay, all external circuit resistance must be minimized, and the magnetic-field energy must somehow be deposited into plasma kinetic energy.

The first requirement necessitates severe capacitor and circuit requirements. For practical coaxial guns using lumped capacitor energy storage elements producing current in excess of 10^5 amperes, the inductance per unit length is sufficiently low so that external inductances in the low nanohenry range must be realized. For other geometries, where the inductance per unit length is significantly larger or for coaxial guns driven by lower currents, the requirements are less severe.

When the current sheet is stable and its velocity is constant, \dot{L} is approximately constant. Considering the system where these requirements are met, and where the resistance is negligible, it is evident from the last equation that half of the energy is going into work done on the plasma and half is going into field energy within the gun. As the voltage at the capacitor reverses, some of this field energy is used to recharge the capacitor. A secondary discharge is usually set up at the breech some time after voltage reversal and the electromagnetic energy existing in the capacitor and external inductance at this time is sealed off from the plasma and dissipated uselessly in the external circuit. The crowbar may be stationary (refs. V-1, V-4, and V-5) or successive current sheets

may be formed at each voltage reversal (refs. V-5 and V-6). In the latter case, the sheets move against the magnetic field behind the first sheet and usually slow down, never emerging from the end of the gun. For efficient operation, the crowbar must be controlled to occur very near to voltage zero, so that the field energy is trapped in the gun, with a negligible amount having gone back to the external circuit. The magnetic pressure continues to be exerted on the current sheet, and some of the field energy can be recovered as useful work on the plasma.

Efficiency Considerations

A series of energy transfer processes are involved in achieving the desired goal of transferring a very high fraction of initially-stored capacitor energy to directed kinetic energy of the propellant. Since each process involves energy losses, an efficiency may be assigned to it. The energy efficiency of these devices can be subdivided into the efficiencies of the following processes: (1) transfer of stored capacitor energy to the gun terminals

$$\left(\eta_1 = \frac{\int_0^{\tau} VI \, dt}{\frac{1}{2} CV_0^2} \right)$$

(2) transfer of gun terminal energy to magnetic field energy within the gun plus work done on the current sheet

$$\left(\eta_2 = \frac{\frac{1}{2} LI^2 + \int_0^{\tau} \frac{1}{2} I^2 \dot{L} \, dt}{\int_0^{\tau} VI \, dt} \right)$$

and (3) the transfer of field energy plus work done on the current sheet to directed kinetic energy of the plasma

$$\left(\eta_3 = \frac{\text{kinetic energy}}{\frac{1}{2} LI^2 + \int_0^\tau \frac{1}{2} I^2 \dot{L} dt} \right)$$

τ is taken as the time for useful acceleration and the exact definition varies with different investigators.

The efficiencies of the first two transfers may be maximized largely, through judicious choices for circuit components, correct matching with the gun, and the realization of an opportune crowbar. The efficiency of the third transfer is determined by the detailed plasma processes. Combinations of the individual efficiencies yields the gun efficiency

$$\eta_g = \frac{\text{plasma kinetic energy}}{\int_0^\tau VI dt}$$

and the overall efficiency

$$\eta_f = \frac{\text{plasma kinetic energy}}{\frac{1}{2} CV^2}$$

The overall energy efficiency is frequently used to evaluate performance and differs from the thrust efficiency by factors due to the mass-velocity distribution of the exhaust particles.

Plasma Acceleration Mechanism

The simple theories used to describe the motion of the current sheet and the acceleration process are entirely inadequate in giving quantitative results. This is largely due to the assumption of conditions totally unrealizable in the laboratory and the idealization away from the problem of energy losses. Nevertheless, these models provide a qualitative picture of how the plasma acceleration is accomplished and serve to point out some of the possible loss mechanisms in the plasma. An ideal model and its deficiencies (ref. V-2) is discussed in the following paragraphs. Different models have been de-

scribed by other authors: the snow-plow model (refs. V-1, V-7, and V-8), the slug model (refs. V-9 and V-10), and the gas-dynamic model (refs. V-11 and V-12).

By virtue of their small mass and consequent high mobility, the electrons carry essentially all of the current in the current sheet. Consequently, the $(\vec{j} \times \vec{B})$ force acts only on the electrons. However, as the electrons are accelerated downstream a strong, purely axial coulombian field is produced by the separation of positive and negative space charge, and it is this electric field that accelerates the ions. In the limit of no collisions the electrons will execute cycloidal motions in the crossed fields with a radial drift velocity, V_d , given by

$$\vec{V}_d = \frac{\vec{E} \times \vec{B}}{B^2}$$

The applied radial electric field is equal to the induction field, $\vec{u} \times \vec{B}$, due to motion of the plasma. The former is absent in the frame of reference moving with the plasma. No electrical energy is dissipated within the plasma because the current and electric field are perpendicular. The loss of ions to the electrodes is negligible because their acceleration is parallel to the electrodes, and the kinetic energy of the electrons lost to the anode is small.

In the realistic case, collisions between the ions and electrons are ever present and the current sheet serves as the ionizing agent for the neutral gas into which it moves. These collisions result in joule heating of the electrons. Furthermore, the electron-ion collisions result in heating of ions and the excitation of atomic states of the ions. Even if the thermal energy of the ions is small compared to directed energy, the radial thermal speeds of the ions lead to collisions with the electrodes and the loss of their entire kinetic energy, both thermal and directed, to the electrodes. Equally serious transverse ion losses would result if significant ion current were present or if the ions were shock heated.

The actual processes of plasma acceleration seem to depend very critically on the experimental conditions and are only poorly understood. Electrode and insulator effects on the discharge, as well as that of the gas distribution, are not fully understood, but seem to have a profound effect on the discharge characteristics. Because of these dependences, plasma behavior cannot be studied separately, and simultaneous engineering development of some system components is required. More basic measurements under controlled conditions are necessary before the existing discrepancies can be resolved and a consistent picture of the accelerator behavior presented.

DISCUSSION OF EXPERIMENTAL RESULTS

The experimental results of a number of propulsion-oriented pulsed plasma accelerator programs are presented and discussed. These are the coaxial-gun studies at General Dynamics/Convair, The General Electric Company, and Lewis Research Center; the plasma pinch engine study at Republic Aviation; and, the rail-gun study at the General Motors Corporation. The coaxial gun and the pinch accelerator are similar in that they both exhibit θ -symmetry and presently use gaseous propellants. The two devices are discussed together. Some of the earlier work can be found in references V-5, V-13, V-14, and V-15.

θ -Symmetry Devices

The coaxial geometry has inherent advantages as well as disadvantages. This configuration is topologically free from edges, thereby avoiding the leakage of propellant and possible instabilities initiated at the edges. The magnetic field, under conditions of azimuthal symmetry, is limited to the plasma region, and ideally, the acceleration is in a straight line. The geometrical symmetry makes the interpretation of electromagnetic field data much simpler than in the other devices. However, this geometry presents a very large electrode area in contact with the plasma, and the relatively small inductance per unit length places more severe demands on the external circuit components.

The curved, axially symmetric configuration generally called the pinch plasma engine, is likewise topologically free from edges. The electrode area in contact with the plasma is even larger than in the coaxial geometry and the ion trajectories must be curved to prevent interception with the electrodes.

Pulsed plasma accelerators may be triggered by the propellant influx (refs. V-1, V-16, and V-17) by means of an external switch (refs. V-4 and V-5) or by auxiliary triggering schemes (refs. V-11, V-16, and V-18). Only the external switch mode permits the investigation of discharge conditions under the full variety of initial pressure distributions. The disadvantages of switched operation are reduced reliability and the parasitic inductance and energy dissipation of the switch. A wide variety of gaseous propellants is possible. Typically, nitrogen, argon, xenon, krypton, and helium have been used for convenience.

General Dynamics/Convair coaxial gun program. - The NASA-sponsored program at GD/C has been largely oriented toward the development of reliable diagnostic tools and their use in the investigation of physics of the acceleration process within the gun, determination of the energies within the system as the acceleration proceeds, and a study of exhaust-beam characteristics.

Initially, a single-shot, propellant-triggered coaxial gun was used (refs. V-1 and V-19). The gun geometry and associated electrical system was designed to give short, but strong acceleration, in order to minimize ion heating, plasma cooling to the electrodes, and the formation of troublesome instabilities. A system capable of repetitive operation has been added (ref. V-20).

Measurements made during this time included the following: the magnetic field; the axial and radial electric field; the velocity distribution of individual species; the voltage, current, and power distribution; calorimetric measurements of the total beam energy and its cross-section characteristics; and an optical study of the discharge characteristics.

For purposes of this discussion, the work done may be conveniently divided into two areas: Physics studies that attempt to determine a picture of gun behavior, the acceleration process, and plasma loss mechanisms, consistent with experimental results; and, the feasibility studies which attempt to determine the efficiency of this mode of plasma acceleration.

Physics studies: The magnetic and electric field measurements, together with a determination of exhaust characteristics, have been used to infer plasma properties and shed some light on the mechanism and efficiency of that mode of plasma acceleration where a moving current sheet continually sweeps up neutral gas.

The current sheet may be broad and diffuse with strong axial currents (refs. V-1 and V-19) or thin and well defined (refs. V-20 and V-21) depending on the experimental conditions. For the latter case the current sheet generally reaches terminal velocity in a few tenths of a microsecond and, under the condition of essentially uniform neutral gas density throughout the barrels, this terminal velocity varies approximately as $E^{1/2}$.

A pulse of E_z accompanies the current layer as it advances toward the muzzle. In general, this field cannot accelerate ions to the velocity of the current sheet. The variation between the E_z determined velocity, $\Delta u_z = \ell/m_i \int E_z dt$, and the current sheet velocity has been found to increase with increasing atomic weight of the propellant and decreases with increasing initial capacitor voltage (ref. V-1).

A mass-velocity distribution of the plasma exhaust is necessary to determine if the axial electric field is the primary accelerating mechanism for the ions (ref. V-1). If ions are found to have velocities higher than the E_z determined velocities, direct acceleration of ions and ion currents must be postulated. A complete set of data on one system is not available to make such a determination. However, recent ion probe measurements of the exhaust velocity distribution indicate that under the conditions of correct matching of the energy source to the accelerator the velocity spread in the exhaust is fairly narrow with the average velocity being close to the sheet speed (ref. V-21). Consequently, it seems likely that ion current is important, and that the plasma is either accelerated to the sheet velocity, or driven into the electrodes.

In the event that the accelerator barrels are so long that the magnetic body forces

drop substantially before the current sheet reaches the muzzle, the velocity distribution is broadened and the average velocity reduced. On the other hand, if the current sheet reaches the muzzle early in the energy input phase the velocity distribution is determined by an unknown end effect.

These measurements and others described in reference V-21 suggest strongly that the uniform fill moving current sheet accelerator is behaving at least qualitatively as predicted on the basis of the snowplow model. Similar indications have resulted from work at General Atomic/General Dynamics on a parallel plate accelerator (refs. V-22 and V-23).

Feasibility study: During the first two years, a number of systems, with capacitances ranging from 1 to 5 microfarads, were investigated (refs. V-1 and V-19). Due to limitations imposed by commercially available capacitors and to a mismatch in the gun-electrical system, the large relative inductance change that is a necessary but not sufficient condition for efficient operation, was not obtained. No significant motion of the current sheet, which was found to be broad and diffuse, was observed up to the time an inopportune crowbar isolated the external circuit from the plasma region. The transfer efficiency of initially stored energy to the gun was found to be considerably more than could be expected from the ratio of parasitic inductance to gun inductance.

During the third year, a system consisting of an 11.6-microfarad capacitor bank, with a total system parasitic inductance of 1.5 nanohenrys, was constructed (ref. V-20). An appreciable inductance change due to motion of the plasma during the first half current cycle was realized. The current sheet was again found to be broad and diffuse at early times. The overall calorimetric efficiencies of 25 to 35 percent for this system were not significantly higher than previously obtained, although considerably more energy was deposited in the plasma.

A distributed parameter pulse line has been subsequently used as the energy source for the coaxial gun (ref. V-20). Such a source is characterized by the fact that the transit time of the electromagnetic wave through the capacitor is larger than the characteristic discharge time determined by the circuit parameters. An advantage of this mode of operation is that the pulse time and impedance of the energy source can be independently specified to match the characteristics of the accelerator; for instance, to insure the efficient transfer of stored energy to the gun and a large inductance change due to plasma motion while preventing the withdrawal of the field energy. The constant current from the pulse line makes the interpretation of electromagnetic field data and energy distributions much simpler.

The observed current and voltage waveforms are presented in figure V-3. The pulse line impedance was 17 milliohms. A typical propagation of the current sheet, as determined from B_{θ} measurements, during the energy input phase is shown in figure V-4. The current sheet has been found to be relatively thin and well defined. The cur-

rent sheet reaches a terminal velocity in a few tenths of a microsecond and propagates at constant velocity for the duration of the pulse, producing an almost constant \dot{L} of 14 milliohms for this particular gun geometry. Except for the initial 0.2 microsecond, the ohmic resistance of the plasma is small compared to \dot{L} .

The current and voltage characteristics of any pulse line under various loads can be theoretically calculated. A significant conclusion of the comparison of the theoretical and observed waveforms is that the plasma can be realistically characterized purely as an \dot{L} .

Figure V-5 shows the total energy input, the magnetic field energy, and the work done on the current sheet as functions of time. It is evident that a large fraction of the input energy is converted, in approximately equal amounts, into field energy within the gun and work done on the current sheet. Of the 88 percent of the initial stored energy that was transferred to the gun, 18 percent of the initial energy was withdrawn between the time of voltage reversal and crowbarring of the gun. The work done on the current sheet was 58 percent of the initial stored energy. This represents a very significant fraction of the net 70 percent of initial stored energy deposited in the gun.

In view of the low ohmic losses it seems possible to transfer the initially stored energy to work done on the current sheet with 80 to 90 percent efficiency simply by properly adjusting the pulse-line impedance and discharge time (ref. V-20). However, it should be noted that not all of the work done on the plasma appears as useful kinetic energy of the exhaust. In fact the calorimetric efficiency of the above system was found to be 15 percent.

This was raised to 26 percent by reducing the length of the gun from 6 to 3 inches, and further raised to 44 percent by increasing the diameter of the outer electrode from 3 to 6 inches while keeping the same 1.5-inch inner electrode (ref. V-20).

For all the data just mentioned, the propellant distribution at the time of initiation of the discharge was essentially uniform along most of the length of the barrels. Such a distribution has been used because it was found that stability could be maintained if the current sheet continually swept up gas (ref. V-19). For a relatively narrow peaked propellant distribution the current sheet tended to collapse into a single localized spoke with disastrous effects on gun efficiency and propellant utilization.

General Dynamics/Convair has now concluded that energy which goes into shock heating of the gas swept up by the current sheet cannot be recovered as useful kinetic energy of the exhaust. Rather, it is lost to excitation and radiation in times short compared to the acceleration time (ref. V-21).

There are, however, a number of distinct modes of accelerator operation in which the efficiency is not limited in this manner. Two of these that are presently being investigated at GD/C are the slug mode and the stationary current-sheet mode (ref. V-21). In the former mode, where the propellant is localized within the current sheet and accelerated,

the recent experiments have not been plagued by the instabilities encountered in the earlier experiments (ref. V-19). Calorimetric efficiencies of 64 percent have been obtained (ref. V-21). The latter mode seems to have a number of distinct advantages. The current carrying region remains stationary and neutral gas flowing into this region is ionized and accelerated. Magnetic energy, later to be recovered as plasma energy, does not have to be continuously supplied once the current is established. The particle density continuously decreases eliminating the compression heating of the moving current-sheet accelerator.

This accelerator can be pulsed with pulse durations ranging from the order of tens to hundreds of microseconds, and the desirable high instantaneous-power levels can easily be attained.

General Electric coaxial gun program. - The experimental program at General Electric has been oriented largely toward the evaluation and optimization of gun performance and the investigation of exhaust beam characteristics under repetitive operating conditions.

The measurements made include the following: a direct measurement of thrust, calorimetric measurements of the beam energy and its cross-sectional characteristics, voltage and current measurements and the resulting power distribution in the system, magnetic field measurements, and gas probe measurements of the neutral gas distribution. In the early part of the program a two-stage, triaxial electrode configuration with continuous propellant flow was used (ref. V-11). In this system the pressure in the main electrode region is insufficient to produce a breakdown. Triggering is achieved from a burst of gas produced by the triggering electrode. Calorimetric efficiencies up to 17 percent were obtained. However, the experimental results pointed out the need for heavier mass loading in the interelectrode region.

A number of different mass-injection schemes and various gun geometries were investigated under different operating conditions in order to identify the relative importance of various gun-system parameters and to improve the overall efficiency of the accelerator. The variables in this study included capacitance, voltage, gas density and density profile, and gun geometry. The detailed results of this study are reported in references V-17, V-24, V-25, and V-26.

In general, the propellant distribution prior to discharge and the gun geometry were found to exert the strongest influence on gun efficiency. Initial capacitor voltage was found to be an important parameter, however, operation of the more efficient gun systems in excess of 2 kilovolts lead to excessively high \int_{sp} , that is, in excess of 10 000 seconds. The effects of capacitance and parasitic inductance variations were relatively small.

With regard to gun geometry, the greatest gains in efficiency were realized by reducing the length of the gun barrels and increasing the ratio of outer to inner electrode diameters. Smaller gains were made by using a divergent outer electrode and optimizing the difference in length of the inner and outer electrodes.

Improvements in efficiency due to changes in the initial propellant distribution were made by changing from radial to axial propellant injection, using two-stage operation to reduce the minimum mass required for triggering and to postpone initiation of the discharge until the greatest admitted mass fraction is available for acceleration, and improving the injector port and gas valve design.

Typical current and voltage waveforms for a gun configuration similar to that shown in figure V-6 are shown in figure V-7. The waveforms indicate a large inductance change due to work done on the plasma during the energy input phase and the heavy damping due to the efficient deposition of the stored energy into the gun.

Magnetic-probe measurements indicated that substantial currents of a very complex structure flow behind the leading edge. For the case of 3 kilovolts initial voltage the current sheet propagated to the muzzle in approximately 1.5 microseconds while significant external-circuit currents flowed for about 8 microseconds. Little plasma current was detected by Rogowsky loops a few centimeters downstream from the muzzles. The complex structure behind the sheet which seemed to be fairly steady with time subsequently persisted until power flow into the gun had ceased at approximately 5 microseconds (ref. V-17).

The performance results in figure V-8 were obtained with the gun shown in figure V-6 powered by a 45-microfarad capacitor bank. The I^2R losses in the capacitor bank to the time of voltage zero were found to be about 14 percent. This loss can be reduced to a few percent by using presently available higher Q capacitors. Almost all of the remaining 86 percent of the energy was delivered to the gun with only a few percent of the energy being stored as magnetic energy in the parasitic inductance due to the low currents (refs. V-17 and V-26).

The thrust efficiency against \int_{sp} curves for nitrogen and xenon, propellants are shown in figure V-8. These data were taken at a repetition rate of 10 pulses per second with firing durations of 1 to 2 minutes. Thrust was found to be constant at fixed operating conditions and was found to vary linearly as the pulse rate was varied. The gun was triggered with the first-stage trigger electrodes, with the mass flows used being from 20 to 60 percent of that required for self-triggering of the gun. The erosion rate was found to be about 2 percent of the typical propellant flow rate. In general, calorimetric efficiencies were found to be only slightly higher than the thrust efficiencies.

A neutral gas density probe has been used to determine the propellant distribution prior to the discharge. The results for xenon propellant are shown in figure V-9. Evidently no more than 55 percent of the propellant can be found between the barrels at any instant of time. In obtaining the thrust efficiency against \int_{sp} curve the delay time between valve actuation and first-stage triggering was varied to determine its effect on the efficiency. Highest efficiencies were obtained at a delay time of 0.7 millisecond which corresponds to the greatest propellant fraction within the gun. Nitrogen propellant gave

similar results, with the highest propellant fraction being over 70 percent (ref. V-26).

These experiments have demonstrated the need for improvements in the propellant injection scheme in order to raise the mass utilization. The problem seems to be one of increasing the conductance of the nozzles so that the volume between the valve and the front of the nozzles can be pumped out much faster. The gas valve itself has been found to be adequately fast.

The mass fraction numbers do not necessarily represent the upper limit for the mass utilization. Some of the propellant beyond the electrodes could still be usefully accelerated. However, because the mass utilization is unknown, the species in the exhaust have not been identified, the calorimetric efficiency is only slightly higher than the thrust efficiency, and long term operation was not achieved, it is necessary to confirm the performance results by an independent means, such as the measurement of the mass velocity distribution in the exhaust from which both thrust and \int_{sp} can be calculated.

Lewis Research Center experimental coaxial gun program. - Lewis Research Center has conducted a research program to define some of the factors influencing the coaxial gun efficiency and to study particular phases of the acceleration process. The system used has not been one that is optimized for propulsion application, but rather one which permits the evaluation of gun performance under a wide variety of conditions.

The single-shot gun employs a fast gas valve and the variable-delay ignitron-switched capacitor bank, described in reference V-27, permits the evaluation of gun performance under controllable propellant quantity and distribution conditions.

The diagnostics used include the following: magnetic probes to determine magnetic front velocities and self-crowbarring characteristics; voltage and current measurements to determine the power distribution in the system; calorimetric measurements of the exhaust; and, frame and streak photographs of the exhaust.

The effect on gun performance of the delay time between gas injection and switching of the capacitor bank was investigated. The performance against delay-time curves were rather flat but indicated an optimum delay time for each gas. These delay times appeared to be related to the diffusion times of the gases in the gun. For short delay times on the order of a few hundred microseconds, where the gas distribution was peaked over the gas ports, the discharges were invariably found to go unstable. For longer delay times, such that the propellant had diffused throughout the inner-electrode region, the current sheet was found to be stable over its entire length of travel.

A parametric survey of gun performance for various initial voltages and varying amount of mass for each of three propellants, argon, nitrogen, and hydrogen, was made (ref. V-4). The calorimetric efficiency as a function of mass admitted to the gun is shown in figure V-10. The smallest mass input for each gas was the minimum for which reliable triggering could be achieved at 15 kilovolts. The magnetic front velocity was found to be a function of the initial voltage, type of propellant, and mass of propellant.

This velocity increased with initial voltage and decreased with the atomic weight of the propellant. However, for the 20-kilovolt data, the magnetic-front velocity against mass-admitted curve showed a peak for each of the three propellants. These peak velocities corresponded approximately to those values of mass for which peak system efficiency was obtained.

The transfer efficiency of initial-stored energy to energy delivered to the gun terminals during the first half power cycle ranged from 50 to 80 percent. This efficiency was apparently related to the degree of early motion of the current sheet and decreased with the atomic weight of the propellant. It also generally decreased with increasing mass of a given propellant. Consequently, the efficiency against admitted-mass curves based on the energy delivered to the gun terminals showed trends different from those in figure V-10 (ref. V-4).

A second stationary discharge developed in the breech region of the gun under all operating conditions. The self-crowbar was found to strike before the magnetic front reached the gun muzzle, setting up a circular current loop within the gun and isolating the external circuit from the primary current sheet. The decaying trapped magnetic field continued to accelerate the plasma out of the muzzle.

A study of the plasma exhaust in this mode of acceleration was made using magnetic probes, Rogovsky loops in the exhaust, and an image-converter camera (ref. V-28). The framing mode was used to study the plasma configuration, and the streak mode was used to determine luminous front velocities. The experimental setup is shown in figure V-11. The data was taken with a bank voltage of 15 kilovolts and with 45 micrograms of hydrogen propellant per pulse.

The photographic results indicated that an initial weak-intensity diffuse plasma front, moving at approximately the magnetic-front velocity, emerged from the muzzle. A very short time later, an intense well-collimated core formed at the end of the negative inner electrode and moved downstream at a velocity somewhat less than that of the initial front. This core was found to extend far downstream before fading as the magnetic-field energy decreased.

The Rogovsky loop measurements indicated that this core carried appreciable current well downstream of the gun and formed part of a closed current loop between the electrodes. The results of the current measurements are shown in figure V-12. The current is largest on the gun axis, decreases with increasing distance from the axis, and becomes negative at the edge of the duct. The external Rogovsky loop showed negligible currents. The erosion effects on a mirror and a calorimeter located more than 30 centimeters downstream indicated that the highest energy intensity in the beam was concentrated in an area approximately equal to the cross section of the inner electrode. One of the conclusions of this work was that care had to be exercised in interpreting exhaust data since currents connected to the gun were carried well downstream of the gun muzzle.

Attempts have been made to control the self-crowbar by geometrical changes in the breech region of the gun (ref. V-6). None of these has resulted in appreciably higher efficiencies. Perhaps the most profound change was obtained simply by inserting a boron-nitride disk behind the gas ports. The disk prevented the diffusion of propellant to the breech region of the gun, and current sheets, at each successive voltage reversal, were formed at the disk surface. The minimum mass needed to trigger the gun was far less than before. However, all of the current sheets initiated in the immediate vicinity of the insulator, and considerable mass addition from the insulator, can be expected under these conditions. The efficiency of this mode was very low because the magnetic-field energy stored in the 38-percent length of gun barrel behind the disk is isolated from the plasma and consequently not available for plasma acceleration.

The resulting magnetic field is shown in figure V-13(a), in contrast to the stationary crowbar magnetic field shown in figure V-13(b). The lower trace in figure V-13(a) shows the magnetic field a few centimeters from the insulator downstream of the initial location of the discharges, while the upper trace shows the magnetic field an additional 11.5 centimeters downstream. Each sheet advances against the magnetic field of its predecessor, resulting in a compression of the magnetic field between the sheets. The secondary sheets subsequently slow down, never emerging from the gun. Similar observations are reported in reference V-5. Under the conditions of the stationary crowbar only a single unidirectional current loop is formed within the gun. At the instant of the crowbar the magnetic field stops oscillating with the external-circuit current and decays monotonically as the magnetic field behind the first current sheet expands. This is shown in figure V-13(b).

A theoretical model of the plasma acceleration has been developed and the resulting theoretical predictions of gun efficiencies have been compared to experimentally determined calorimetric gun efficiencies (ref. V-29). The model is an extension of the snow-plow model including both variability of the initial mass loading distribution and the effect of losses associated with wall drag. The experimental results on three gun configurations, not previously reported, as well as those reported in reference V-4, have been used in the comparison.

The model demonstrates the profound effect of the initial mass distribution on the gun efficiency: it predicts the monotonical increase in kinetic efficiency from 28 to 95 percent as the mass distribution is varied from uniform fill to that of a slug. The experimentally determined efficiencies have been found to be about half of those predicted by a simplified version of the model, that is, neglecting radiation, ionization, and wall losses. Preliminary results of comparison of experiment with the complete theory indicate experimental efficiencies about three-quarters of those theoretically predicted for one of the gun configurations.

Republic Aviation pinch engine program. - Basic studies on the application of the pinch accelerator, shown schematically in figure V-14, as a space propulsion device have

been carried out by the Republic Aviation Corporation for a number of years. The results of only the Air Force-sponsored Program (Contract AF 33(616)-8476) for research and development of a 30-kilowatt pulsed pinch plasma engine system are presented in the following paragraphs (ref. V-16).

A number of engine configurations, together with various engine-triggering techniques were investigated. Extended operation of a 1-kilowatt power level was achieved, and the stabilization of engine performance with time was demonstrated. Reliable stabilized performance data were obtained. Continuous operation for 100 hours at a repetition rate of 3 pulses per second and a power level of 0.63 kilowatt was demonstrated.

A noticeable dropoff in thrust and significant changes in discharge characteristics with time under repetitive firing condition have been observed. This has been the case under all operating conditions. These effects have been attributed to electrode conditioning, electrode outgassing, and long-term changes in the electrodes. The largest thrust drop was found to occur during the first few hundred shots, whereafter a smaller drop takes place until approximate stabilization of performance is achieved at the end of about 1 hour of operation. The high initial thrust can probably be attributed to the erosion of microscopically-sharp edges on the electrodes and desorption of monolayers from the electrode surfaces. The slower dropoff is apparently due to diffusion of gases from within the electrodes, chemical changes of the electrodes, and possibly, due to a resistive layer built up on the electrodes.

The performance data for the XE-IS engine after 1 hour of continuous operation are shown in figure V-15. The pulse rates at different voltages were adjusted to give a 1-kilowatt power level. Erosion was obtained by weighing the engine before and after performance evaluation. Consequently, the erosion was averaged over the full hour of operation and added to the injected propellant mass to give the total mass flow. The erosion rate was found to increase with initial voltage and with initial stored energy. The insulator material affected the erosion rate while the electrode material had little influence. In the typical case the eroded material contributed 1 to 2 percent to the total mass flow. Other propellants such as argon, freon, and oxygen produced results similar to those for nitrogen.

The presence of an externally imposed axial magnetic field was found to lower the minimum pressure and minimum mass required for breakdown. For this minimum mass, thrust was found to decrease slightly but the efficiency and \int_{sp} were found to increase. At the same mass flow, the magnetic field had an adverse effect on both the thrust and the efficiency.

Performance data on a two-stage engine are shown in figure V-16. This system was designed to produce breakdown and initial current-sheet motion with a small capacitor bank and then accelerate the sheet with a larger bank. For the data given, the smaller bank was 140 microfarads, with the larger one being 280 microfarads. Both higher effi-

ciencies and higher \int_{sp} were obtained with this configuration.

The energy transfer from the capacitors to the electrodes was found to be very high for the XE-IS engine configuration, typically 90 percent or more. The current and voltage waveforms for this device were found to be almost critically damped. None of the field energy within the engine was returned to the capacitors during the time of plasma acceleration.

Tests on the gas valve indicated that the valve remained open for some time after the discharge was initiated, resulting in propellant loss, and consequently, reduced mass utilization. Because of the adsorption of unknown quantities of this propellant on the electrode surfaces and because of the lack of knowledge of the rate of propellant influx as a function of time during which the valve is open, it is impossible to say what improvement in efficiency can be realized by the use of a faster gas valve.

Magnetic probes have been used to study the field distribution, the motion and form of the current sheet, and to infer the current distribution within the accelerator. The effects of delayed triggering on engine performance have been investigated. Basic studies on the gas injection-breakdown phenomena and on dynamic density measurements have been conducted. The results of all these studies are only in the preliminary stage.

The characteristics of a modified accelerator configuration and how they vary with accumulated discharges have been studied by measuring the net interelectrode current, the magnetic field within the accelerator, the voltage at various stations along the accelerator, and the total magnetic flux in the interelectrode space. The results of this study are reported in reference V-30. A symmetric, well-defined, and relatively thin current sheet was found to propagate toward the muzzle with slow moving diffuse axial currents flowing behind it. The fraction of the total current associated with the sheet was found to decrease as the current sheet moved toward the muzzle. The change of flux in the interelectrode space was found to be primarily a function of the current associated with the thin current sheet and its velocity. The velocity of the current sheet, the fraction of the total current flowing in the sheet, and the degree of dependence of discharge characteristics on propellant species were found to increase with accumulated number of discharges following the exposure at the system to the atmosphere.

Rail Gun

The rail gun, consisting of nothing more than two parallel linear electrodes, is perhaps the simplest of all the pulsed accelerators. It has the advantages of very high inductance per unit length and small electrode area in contact with the plasma. Its disadvantages are the possibilities of propellant leakage and initiation of instabilities at the current-sheet edges. Because of the mass loss problem, gaseous propellants are not practical and the best results have been obtained with metal-derived plasmas.

Allison Division of General Motors Corporation rail gun program. - Allison, under Air Force Office of Scientific Research and company funding, has conducted a 4-year program of analytical and experimental study of a rail-type plasma accelerator. The topics studied include the following: the acceleration process, the effects on efficiency of the external circuit components, the determination of the propellant material and accelerator configuration leading to highest efficiency operation, a study of plasma dispersion and the mass confinement problem, and an evaluation of some of the loss mechanisms in the plasma.

During the first 3 years, a single-shot exploding wire rail gun with a switched capacitor bank, was investigated (ref. V-31). Subsequently, a vapor-deposited, self-triggered, exploding-film system with repetitive operation capabilities has been developed (ref. V-18).

Measurements made on the single-shot system include the following: current and voltage waveforms, power and energy distributions in the circuit, magnetic-field measurements, determination of the mass distribution in the exhaust, erosion measurements, measurements of the total exhaust momentum, measurements of the total beam energy, and optical studies of the plasma configuration.

In an exploding wire rail gun the wire explodes with a high radial velocity. This results in the dispersion of the propellant out of the accelerating fields and reduced performance. All attempts at the application of auxiliary magnetic fields, either externally excited or self-induced, for enhancement of plasma containment or increased accelerating force, resulted in a deterioration of performance. The highest performance was obtained with two parallel 0.25-inch-diameter electrodes, 11.5 inches long and separated by 1 inch. These electrodes had the attributes of highest inductance per unit length of those tested and with the minimum electrode surface area exposed to the plasma. All the data presented below were obtained with this geometry.

The system used is shown in figure V-17(a). Figure V-17(b) represents the equivalent electric circuit.

In the evaluation of the performance of the gun, the linear momentum, measured with a closed-configuration ballistic pendulum, was combined with propellant mass used and the initially stored capacitor energy to calculate a gun efficiency. This is exactly analogous to the thrust efficiency $T^2/2mP$ under repetitive operating conditions.

In the closed-configuration pendulum used, any momentum components due to surface sputtering of the pendulum are canceled through multiple collisions with the walls, with the possible exception of a small amount of impingement of sputtered material on the electrodes. In order to check the validity of the measurement, both electrically conducting and nonconducting, target materials of various heat conductivities and boiling points were used. No significant variation in the measured momentum was observed.

The mass used in the efficiency calculations was that of the wire. The mass of eroded electrode material, in typical cases, was found to be very small relative to the propellant mass, and decreased with accumulated discharges. In the case of silver propellant as high as one-third of the initial propellant was found deposited on the electrodes. Possible contributions, in the form of gases desorbed from the electrodes, to the total mass participating in the discharge were not evaluated. In the event that such contributions are present, the true thrust efficiency would be correspondingly reduced.

The results of a survey of various propellant materials and masses are presented in figure V-18. The data were taken with an external chamber pressure of 4×10^{-4} millimeter of mercury. It was later determined that chamber pressure exerts a significant influence on device performance and that, for silver propellant, an approximately 10-percent gain in linear momentum of the exhaust could be realized by reducing the pressure to the low 10^{-5} millimeter of mercury range. Increased performance was also realized later with accumulated discharges on the electrodes. In the case of 1-mil silver propellant, the energy efficiency increased from 36 to 45 percent. Further gains were realized by replacing the brass electrodes by either molybdenum or Mallory 1000.

Calorimetric measurements of the device efficiency have been made to confirm the preceding data (ref. V-32). The results are summarized in figure V-18. Comparison of calorimeter and ballistic-pendulum data is given in figure V-19. Also shown is a curve for the minimum directed energy. This was calculated on the assumption that the macroscopic trajectories of all the plasma elements were radial lines from this initial propellant location. A possible explanation for the comparison characteristics may be found by considering factors such as a velocity distribution in the plasma, less than perfect mass utilization, and less than unity collecting efficiency of the calorimeter.

It was determined that secondary discharges, at approximately the initial wire location, formed at subsequent voltage reversals. Since the insulator did not appear in the discharge region, apparently a sufficient residue is left behind the main body of plasma. This effect was not investigated in detail. Observations of the discharge configuration, with an image converger camera, indicated that the acceleration process is much more complicated than predicted by the simple model of linear acceleration of the main plasma body.

The repetitively fired system (ref. V-18) shown in figure V-20 utilizing vapor deposited film propellant has several distinct advantages over the exploding-wire gun. Because quasi-unidirectional explosion velocities are obtained with film propellants, explosive dispersion losses are minimized. Ohmic losses and parasitic inductance are reduced by the elimination of the external switch. Plasma diffusion losses may be reduced by stronger acceleration of the plasma. The feasibility of this mode of operation has been experimentally demonstrated. Total scavenging of metal films from electrically inert substrates, without visual erosion of the substrates, has been obtained. Some

unpublished preliminary results with the repetitively fired system are shown in figure V-27. The quoted efficiencies are based on direct thrust stand and total mass flow measurements.

CONCLUDING REMARKS

The capability of high power operation in the required range of J_{sp} has already been demonstrated. The most serious unresolved problems are the achievement of high overall efficiency operation and the demonstration of long-life potential at power levels such that the system becomes competitive in terms of pounds per kilowatt. A number of fundamental problems must be resolved before a full-scale program to develop a space propulsion system can be justified. However, because of the great influence that certain critical system components exert on plasma behavior and gun performance, concurrent development of these, notably the energy storage element and a suitable pulsed propellant feed system, is necessary.

The problem to be resolved before the feasibility of the pulsed accelerators for space propulsion application can be demonstrated fall largely in the following areas: (a) those related to the physics of the acceleration process and the determination of the exhaust beam characteristics; (b) the determination of the "optimum" mode of operation and "optimum" system configuration leading to best performance; and (c) those related to a complete performance evaluation including time variations under long-term operation.

(a) The acceleration mechanism, current sheet dynamics, and the roles of electrons and ions as current carriers are not well understood. The influence on the discharge characteristics of the initial gas distribution, of the insulator, and of the energy source characteristics are only poorly understood. Only preliminary data are available on the velocity distribution for each species in the exhaust. In most cases the individual species have not been identified and no information on the contribution of the gases desorbed from the electrodes and insulator to the total mass flow and of the utilization of the injected mass is available. It now seems possible to deposit the initial stored energy efficiently into work done on the plasma. The problem is getting this work out as useful kinetic energy of the exhaust. The time history of the energy deposited in the plasma is not known, and this precludes the identification of the major loss mechanisms in the accelerator and the determination if they can be reduced to tolerable levels.

Present diagnostic techniques must be refined, new techniques developed, and a great deal more basic measurements under controlled conditions are necessary before these basic problems can be resolved. Only then can a consistent picture of accelerator behavior (a model) be presented and the scaling relations among the important parameters be determined. The development of a theoretical model of the processes in coaxial

guns must be furthered to at least such a degree that scaling becomes understood by enabling the designer to optimize a set of parameters required for any particular mission.

(b) The variation in accelerator performance and in the discharge characteristics as the important system parameters are changed over a wide range must be determined experimentally. In this manner an optimum accelerator configuration and associated electrical system may be found. The effects on gun operation and performance of realistic propellants such as liquid metals must be evaluated.

The "optimum" mode of operation, with respect to type of switching or triggering, the propellant admission scheme, pulsing frequency, etc. , must be evaluated with overall system considerations in mind. For instance, component reliability and capacitor lifetime are of primary importance.

(c) A complete set of performance data is needed, and long-term effects on the performance must be evaluated. This includes long-term operation such that performance stabilizes, the effects of adsorbed or absorbed gases can be eliminated, and erosion evaluated. Mass utilization must be evaluated to determine if it is a basic limitation.

The final pulse rate will be limited only by the heat handling capabilities of the system and the lifetime of the energy storage element. A large fraction of the nonpropulsive energy loss necessarily appears as heat transferred to the electrodes. This may prove to be the most severe problem in achieving very high repetitive operation. Resolving these problems involves extensive development of all system components and has largely been postponed until efficient operation is demonstrated.

REFERENCES

- V-1. Lovberg, R. H. : Hayworth, B. ; and Gooding, T. : The Use of a Coaxial Gun for Plasma Propulsion. Rept. No. AE62-0678, General Dynamics, May 15, 1962.
- V-2. Lovberg, R. H. : Impulsive MHD Devices as Space Engines. Vol. 1 of Advanced Prop. Concepts, Gordon and Breach Sci. Pub., Inc., 1963, pp. 95-113.
- V-3. Kash, Sidney W. : Efficiency Considerations in Electrical Propulsion. Plasma Acceleration, S.W. Kash, ed., Stanford Univ. Press, 1960, pp. 79-93.
- V-4. Michels, Charles J. ; and Ramins, Peter: Performance of Coaxial Plasma Gun with Various Propellants. CONF-93-2, Int. Coaxial Plasma Gun Symposium, Cleveland (Ohio), Sept. 1962.
- V-5. Marshall, John: Hydromagnetic Plasma Gun. Plasma Acceleration, S.W. Kash, ed., Stanford Univ. Press, 1960, pp. 60-72.
- V-6. Michels, Charles J. : Some Transient Electrical Characteristics of the Exhaust of a Self-Crowbarred Coaxial Plasma Gun. NASA TN D-2571, 1965.
- V-7. Vargo, Donald J. : Electromagnetic Acceleration of a Variable-Mass Plasma. NASA TN D-2164, 1964.
- V-8. Hart, Philip J. : Modified Snowplow Model for Coaxial Plasma Accelerators. J. Appl. Phys., vol. 35, no. 12, Dec. 1964, pp. 3425-3431.
- V-9. Schock, A. : Electromagnetic Acceleration of Plasma for Space Propulsion. Planetary and Space Sci., vol. 4, Jan. 1961, pp. 133-144.
- V-10. Mostov, Philip M. ; Neuringer, Joseph L. ; and Rigney, Donald S. : Electromagnetic Acceleration of a Plasma Slug. Rept. No. PPL TR-61-5, Republic Aviation Corp., Feb. 24, 1961.
- V-11. Gorowitz, B. ; Gloersen, P. ; and Rowe, J. H. : Performance Study of a Repeatedly Pulsed Two-Stage Plasma Propulsion Engine. General Electric Company (NASA CR-55248), 1963.
- V-12. Kemp, Nelson H. : and Petschek, Harry E. : Theory of the Flow in the Magnetic Annular Shock Tube. Res. Rept. No. 60, AVCO Corp., July 1959.
- V-13. Gloersen, P. ; Gorowitz, B. ; and Palm, W. : Experimental Performance of a Pulsed Gas Entry Coaxial Plasma Accelerator. ARS J., vol. 31, no. 8, Aug. 1961, pp. 1158-1161.
- V-14. Burkhardt, L. C. ; and Lovberg, R. H. : Current Sheet in a Coaxial Plasma Gun. Phys. Fluids, vol. 5, no. 3, Mar. 1962, pp. 341-347.

- V-15. Mawardi, O. K. , ed. : Proceedings of an International Symposium on Plasma Guns. Phys. Fluids Supplement, pt. 2, vol. 7, no. 11, Nov. 1964, pp. S1-S74.
- V-16. Pearson, J. J. ; Loddengaard, R. A. ; and McIlroy, W. : Research and Development of a Pulsed Pinch Plasma Engine. Rept. No. PCD TR-63-10, Republic Aviation Corp. , May 1963.
- V-17. Gorowitz, B. ; Gloersen, P. ; Ruess, A. ; and Kenney, J. : Performance Study of a Repetitively Pulsed Two-Stage Plasma Propulsion Engine. General Electric Company (NASA CR-54064), 1964.
- V-18. Rosebrock, T. L. ; Glingman, D. L. ; and Gubbins, D. G. : Pulsed Electromagnetic Acceleration of Metal Plasmas. AIAA J. , vol. 2, no. 2, Feb. 1964, pp. 328-334.
- V-19. Gooding, Terence J. ; Hayworth, Bruce R. ; and Lovberg, Ralph H. : Development of a Coaxial Plasma Gun for Space Propulsion. Rep. No. GDA 63-0454, General Dynamics/Astronautics (NASA CR-52339), 1963.
- V-20. Gooding, Terence J. ; Hayworth, Bruce R. ; and Lovberg, Ralph H. : Development of a Coaxial Plasma Gun for Space Propulsion. Rep. No. GD/A63-0927, General Dynamics/Astronautics (NASA CR-52382), 1963.
- V-21. Gooding, Terence J. ; Larson, Alan V. ; Hayworth, Bruce R. ; and Ashby, David, E. T. F. : Development of a Coaxial Plasma Gun for Space Propulsion. Rep. No. GDA-DBE-64-052-4, General Dynamics/Convair (NASA CR-54245), 1965.
- V-22. Lovberg, R. H. : Acceleration of Plasma by Displacement Currents Resulting From Ionization. Rept. No. GA-4363, General Dynamics Corp. , June 28, 1963.
- V-23. Lovberg, R. H. : Measurement of Plasma Density in a Rail Accelerator by Means of Schlieren Photography. Rept. No. GA-4735, General Dynamics Corp. , Nov. 1963.
- V-24. Gorowitz, B. ; Karras, T. ; and Gloersen, P. : Performance of a Two-Stage Repetitively Pulsed Coaxial Plasma Engine. Preprint No. 65-342, AIAA, July 1965.
- V-25. Karras, T. ; Gorowitz, B. ; and Gloersen, P. : Neutral Mass Density Measurements in a Repetitively Pulsed Coaxial Plasma Accelerator. Preprint No. 65-341, AIAA, July 1965.
- V-26. Gorowitz, Bernard; Ruess, Allen; Kenney, J. ; and Gloersen, P. : Overall Efficiency Trends in a Coaxial Gun Plasma Engine System. Paper No. 64-706, AIAA, Aug. 1964.
- V-27. Michels, C. J. ; and Terdan, F. F. : Characteristics of a 5-Kilojoule Ignitron-Switched, Fast-Capacitor Bank. NASA TN D-2808, 1965.

- V-28. Michels, Charles J.: Some Transient Electrical Characteristics of the Exhaust of a Self-Crowbarred Coaxial Plasma Gun. NASA TN D-2571, 1965.
- V-29. Michels, C. J.; Heighway, J. E.; and Johansen, A. E.: Analytical and Experimental Performance of Capacitor Powered Co-axial Plasma Guns. Paper Presented at AIAA Meeting, San Francisco (Calif.), July 26-29, 1965.
- V-30. Donner, T.; and McIlroy, W.: Characteristics of a Pulsed Plasma Accelerator. Proc. Fifth Symposium on Eng. Aspects of Magnetohydrodynamics, M. I. T., 1964, pp. 203-215.
- V-31. Rosebrock, T. L.; Clingman, D. L.; and Gubbins, D. G.: Rail Type Pulsed Plasma Acceleration. Rept. No. 3255, General Motors Corp., Apr. 1963.
- V-32. Rosebrock, T. L.; Clingman, D. L.; and Gubbins, D. G.: Calorimetric Measurements of Efficiency of a Pulsed Rail Type Plasma Accelerator. Rept. No. 3719, General Motors Corp., Dec. 1963.

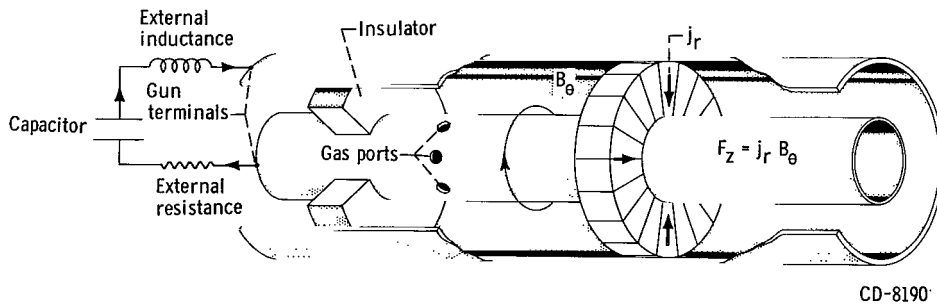


Figure V-1. - Coaxial plasma gun.

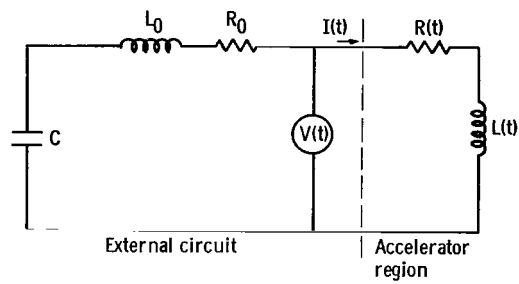


Figure V-2. - Equivalent circuit for pulsed plasma accelerator.

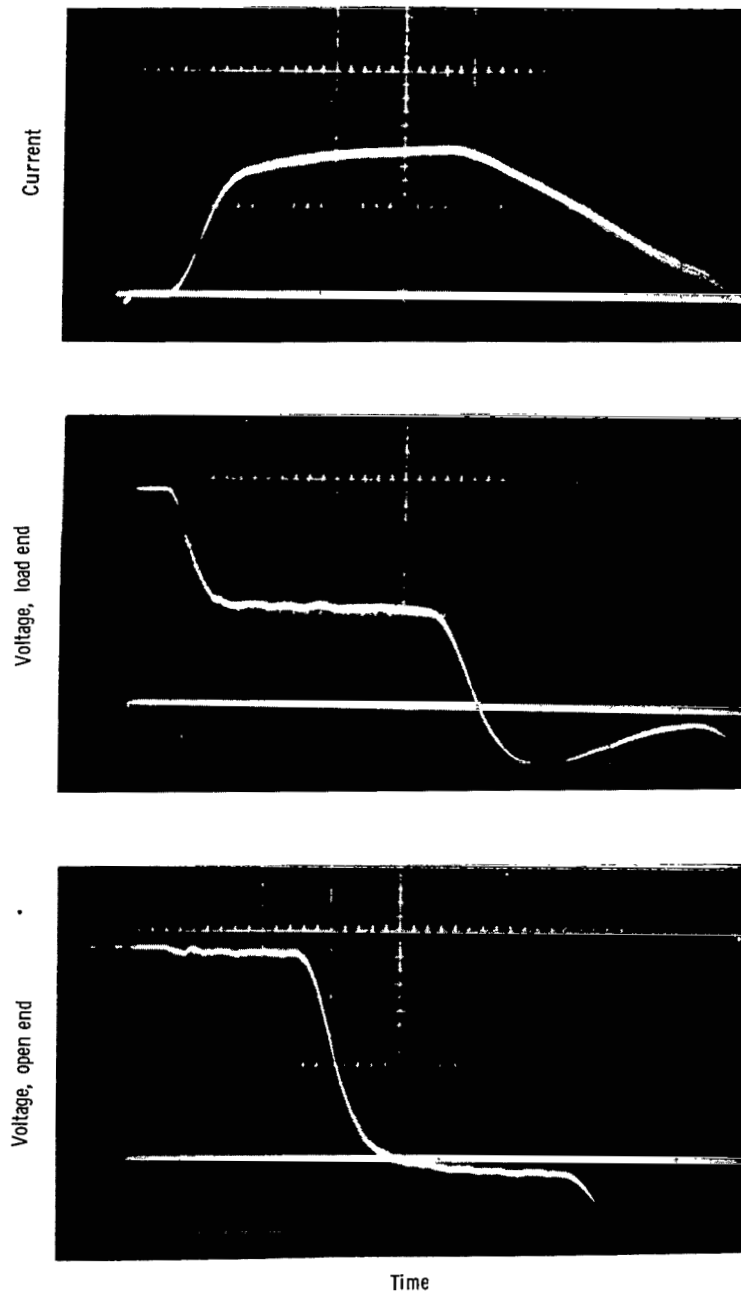


Figure V-3. - Current and voltage waveforms for pulse line. Current, about 100 000 amperes per centimeter; voltage, about 2 kilovolts per centimeter; time, 0.2 microsecond per centimeter.

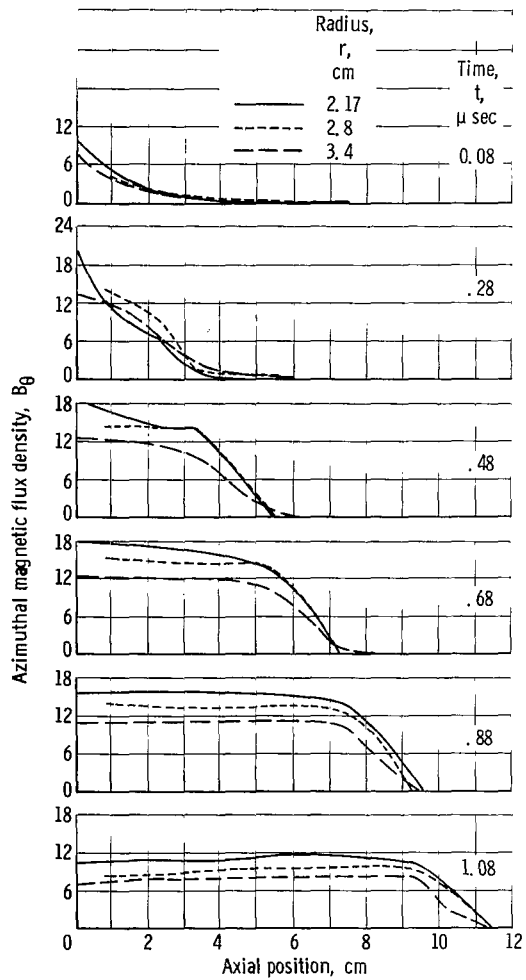


Figure V-4. - Axial magnetic field distributions of nitrogen at 6.3 kilovolts.

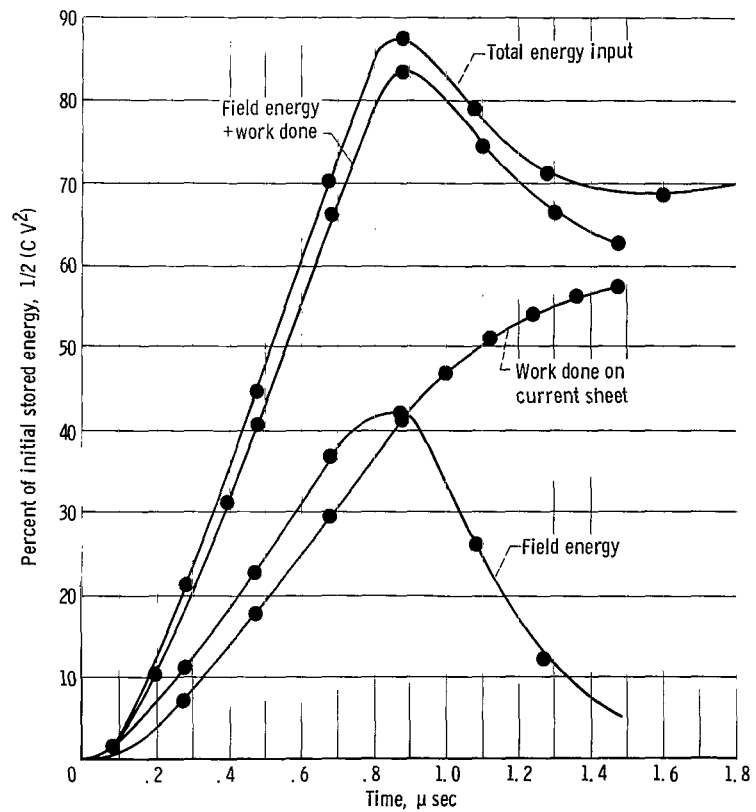


Figure V-5. - Energy balance as function of time.

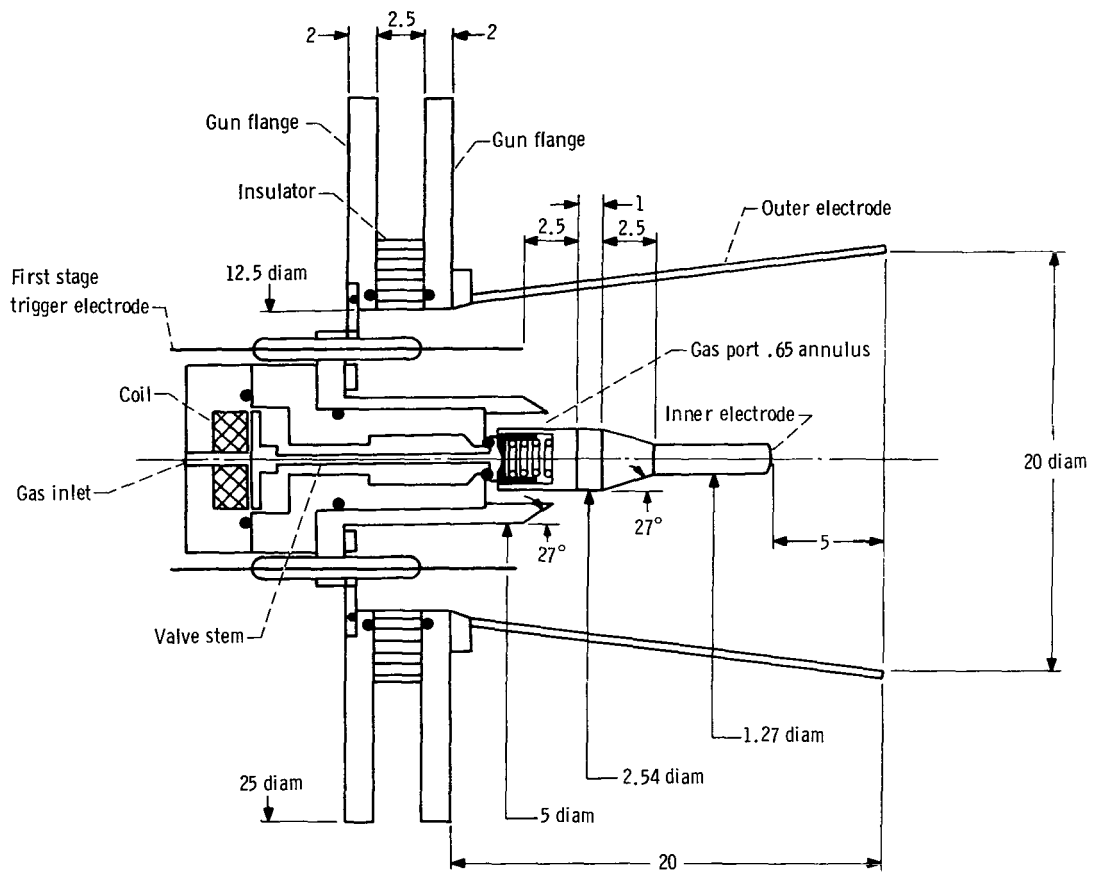


Figure V-6. - General Electric two-stage Mod A-7D engine. (Dimensions in centimeters.)

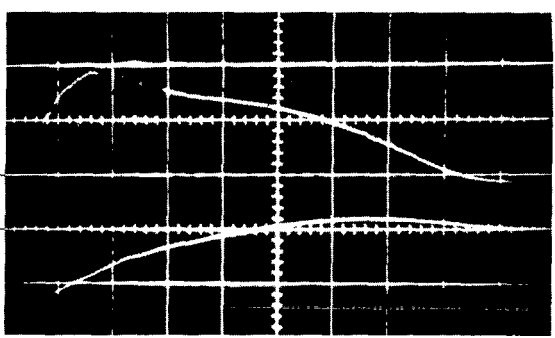


Figure V-7. - Current and voltage transient at breech of Mod. A-4 accelerator (10:1 radius ratio). Upper trace current, 11.2 kiloamperes per centimeter; lower trace voltage, 2 kilovolts per centimeter; time, 1 microsecond per centimeter.

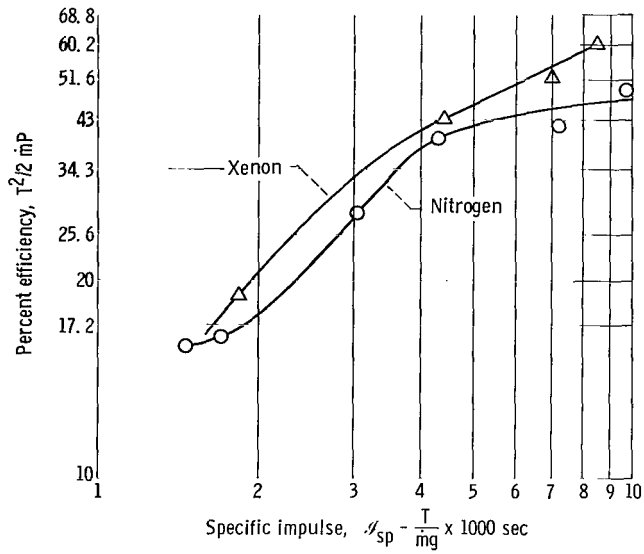


Figure V-8. - Efficiency as for function of specific impulse for two-stage Mod A-7D engine.

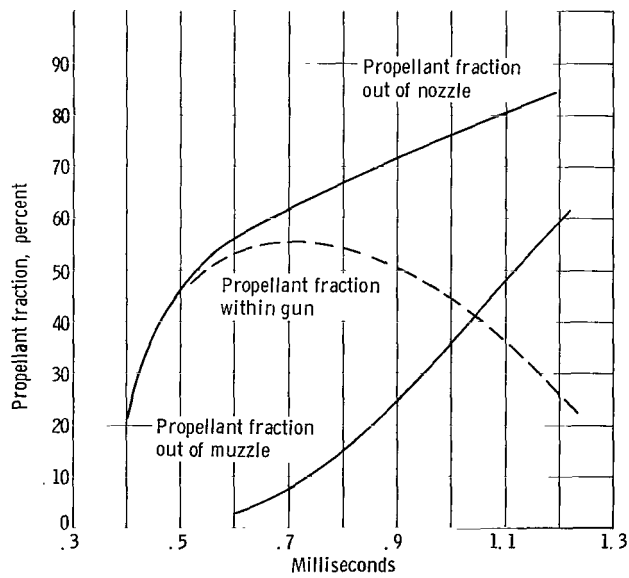


Figure V-9. - Xenon propellant fraction curves (4400 valve voltage).

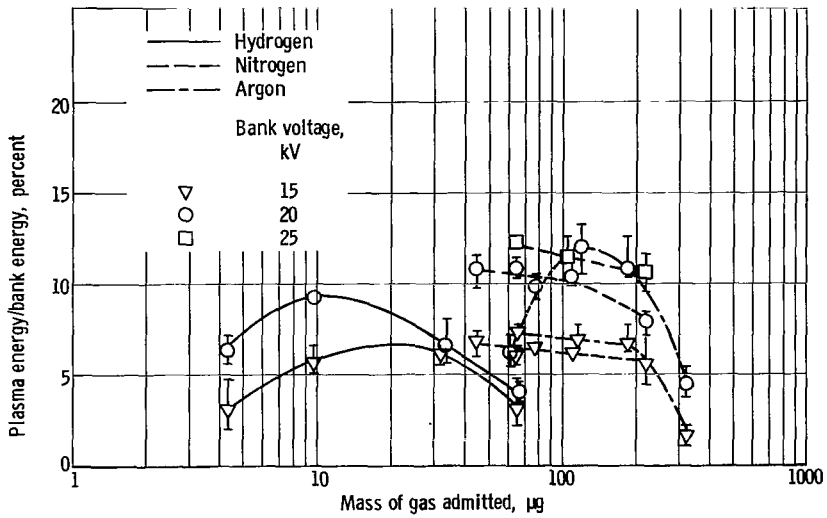


Figure V-10. - Effect of mass of propellant admitted on different system efficiency bank voltages.

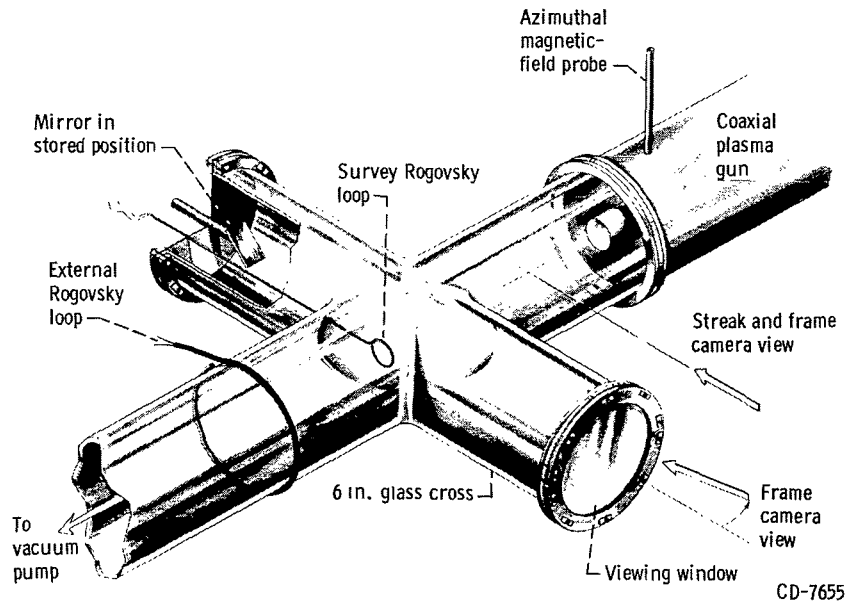


Figure V-11. - Gun and measurement section.

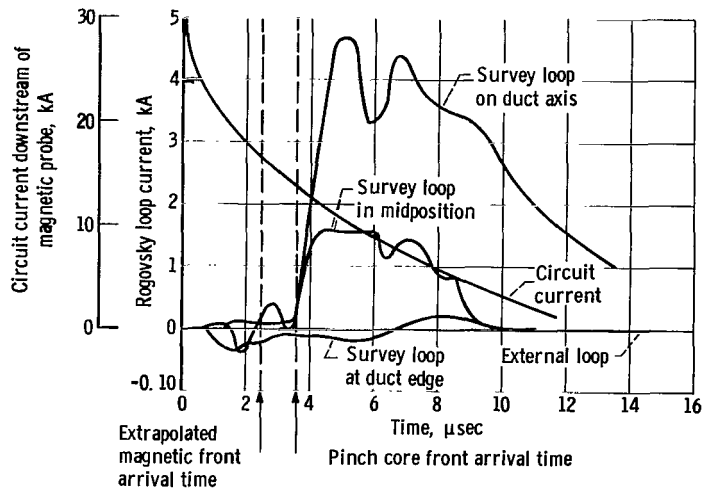
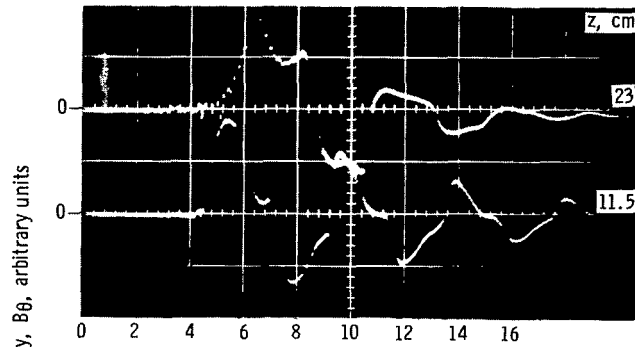
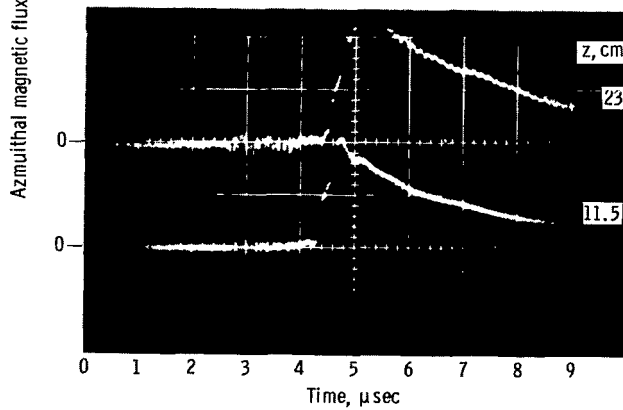


Figure V-12. - Radial survey Rogovsky loop records.



(a) Successive moving current sheets.



(b) Stationary self crobar discharge.

Figure V-13. - Magnetic field as function of time for two types of secondary discharges in coaxial gun.

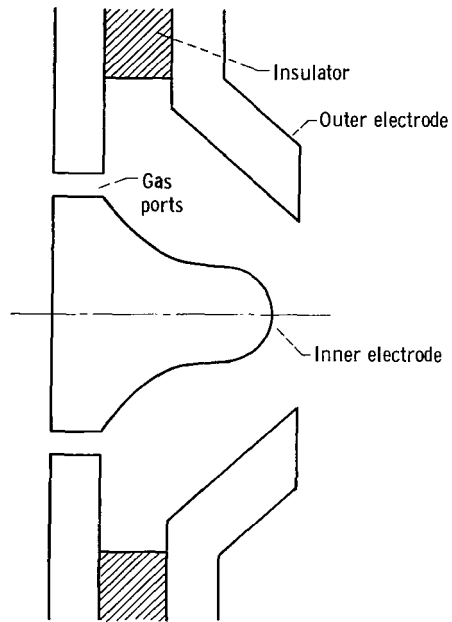


Figure V-14. - Pinch engine electrode configuration.

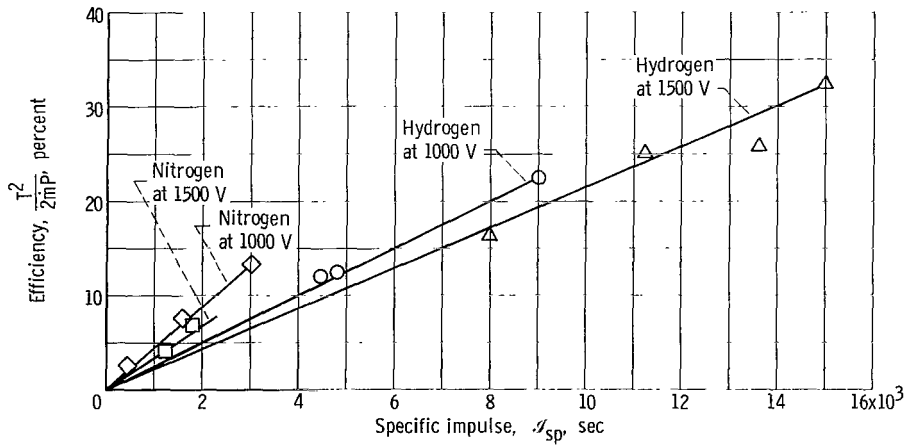


Figure V-15. - Efficiency as function of specific impulse. XE-IS engine configuration, 420 microfarad capacitor bank, 1 hour data.

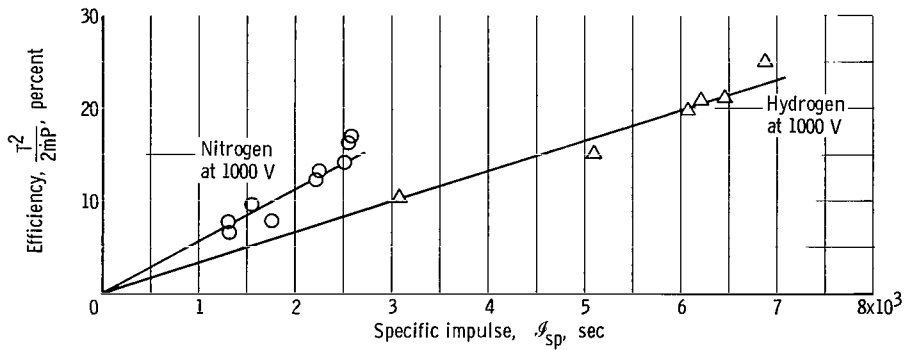


Figure V-16. - Efficiency as function of specific impulse for two-stage configuration. Capacitances, 140 and 280 microfarads; 1 hour data.

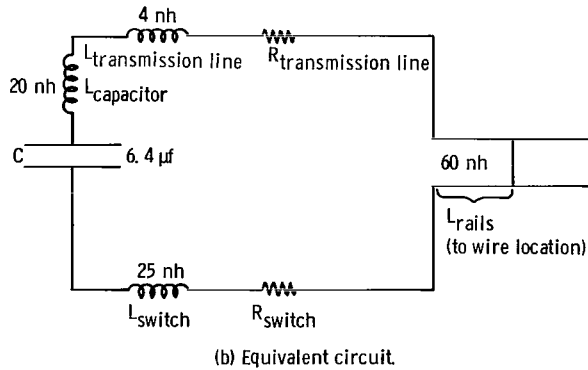
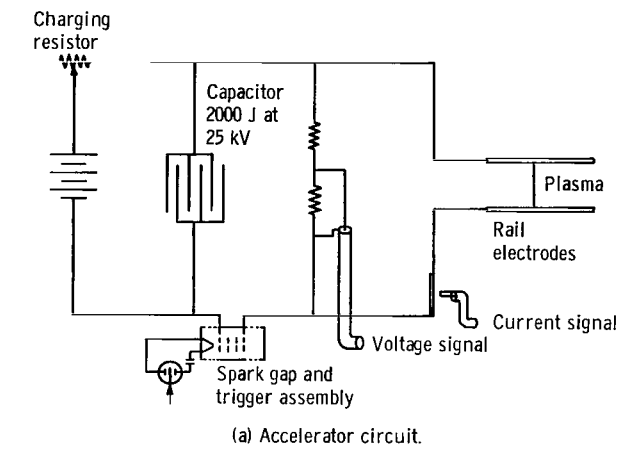


Figure V-17. - Rail gun circuit schematics.

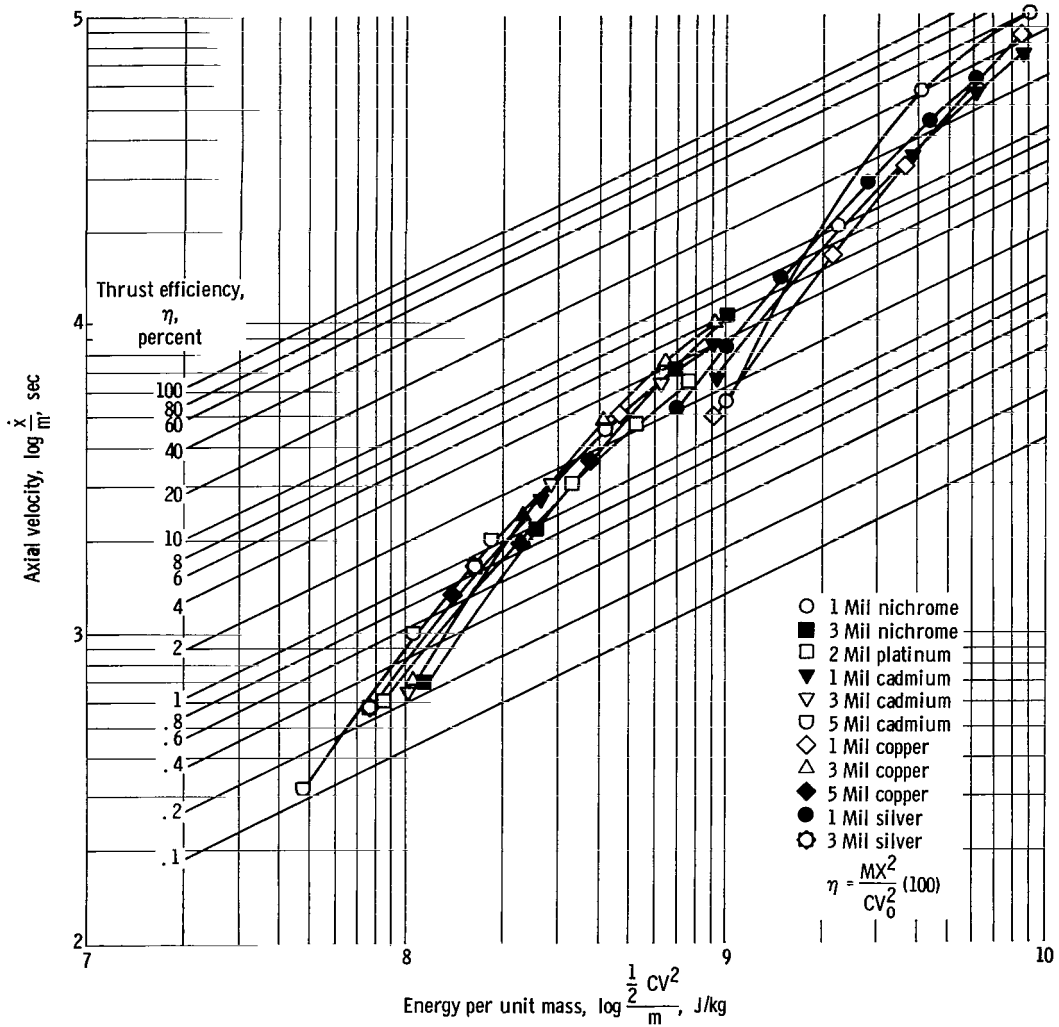


Figure V-18. - Effect of energy per unit mass on axial velocity. Chamber pressure, 4×10^{-4} millimeter of mercury.

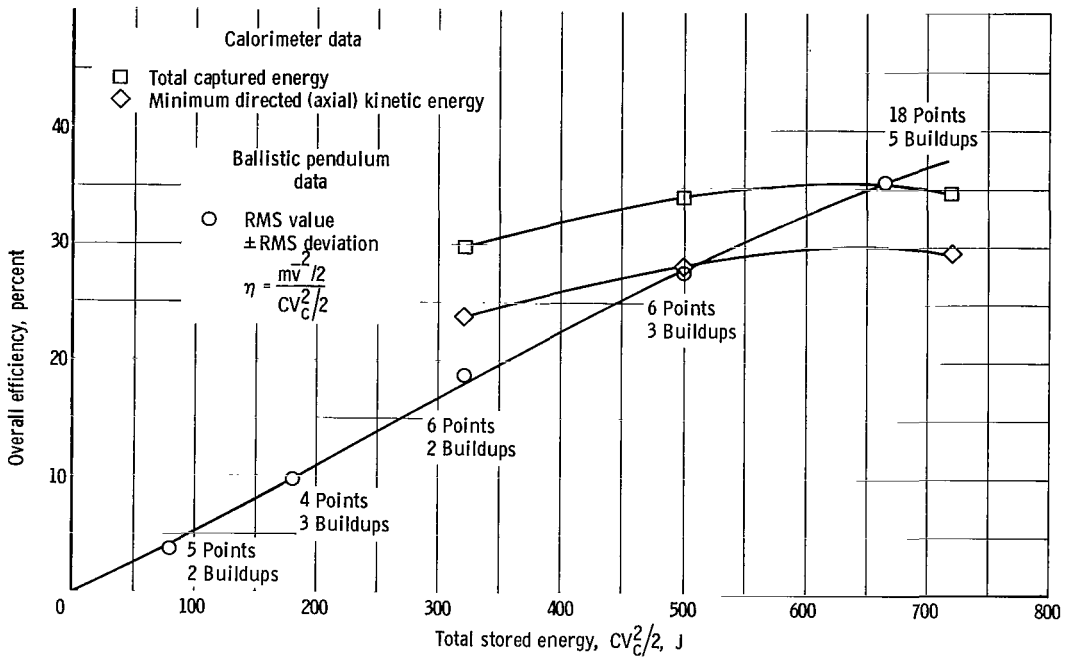


Figure V-19. - Comparison of calorimeter and ballistic pendulum efficiency data. Propellant, 1-mil silver wire; plasma total mass flow, 1.19×10^{-7} kilogram.

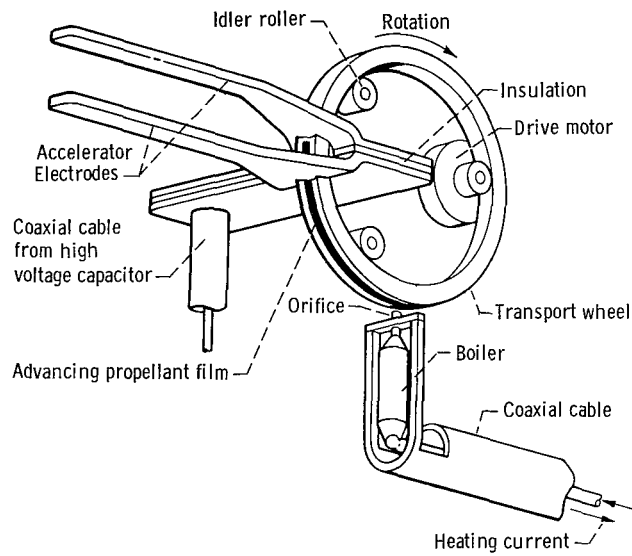


Figure V-20. - Repetitively pulsed plasma accelerator.

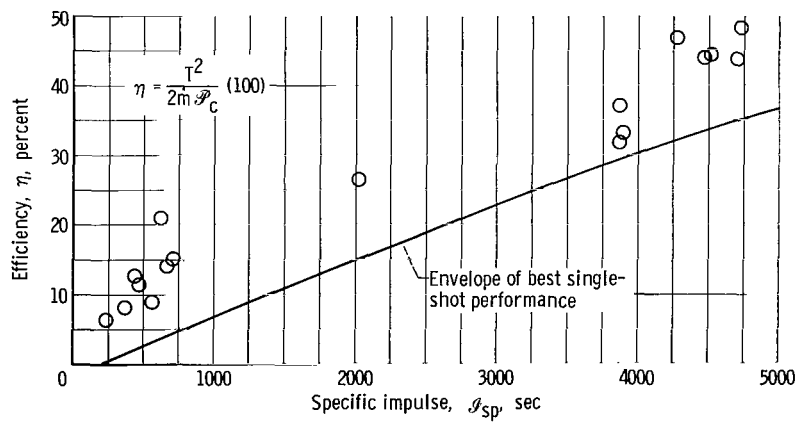


Figure V-21. - Allison pulsed plasma accelerator thrust efficiency.

CHAPTER VI

GENERAL CONCLUDING REMARKS

At present, plasma accelerators are at the stage of experimental evaluation for propulsion applications, collecting performance data, and investigating the problems of operation. A number of different types of plasma accelerators requiring a wide range of input powers are being investigated. Development of flyable systems and the technology associated with these efforts has been logically postponed until acceptable performance of the accelerators has been firmly established.

Substantial improvements in the performance of the accelerators as well as an understanding of their operation have been made. The accelerators have demonstrated the capability of producing high thrust densities and relatively high efficiencies over a wide range of specific impulse. In dc accelerators the most significant advance is the development of the steady-state arc-type accelerators, which, for the first time, have accelerated relatively-dense plasmas to very high exhaust velocities. Alternating current accelerators have demonstrated a definite improvement in thrust efficiencies, increasing this value from a few percent to moderately good levels. This was accomplished with both low and relatively high density plasmas (micron and millimeter pressure ranges). In the class of pulsed plasma accelerators efficient deposition of stored energy into work done on the plasma has been demonstrated. Relatively high thrust efficiencies at relative low voltages and energy per discharge have been achieved.

Recently there has appeared a definite tendency toward devices using coaxial geometry, minimum electrode areas, and short interaction lengths. Linear cross-field accelerators are now being studied primarily for wind-tunnel applications rather than for propulsion-oriented devices. Investigations of the traveling-wave accelerators have largely been discontinued. Emphasis presently is primarily being focused on accelerators capable of being easily mated with solar-cell power sources. The availability of alternative sources of electric space power appear presently to be in the distant future.



APPENDIX - SYMBOLS

| | | | |
|---------------------|---|---------------------------|---|
| A | area, m^2 | \dot{m} | mass, kg |
| \mathcal{A}_t | exit area, m^2 | \dot{m}_t | total mass flow, kg/sec |
| \vec{a} | unity vector of area, m^2 | n | number density of particles, m^{-3} |
| B | magnetic flux density, tesla | P | power, W |
| \bar{B} | maximum axial magnetic flux density produced in polyphase system, weber/ m^2 | \mathcal{P}_c | chamber pressure, torr |
| B_0 | magnetic flux density at geometric center of single-turn loop of coil radius for maximum coil current, weber/ m^2 | Q | ratio of energy dissipated to stored energy, dimensionless |
| C | capacitance, F | R' | resistance, ohm |
| E | electric field strength, V/m | \mathcal{R} | radial length, m |
| E' | moving-frame electric field, V/m | r | radius coordinate, m |
| e | electron charge, C | r_1 | anode radius, m |
| F | force, N | r_2 | cathode jet radius, m |
| F_m | force on magnetic dipole, N | s | distance, m |
| f_V | volume force, N/m^3 | T | thrust, N |
| g | acceleration due to gravity, m/sec^2 | \mathcal{T} | temperature, deg |
| h | electrode separation, m | t | time, sec |
| I | current, A | u | velocity, m/sec |
| \mathcal{I}_{sp} | specific impulse, sec | V | voltage or potential, V |
| \mathcal{I}_{tot} | total impulse, N/sec | v_D | drift velocity, m/sec |
| j | current density, A/m^2 | x, y, z | coordinate system, m |
| k | Boltzmann constant, $J/^\circ K$ | α | fraction ionized, dimensionless |
| L | inductance, H | $\beta = \omega_e \tau_e$ | ratio of cyclotron to collision frequencies of electrons, dimensionless |
| l | length, m | $\omega_i \tau_i$ | ratio of cyclotron to collision frequencies of ions, dimensionless |
| m | mass of particles, kg | δ | distance between coils, m |
| | | ϵ | energy, J |

| | |
|----------------------|--|
| ζ | dimensionless axial coordinate |
| η | thrust efficiency, percent |
| Λ | Debye shielding length, m |
| λ | wavelength of driving-electromagnetic wave, m |
| μ | magnetic dipole moment, A/m ² |
| μ_0 | permeability of free space, H/m |
| ν | frequency, Hz |
| ρ | mass density, kgm/m ³ |
| σ | conductivity, mho/m |
| τ | time between collisions, sec |
| Φ | tensor conductivity, mho/m |
| φ | magnetic flux, Wb |
| Ψ | design parameter, dimension- less |
| ψ | dimensionless coil spacing factor |
| ω | angular velocity, radians/sec |
| ω_e, ω_i | electron and ion cyclotron fre- quency, sec ⁻¹ |
| ω_{rf} | microwave frequency, sec ⁻¹ |

Subscripts:

| | |
|----------|--|
| a | pertaining to linear crossed- field accelerator |
| c | cyclotron |
| dir | directed properties |
| e | pertaining to electrons |
| eff | effective |
| em | electromagnetic |
| f | final or exit conditions |
| i | pertaining to ions |
| inp | input properties |
| n | pertaining to neutrals |
| o | entrance or initial conditions |
| p | pertaining to plasma properties |
| r | radial components |
| s | sheath |
| th | thermal |
| x, y, z | coordinate system |
| θ | azimuthal direction |
| 0 | pertaining to neutral atoms |